27603

National Library of Canada | Bibliothèque nationale du Canada

CANADIAN THESES ON MICROFICHE | THÈSES CANADIENNES SUR MICROFICHE

D

NAME OF AUTHOR/*NOM DE L'AUTEUR* GRAYDON WELLS ARKSEY

TITLE OF THESIS/*TITRE DE LA THÈSE* SYSTEM DESIGN OF A PORTABLE RECEIVER-RECORDER FOR EXTREMELY-LOW-FREQUENCY (ELF) RADIO WAVES

UNIVERSITY/*UNIVERSITÉ* UNIVERSITY OF ALBERTA, EDMONTON

DEGREE FOR WHICH THESIS WAS PRESENTED/*GRADE POUR LEQUEL CETTE THÈSE FUT PRÉSENTÉE* M.Sc. (ELEC ENG)

YEAR THIS DEGREE CONFERRED/*ANNÉE D'OBTENTION DE CE GRADE* 1976

NAME OF SUPERVISOR/*NOM DU DIRECTEUR DE THÈSE* DR. C.R. JAMES

Permission is hereby granted to the NATIONAL LIBRARY OF CANADA to microfilm this thesis and to lend or sell copies of the film.

The author reserves other publication rights, and neither the thesis nor extensive extracts from it may be printed or otherwise reproduced without the author's written permission.

L'autorisation est, par la présente, accordée à la BIBLIOTHÈQUE NATIONALE DU CANADA de microfilmer cette thèse et de prêter ou de vendre des exemplaires du film.

L'auteur se réserve les autres droits de publication; ni la thèse ni de longs extraits de celle-ci ne doivent être imprimés ou autrement reproduits sans l'autorisation écrite de l'auteur.

DATED/*DATÉ* DEC. 17, 1975 SIGNED/*SIGNÉ* Graydon W Arksey

PERMANENT ADDRESS/*RÉSIDENCE FIXÉ* 8717- 88 AVE

EDMONTON, ALBERTA

NL-91 (3-74)

INFORMATION TO USERS

THIS DISSERTATION HAS BEEN MICROFILMED EXACTLY AS RECEIVED

This copy was produced from a microfiche copy of the original document. The quality of the copy is heavily dependent upon the quality of the original thesis submitted for microfilming. Every effort has been made to ensure the highest quality of reproduction possible.

PLEASE NOTE: Some pages may have indistinct print. Filmed as received.

Canadian Theses Division
Cataloguing Branch
National Library of Canada
Ottawa, Canada K1A 0N4

AVIS AUX USAGERS

LA THESE A ETE MICROFILMEE TELLE QUE NOUS L'AVONS RECUE

Cette copie a été faite à partir d'une microfiche du document original. La qualité de la copie dépend grandement de la qualité de la thèse soumise pour le microfimage. Nous avons tout fait pour assurer une qualité supérieure de reproduction.

NOTA BENE: La qualité d'impression de certaines pages peut laisser à désirer. Microfilmée telle que nous l'avons reçue.

Division des thèses canadiennes
Direction du catalogage
Bibliothèque nationale du Canada
Ottawa, Canada K1A 0N4

THE UNIVERSITY OF ALBERTA

SYSTEM DESIGN OF A PORTABLE RECEIVER-RECORDER FOR EXTREMELY-LOW-FREQUENCY (ELF) RADIO WAVES

by

GRAYDON WELLS ARKSEY

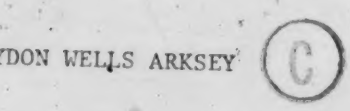

A THESIS

SUBMITTED TO THE FACULTY OF GRADUATE STUDIES AND RESEARCH

IN PARTIAL FULFILMENT OF THE REQUIREMENTS FOR THE DEGREE

OF MASTER OF SCIENCE

IN

ELECTRICAL ENGINEERING

DEPARTMENT OF ELECTRICAL ENGINEERING

EDMONTON, ALBERTA

SPRING, 1976

THE UNIVERSITY OF ALBERTA

RELEASE FORM

NAME OF AUTHOR ..... GRAYDON WELLS ARKSEY

TITLE OF THESIS ..... SYSTEM DESIGN OF A PORTABLE RECEIVER-RECORDER FOR EXTREMELY-LOW-FREQUENCY (ELF) RADIO WAVES

DEGREE FOR WHICH THESIS WAS PRESENTED ..... MASTER OF SCIENCE

YEAR THIS DEGREE GRANTED 1976

Permission is hereby granted to THE UNIVERSITY OF ALBERTA LIBRARY to reproduce single copies of this thesis and to lend or sell such copies for private, scholarly or scientific research purposes only.

The author reserves other publication rights, and neither the thesis nor extensive extracts from it may be printed or otherwise reproduced without the author's written permission.

(Signed) Graydon W. Arksey

PERMANENT ADDRESS:

8717 - 88 Ave.,

Edmonton,

Alberta. T6C 1L4

DATED Dec. 17, 1975

THE UNIVERSITY OF ALBERTA

FACULTY OF GRADUATE STUDIES AND RESEARCH

The undersigned certify that they have read, and recommend to the Faculty of Graduate Studies and Research, for acceptance, a thesis entitled "System Design of a Portable Receiver-Recorder for Extremely-Low-Frequency (ELF) Radio Waves" submitted by Graydon Wells Arksey in partial fulfilment of the requirements for the degree of Master of Science in Electrical Engineering.

C. R. James
Supervisor

Gordon Rostoker

[illegible]

R. E. Rink

Date Dec 15, 1975

DEDICATION

To my wife Edith, whose patience and tolerance remained limitless, and whose faith and encouragement was unfailing.

ABSTRACT

In the past decade there has been renewed scientific interest in Extremely-Low-Frequency (ELF) radio waves, in the range from 3 Hz to 3 kHz. A brief historical review is included of investigations related to ELF phenomena, and the spectrum characteristics are outlined with special reference to the Earth-ionosphere cavity "Schumann Resonances" and to transient disturbances related to global lightning activity. The current technology of measurement at ELF frequencies is briefly examined and the design criteria are discussed for a special field-portable receiver and magnetic-tape recording system for ELF signals. The detailed design equations and schematics of a tested prototype system are then presented, with special emphasis on the subsystems involved: a convenient charge-induction type of E-field sensor, a modified 60-Hz notch filter with a controlled transient response, a Pulse-Duration-Modulation (PDM) method for recording the ELF signals on magnetic tape, and a PDM demodulator system with a tape-speed-variation compensator, to recover the ELF signals from the magnetic tape. A number of examples are included of field-recorded natural ELF transients and background noise.

ACKNOWLEDGEMENTS

The author wishes to thank Dr. C.R. James and Dr. G.S. Christensen for many long-past conversations and for their continued encouragement which eventually led to the present research theme. The author also wishes to thank Dr. G.B. Walker for a number of constructive criticisms and for his unfailing encouragement.

The financial support provided by an Alberta Government Telephones Centennial Fellowship and by the Department of Electrical Engineering is gratefully acknowledged.

TABLE OF CONTENTS

CHAPTER		PAGE
1.	INTRODUCTION	1
	1.1 The Extremely-Low-Frequency (ELF) Spectrum	1
	1.1.1 Historical Background	1
	1.1.2 Spectrum Characteristics	4
	1.2 Existing ELF Measurement Techniques	11
	1.2.1 H-Field Sensors	11
	1.2.2 E-Field Sensors	12
2.	GENERAL DESIGN CONSIDERATIONS	15
	2.1 Portability	15
	2.2 System Frequency Response	17
	2.3 Transient Response	19
	2.4 Magnetic-Tape Recording	23
	2.4.1 Digital vs F.M. Recording	23
	2.4.2 Pulse-Duration Modulation	25
	2.4.3 Record-Playback of PDM Waveforms	28
	2.4.4 Compensation For Tape-Speed Variation	31
3.	DETAILED SYSTEM DESIGN	35
	3.1 The E-Field Sensor	36
	3.1.1 The Charge-Induction Plate	37
	3.1.2 The Sensor Equations	38
	3.1.3 The Electrometer-Amplifier Circuits	41
	3.1.4 Sensor Characteristics	46

3.2 Amplifiers and Filters 51

3.2.1 The Input and Summing Amplifiers 52

3.2.2 The 60-Hz Notch Filter 53

3.2.3 The High-Pass Filter 58

3.3 The Pulse-Duration Modulator 63

3.3.1 The Buffer-Limiter Amplifier 64

3.3.2 The 1-kHz Ramp Generator 66

3.3.3 The Voltage Comparator 69

3.3.4 Differentiation and Scaling 71

3.3.5 The Modulation Indicator 71

3.3.6 The PDM-Modulator Transfer Characteristic 73

3.3.7 The Battery Power Supply 75

3.4 The Pulse-Duration Demodulator 77

3.4.1 Input Amplifier and Zero-Crossing Detector 78

3.4.2 Measurement of Periods T_1 and T_2 80

3.4.3 Reset and Sample Pulses 85

3.4.4 Tape-Speed Compensation 87

3.4.5 Power Supply 92

3.5 Physical Design Details 94

3.6 The Magnetic-Tape Recorder 99

3.7 System Transfer Characteristics 102

4. CONCLUSION 107

4.1 Typical Field Records of ELF Signals 107

4.2 Comments 115

4.3 Summary 120

REFERENCES 122

APPENDIX A: THE MODIFIED TWIN-T NOTCH FILTER 128

A.1 The Passive Twin-T Notch Filter 128

A.2 The High-Q Twin-T Notch Filter 132

A.3 The 60-Hz Peaked Amplifier 136

A.4 The Modified 60-Hz Notch Filter 138

A.5 Phase Responses 143

A.6 Effectiveness and Limitations 145

APPENDIX B: THE "GYRATOR" NOTCH FILTER 147

B.1 Schematic and Transfer Function 147

B.2 Pole-Zero Locations 148

B.3 Practical Limitations 149

B.4 Advantages 150

LIST OF FIGURES

FIGURE		PAGE
1.1	ELF Attenuation vs Frequency	4
1.2	Narrow-Band ELF Noise Records	6
1.3	Wide-Band ELF Noise	7
1.4	Lightning-Flash Pulse Trains	8
1.5	A Schumann-Resonance Fundamental-Mode Transient	9
1.6	Short-Period ELF Power Spectra	10
2.1	Low-Frequency Cut-Off For Baseline Stability	17
2.2	Notch-Filter Removal of 60-Hz Interference	18
2.3	Typical Signal Artifacts Due to Filter Transients	20
2.4	High-Pass Filter Transients	21
2.5	Low-Pass Filter Impulse Response	22
2.6	Pulse-Duration-Modulation Waveforms	26
2.7	Basic PDM Waveforms During Record-Playback	28
2.8	Modified Record-Playback System Waveforms	30
3.1	System Block Diagrams	35
3.2	The E-Field Sensor Block Diagram	36
3.3	The Charge-Induction Plate System	37
3.4	Equivalent Circuits For The E-Field Sensor	38
3.5	The Electrometer Input Circuit	41
3.6	The Cable-Drive Amplifier	43
3.7	The E-Field Sensor Detailed Schematic	45
3.8	Sensor Calibration Arrangement	46
3.9	Sensor Calibration Waveforms	47

3.10	Equivalent-Input Noise Records	48
3.11	Thevenin-Equivalent Circuit For Input Noise	49
3.12	Amplifiers and Filters: Block Diagram	51
3.13	The Input and Summing Amplifiers	52
3.14	The Passive Twin-T RC Notch Filter	54
3.15	The Modified Notch Filter Block Diagram	55
3.16	Pulse Response of the Modified Notch Filter	57
3.17	The High-Pass Filter Modification	58
3.18	High-Pass Filter Pole-Zero Modifications	60
3.19	Frequency Response of the High-Pass Filter	61
3.20	Transient Response of the Modified High-Pass Filter	61
3.21	Detailed Schematic of the Amplifiers and Filters	62
3.22	Pulse-Duration Modulator Block Diagram	63
3.23	The Buffer-Limiter Amplifier	64
3.24	The 1-kHz Ramp Generator	66
3.25	The 1-kHz Ramp-Voltage Waveform	68
3.26	The Voltage Comparator	69
3.27	Pulse-Duration Modulator Waveforms	70
3.28	The Modulation-Level Indicator	72
3.29	The PDM-Modulator Transfer Characteristic	73
3.30	Detailed Schematic of the Pulse-Duration Modulator	74
3.31	Battery Power Supply Schematic	76
3.32	Demodulator Block Diagram	77
3.33	Input Amplifier and Zero-Crossing Detector	78
3.34	Zero-Crossing Detector Waveforms	80
3.35	Typical Period Measurement	81

3.36	Schematic: Pulse-Duration Demodulator	82
3.37	Square-Wave Response of the PDM System	84
3.38	Schematic: Generation of Reset and Sampling Pulses	86
3.39	Tape-Speed Compensator Waveforms	87
3.40	Schematic: Tape-Speed Compensator	88
3.41	Tape-Speed-Variation Compensation	91
3.42	Demodulator Power Supply	93
3.43	E-Field Sensor: Physical Design	95
3.44	Amplifier-Modulator: Panel Layout	96
3.45	Demodulator: Panel Layout	98
3.46	Signal Drop-Out During Tape Playback	100
3.47	System Frequency Response	102
3.48	Sampling Rates and Waveform Reconstruction	103
3.49	System Pulse Response	104
3.50	Input-Output Transfer Characteristics	105
4.1	Typical ELF Field Recording (Sample #1)	108
4.2	" " " " (Sample #2)	109
4.3	" " " " (Sample #3)	111
4.4	" " " " (Sample #4)	112
4.5	" " " " (Sample #5)	113
4.6	Filter Artifacts and a "Slow-Tail" Waveform	117
4.7	Typical ELF Atmospheric Noise (Evans and Griffith [73])	118
A.1	The Passive RC Twin-T Notch Filter	128
A.2	Poles and Zeros of the Passive Twin-T Filter	129
A.3	Impulse Response of the Passive Twin-T Filter	130
A.4	Pulse Response of the Passive Twin-T Filter	131

A.5	High-Q Active Twin-T Notch Filter	132
A.6	Root Locus for the High-Q Twin-T Notch Filter	133
A.7	The Impulse Response of a High-Q Twin-T Filter	134
A.8	The Pulse Response of a High-Q Twin-T Filter	135
A.9	The 60-Hz Peaked Amplifier	136
A.10	The Freqvency Response of the 60-Hz Amplifier	137
A.11	Pole-Zero Locations for the 60-Hz Peaked Amplifier	138
A.12	Block Diagram of the Modified Notch Filter	138
A.13	Pole-Zero Locations of the Modified Notch Filter	139
A.14	Frequency Response of the Modified Notch Filter	140
A.15	The Impulse Response of the Modified Notch Filter	141
A.16	The Pulse Response of the Modified Notch Filter	142
A.17	The Phase Responses of the Various Notch Filters	144
A.18	The Effectiveness of the Modified Notch Filter	145
A.19	Settling Time of the Modified Notch Filter	146
B.1	The "Gyrator" Notch Filter	147
B.2	Pole-Zero Locations for the Gyrator Notch Filter	149
B.3	Pulse Response of the Gyrator Notch Filter	151

CHAPTER 1

INTRODUCTION

1.1 THE EXTREMELY-LOW-FREQUENCY (ELF) SPECTRUM

1.1.1 HISTORICAL BACKGROUND

The electromagnetic spectrum above 100 kHz has been extensively exploited for many years. The commercial incentives have ensured adequate theoretical and experimental investigations of propagation phenomena and the continuing development of communications systems.

Below 100 kHz, the greatly increased size and cost of transmitting antennae, the decreasing radiation efficiency and the limited channel capacity have almost eliminated commercial interest. However, in the Very-Low-Frequency (VLF) range, nominally 3 kHz-30 kHz, very reliable long-range navigation and time-standard systems have been developed [1],[2], [3],[4]. The attenuation rate is less than 10 dB/1000km at VLF, and propagation is primarily via waveguide modes in the earth-ionosphere cavity, so that such systems are relatively immune to the normal vagaries related to ionospheric disturbances.

Below these frequencies again, at Extremely-Low-Frequencies (ELF), nominally 3 Hz-3 kHz, lies a portion of the electromagnetic spectrum which in recent years is being intensively re-examined.

Historically, about 1900 Nikola Tesla observed periodic excitation of tuned spark-gaps by receding lightning storms, and envisioned broadcast power based on the resonant pumping of the earth's charge at about 10 Hz [5]. His proposals for world-wide communications on the same

theme [6] were never developed, and after Marconi's successful trans-atlantic signal experiments in 1901, commercial exploitation concentrated on the higher frequencies. Barkhausen reported in 1919 [7] that sharp audio whistles were often noted in the high-gain amplifiers used to monitor enemy telephone circuits (via earth-return currents) and in 1930 he postulated that these whistles might be due to a long-path ionospheric dispersion of the audio-frequency components of far-distant lightning flashes [8].

Some theoretical justification for such a dispersion mechanism was offered in 1935 by Eckersley [9] but it was not until 1954 that Storey [10] offered the now accepted theory that ionospheric disturbances due to lightning flashes can find propagation paths far beyond the ionosphere along the Earth's magnetic-flux lines, so that inter-hemispheric transmissions and reflections are possible. Extensive investigation of these 'whistlers' has been made since that time because of their relation to the characteristics of the ionosphere and the magnetosphere [11].

The possibility of earth-ionosphere cavity resonances again became of interest in 1952, when Schumann offered a mathematical analysis of the subject [12],[13] and showed that for the ideal case of perfectly conducting earth-ionosphere boundaries, the eigenfrequencies would in fact be $f_n = 7.46\sqrt{n(n+1)}$ Hz (i.e. 10.6 Hz, 18.3 Hz, 25.9 Hz, . . .). The general background noise at ELF makes it difficult to directly observe these transiently excited resonances, although Schumann and Konig in 1954 [14] offered several recordings of damped oscillations at about 9 Hz showing field strengths in the order of 500 microvolts/metre.

It was not until 1960 that Balser and Wagner [15] secured averaged power spectra of ELF noise levels which clearly verified the existence of the Schumann resonances. The measured eigenfrequencies were at 7.8 Hz, 14.1 Hz, 20.3 Hz . . . and were sufficiently resolved so that estimates of the cavity Q could be made from the lowered frequencies of the mode peaks and their relative amplitudes. Subsequent verifications of these spectra have been made by other investigators using different methods, and military interest has led to much experimental and theoretical work on ELF propagation characteristics and ionospheric conductivity profiles. Extensive bibliographies of relevant ELF investigations have been included in papers by Galejs [16], Jones [17], Wait [18] and others.

In the past decade particularly, the major research into ELF phenomena has been funded by the U.S.Navy under "Project Sanguine". Even one-way communication with submerged submarines on a global scale is considered imperative and appears feasible; below 100 Hz attenuation is less than 1 dB/1000Km and sea-water penetration can be in the order of tens-of-metres. Unfortunately, transmitting antennae must cover literally thousands of square miles and require megawatts of input power for a few watts radiated. For one case cited, the radiation resistance for an ELF antenna 620 miles long was only about 0.01 ohms, so that less than 0.03% of the input power was radiated [19]. (These studies have been of such wide interest that a special issue of the IEEE Transactions on Communications, Vol. COM-22, No.4, April 1974, was devoted entirely to papers related to Project Sanguine.)

Because of the very high ground currents associated with such an ELF transmitting array, and their distribution over such an immense area, the potentially adverse environmental and biological effects were extensively investigated [20] but there remains a wide-spread controversy over system cost-effectiveness and environmental impact [21].

1.1.2 SPECTRUM CHARACTERISTICS

Since the ELF wavelengths are much greater than the height of the ionosphere, propagation between the earth-ionosphere sheet conductors is essentially in the TEM mode. However, the boundaries do have finite conductivities resulting in small horizontal E-field components, and these lead to wave leakages into the bounding media. In practice, this energy loss is a very small fraction of the propagating wave energy, so that the attenuation rate is very low.

Propagation characteristics at ELF over various path lengths and under a wide range of conditions have been measured by many investigators [22],[23],[24], giving the typical attenuation curves shown below . (The dip in the region of 10 kHz is due to a resonance absorption in the earth-ionosphere cavity.)

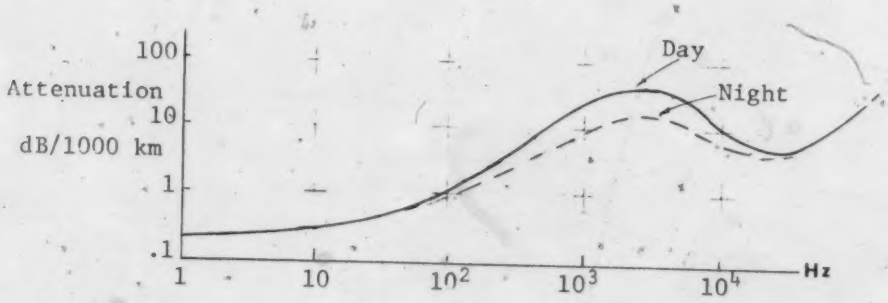

Figure 1.1 ELF Attenuation vs Frequency (from Maxwell [33])

The natural ELF noise spectrum consists primarily of random disturbances related to world-wide lightning activity. The wide spectrum of electromagnetic radiation generated by lightning strokes has been carefully investigated for many years [25],[26],[27],[28],[29] with various portions of the radiation spectrum attributed to specific flash processes. Most of the energy radiated in the 30 kHz - 100 kHz range is related to the very fast pre-discharge "leader" breakdown processes, and attenuation with distance is sufficient to limit the propagation to a few thousand kilometers. The main-discharge "return-stroke" radiation peaks at about 10 kHz, while slower decay currents between the multiple return strokes (described as "slow tails") radiate considerable energy below 1 kHz. At such extremely-low frequencies, the very-low attenuation rate permits world-wide propagation, and this constitutes the ELF "background noise" [30],[31],[32],[33].

The ELF noise below 1 kHz may actually be considered as being made up of two components:

1) A background level of impulse noise, with a Poisson repetition-rate distribution centred on a world-wide lightning-flash average of perhaps 100/sec, with a typical power spectral density of about 0.05 $(mV/m)^2/Hz$ [32].
2) A superimposed random noise, with peak-signal levels one or two orders of magnitude greater than the background (but with a much lower average repetition rate) generated by local or regional lightning storms.

The resultant ELF noise is typically as shown in Figure 1.2, which shows narrow-band (5 Hz-40 Hz) recordings of the horizontal magnetic-field

components, recorded simultaneously at widely-separated geographically-located points. The time correlations of many of the noise bursts are quite evident.

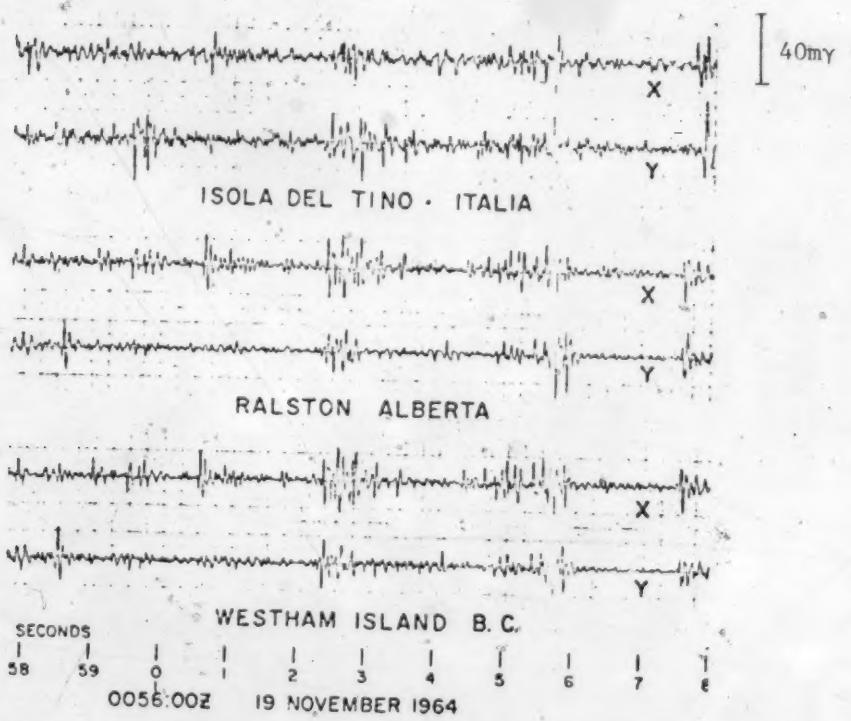

Fig. 1.2 Narrow Band ELF Noise Records (from Shand [34])
(Horizontal Magnetic-Field Components, 5 Hz-40 Hz)

These noise bursts are superpositions of resonant-mode disturbances, with only the first two modes being evident in these recordings. Diurnal variations in activity produce changes in the number of bursts which occur, but in general the average amplitudes remain essentially the same.

Wide-band receivers can of course display the impulsive nature of ELF signals with less modification by the receiving system:

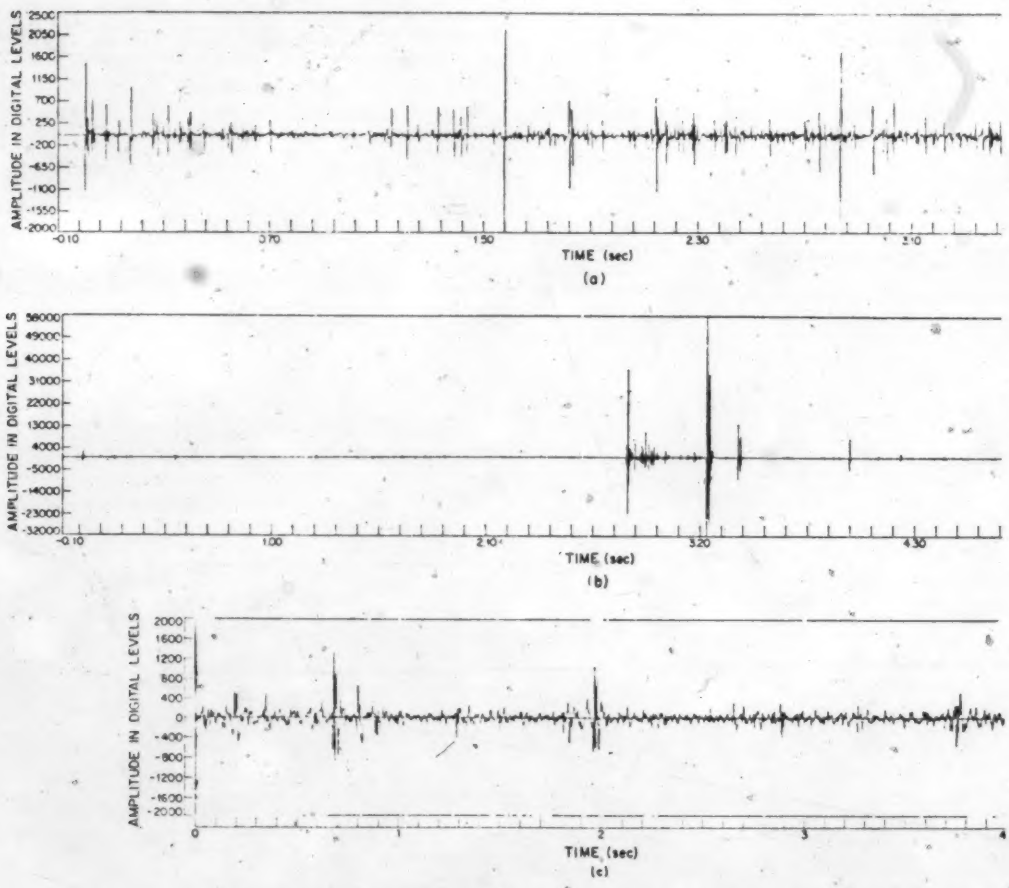

ELF wide-band (20-300-Hz) noise. (a) Saipan median level. (b) Saipan high level. (c) Norway.

Fig. 1.3 Wide-Band ELF Noise (from Bernstein [35])
(recording methods and scaling not specified)

Occasionally, high-speed chart recordings may display the sequence of pulses generated by the multiple strokes of a lightning flash:

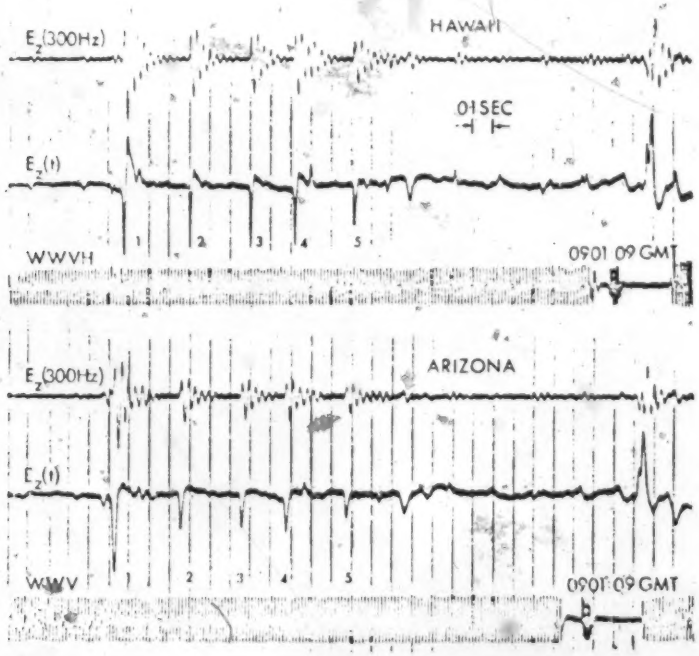

Examples of a pulse train of 'slow tail' ELF atmospherics recorded simultaneously at the Hawaii and Arizona Stations.

Figure 1.4 Lightning-Flash Pulse Trains (from Hughes [36])

Despite the continuous presence of such ELF activity, well-defined oscillations at Schumann-mode frequencies are difficult to observe. Typically, oscillatory disturbances retain their phase coherency for only a few cycles before the random superposition of another disturbance. An isolated mode oscillation such as that shown in Figure 1.5 is therefore a comparatively rare occurrence. Nevertheless, Shand [34] suggests that "excepting the sources of local lightning and man-made

interference, no measurable non-Schumann activity has been found in the frequency range 5 - 40 c.p.s.".

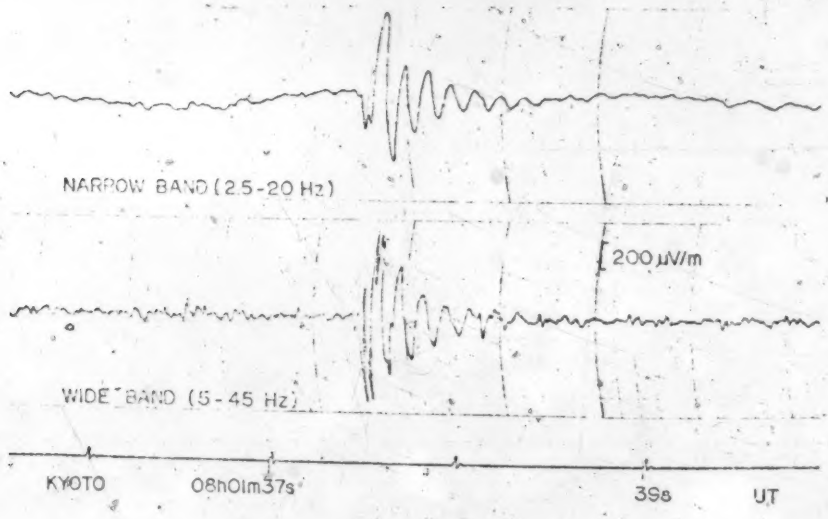

Figure 1.5 A Schumann-Resonance Fundamental-Mode Transient (from Ogawa et al. [37])

Due to the difficulty in measuring the Schumann resonances directly, most of the ionospheric research based on the changing characteristics of the resonances has relied on averages of power spectra integrated over many minutes. (Short-period spectral estimates, as shown in Figure 1.6, may show considerable fine structure and even peak splitting, but Rycroft [32] considers such detail to be spurious, due to statistical fluctuations in signal strength and finite record lengths.)

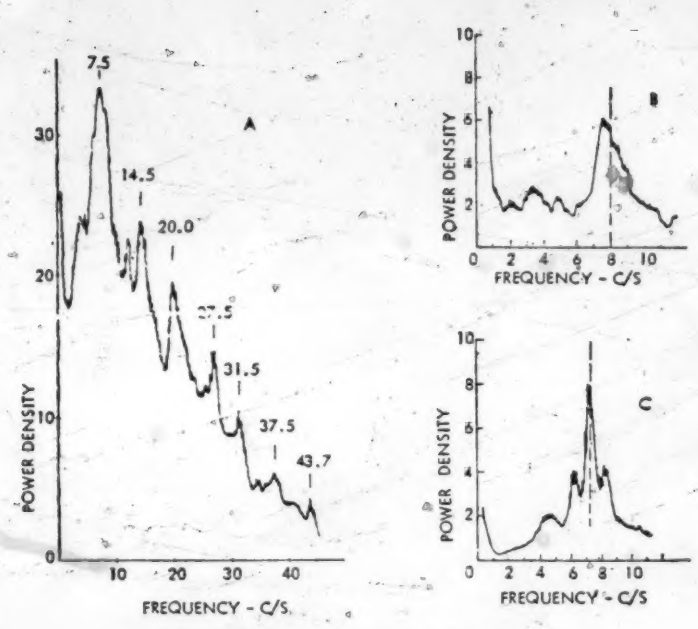

Short-period Spectrum Measurements

(a) Using a 30 sec. data block
(b) Using a 2 min. data block
(c) Using a 2 min. data block

Figure 1.6 Short-Period ELF Power Spectra
(from Larsen and Egeland [38])

1.2 EXISTING ELF MEASUREMENT TECHNIQUES

1.2.1 H-FIELD SENSORS

At ELF, induction coils are of course very inefficient due to the extremely low rate-of-change-of-flux of the magnetic-field components. For useful levels of induced signal voltages, such inductors therefore tend to be a problem because of their physical size, and from a stability standpoint.

The system used by the Pacific Naval Laboratory (Victoria, B.C.) is typical [39]: For the horizontal H-field components, electrostatically-shielded inductors are used, each with some 30,000 turns of #22 wire wound on a laminated mu-metal core some 72 inches long, with a cross-section of approximately 1.4 sq.in., and a nominal weight of about 94 pounds. Inductance is given as 600 Henries, and sensitivity is reported to be approximately 150 microvolts/gamma/Hz. These coils are rigidly supported and shielded from wind buffeting, since mechanical vibration of the coil in the earth's magnetic field can easily generate signal artifacts an order of magnitude (or more) greater than the ELF signals of interest.

For the still weaker traces of vertical H-field components, Barkhausen noise in the high-permeability core becomes unacceptable, so that very large air-core loops must be used (typically a buried shielded loop of 5 to 10 turns, with a loop diameter of 1000 ft. or more). Associated receivers and recording equipment are typically at least 500 ft. away from the sensing coils, with connections made via buried shielded cables.

For geophysical applications, where the ELF signals are integrated over 30 seconds or more, with a number of such readings averaged, considerably smaller coils can be used, but vibration in the Earth's magnetic field remains a problem [40],[41].

1.2.2 E-FIELD SENSORS

As noted previously, far-field propagation at ELF is via a TEM mode, so that above ground, only the vertical E-field component is normally measurable. Also, since the height of a practical E-field antenna will be a very small fraction of a wavelength at ELF, its effective source impedance will be very high and almost totally capacitive.

The original work on the Schumann resonances by Balser and Wagner at M.I.T. [15] made use of a 120-ft. metal tower as the vertical E-field sensor, while Rycroft at Cambridge, England [32] used a 190-metre horizontal wire suspended at an average height of 4.5 metres above the ground. Much shorter whip antennae have been used for special applications; Maxwell made use of an 8.85 metre vertical-whip antenna for ELF noise-field measurements [42] and Hughes used a 21-ft. vertical antenna for making field recordings of ELF lightning-flash waveforms [43].

The absolute calibration of such vertical-whip antennae can be rather difficult, since the "effective height" of the system is a function of antenna capacitance to ground, all mounting and amplifier input capacitances, ground-plane effectiveness, and system geometry. The method suggested by Clayton et al. [44] made use of a near-by reference

monopole to generate a calculated E-field, and a special Schering capacitance bridge to measure the effective whip-antenna capacitance.

A practical problem related to the vertical-whip antenna is the wind-induced swaving and vibration, which can generate spurious signals by modulating antenna capacitance. The low-frequency artifacts below 5 Hz can be minimized by a controlled low-frequency roll-off in the following amplifiers, but any vibration components above 5 Hz are directly in the frequency band of interest.

Two approaches have been used to avoid such motion artifacts; a tripod made up of three 6-ft. aluminum tubes (with the preamplifier in one leg) has been used by Jones and Kemp [45], and a ball antenna rigidly mounted on a supporting mast some 15 metres above a building roof has been used with success by Ogawa et al. in Japan [46].

Horizontal E-field components at ELF appear mainly as leakage fields in the conducting boundaries, and are related to the local earth conductivity. Such horizontal-field components are usually measured in terms of the voltage difference between widely-spaced ground electrodes. The voltage measured by such a grounded horizontal-wire antenna is related to the above-ground vertical E-field, to a good approximation, by the expression [47]

$$V = 7.45 \times 10^{-6} E_v \ell \sqrt{\frac{f}{\sigma}} \cos\phi$$

(e.g. for an E_v = 10mV/m, and antenna length (ℓ) of 100 m, a frequency (f) of 10 Hz, a soil conductivity (σ) of 10^{-3} mhos/m, and ϕ=0 for a wave propagating lengthwise along the antenna, V = 700 μvolts.)

While such signals appear to be of sufficient magnitude to be useful, they tend to be obscured by electrode noises and by artifacts traceable to ground vibration of long cables. As early as 1945, Dahlberg [48] used "porous-pot" ground electrodes a few hundred feet apart and measured signals in the 0.1 Hz to 10 Hz range with amplitudes of a few hundred microvolts, but because of the interfering noises they appeared to be of little use for geophysical studies.

More recently, in 1969, Slankis et al. [49],[50] have used the 8 Hz Schumann fundamental-mode signals for certain types of geophysical surveys, using only simple 3/8 in. diameter brass-rod electrodes with about 100-ft. spacing. They report integrated average telluric-field strengths of approximately 10 mV/Km in a sharply-tuned band at 8 Hz. (Integrated average-noise amplitudes for periods of 40 sec. to 60 sec. were used, and no attempt was made to observe characteristic ELF waveforms.)

For ELF communications with submarines, a towed horizontal-wire antenna in sea water has been used, with the exposed electrodes made of titanium, and with electrodes some 1000 ft. apart [51]. The high electrical conductivity of the sea water reduces the available signal voltages to a very low level, so that special signal encoding and extensive digital data-processing of the received signals is necessary for a data rate of even 1 bit/sec.

CHAPTER 2

GENERAL DESIGN CONSIDERATIONS

From the brief review offered in the preceding chapter, it is evident that most of the research into ELF phenomena has required the support of rather extensive instrumentation systems. Some of these systems required thousands of feet of buried cable and well-equipped instrumentation vans, while others were designed around permanent elaborate facilities and were part of an international monitoring network. Such systems are typically concerned with major and long-established research programs or have been developed under military research contracts. As a result, independent access to such facilities is normally impractical, and even partial duplication can be financially prohibitive.

Nevertheless, many ELF phenomena are of fundamental theoretical interest, so that some ready access to real-time field measurements is highly desirable for specialized studies as well as for general research and teaching purposes. These requirements have led to the development of a special ELF recording system, based on the following design considerations.

2.1 PORTABILITY

For convenience, the field equipment should be readily portable by a single person. This requirement is related to the fact that 60-Hz power-line interference lies within the ELF range of interest (5 Hz - 200 Hz) and despite the effectiveness of a 60-Hz notch filter,

it is often desirable to make field recordings in selected areas as remote as possible from power lines. Since such isolation may also be beyond immediate access to motor vehicles, equipment weight is an obvious concern. Such portability implies battery operation of amplifiers and recorders, which in any case frees the system from dependence on a vehicle-mounted 60-Hz auxiliary power unit, with its attendent cost, inconvenience and added electrical interference.

Some form of magnetic-tape recording is desirable, since this permits field recording in real time, with the ability to play back the data in the laboratory for direct examination or further data processing. From cost, battery operation and weight considerations, the domestic-market portable cassette-tape recorders offer an immediately attractive possibility, although the fixed 1 7/8 inch/second tape speed limits the frequency response, and tape-transport "wow-and-flutter" specifications are far below normal instrumentation-recorder standards.

Again from weight considerations, H-field sensors are not attractive, and because of cable weight and installation time, earth electrodes for the horizontal E-field components are also unattractive. Since the propagating TEM mode leaves the vertical component of the E-field with a more useful magnitude, it appears that an E-field sensor offers the most practical solution. Again for convenience, the commonly used elevated whip-antenna has been avoided, and a more readily portable "charge-induction-plate" sensor has been used. (The details of this type of sensor are fully covered in Section 3.1.)

2.2 SYSTEM FREQUENCY RESPONSE

It was noted in Section 1.1.2 that ELF signals down to at least 7 Hz are of interest because of the Schumann resonances. Below about 5 Hz, the system frequency response must usually be rapidly attenuated to prevent major baseline disturbances due to local space-charge phenomena, geomagnetic signals, and possible artifacts due to vibration of antennae and cables. Figure 2.1 shows the general problem:

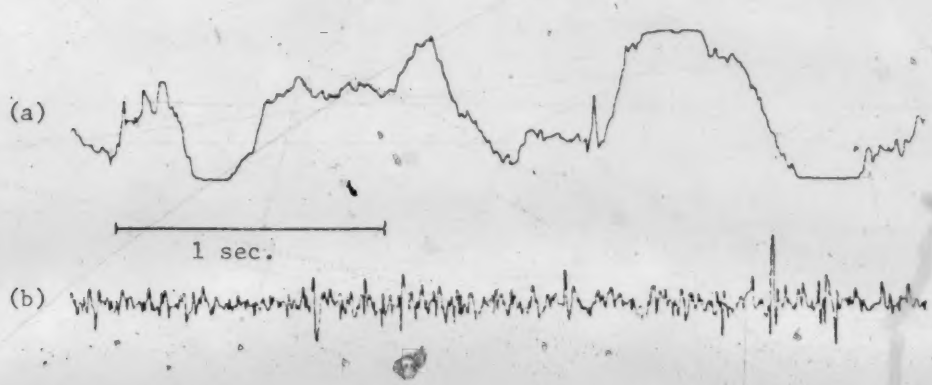

(a) With the lower cut-off frequency at 1 Hz.

(b) With the lower cut-off frequency at 8 Hz.

Fig. 2.1 Low-Frequency Cut-Off For Baseline Stability

Large low-frequency disturbances as shown in Fig. 2.1(a) may saturate the system amplifiers and lead to signal clipping. Careful choice of the low-frequency cut-off can produce the much more useful recording of Fig. 2.1(b).

In the "mid-band" region, interference from 60 Hz and its harmonics is the obvious concern, although a single high-Q notch filter

can usually provide an acceptable solution, (providing that sources such as 220V above-ground power lines are several hundred yards away). Some trace of 3rd-harmonic noise may then be evident, but in the present applications an added 180-Hz notch filter has not been considered necessary.

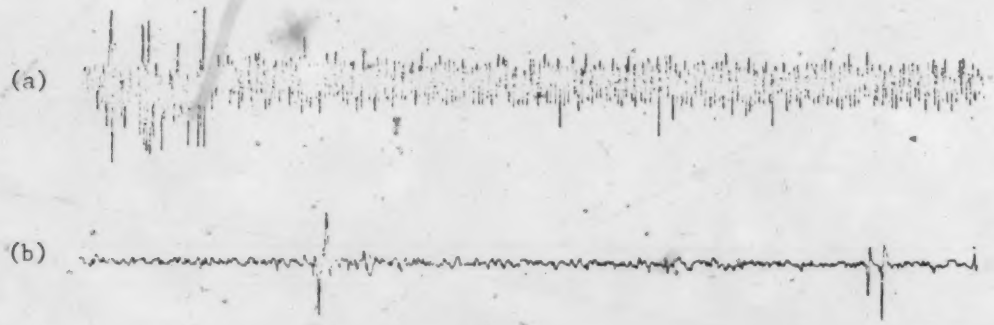

(a) With the 60-Hz notch filter OUT

(b) With the 60-Hz notch filter IN

Fig. 2.2 Notch-Filter Removal of 60-Hz Interference

Above 60 Hz, ELF signals of interest exist up to the nominal 3-kHz band limit, and of course these higher frequencies may be components of lower-frequency waveforms. In such cases the widest available band-pass is always desirable from a signal-resolution standpoint. However, to get magnetic-tape recordings of ELF signals below 50 Hz, a frequency-modulated carrier system is required, and this leads to practical limits on the upper modulation frequency.

As discussed more fully later (under Section 2.4) an F.M. carrier frequency of 1000 Hz has been used in the system, giving a

nominal 200-Hz upper frequency limit for recorded ELF signals. This can still provide considerable resolution of the details of a 10-Hz transient waveform, so that most of the phenomena related to the Schumann resonances are well within the system pass-band, if 5 Hz and 200 Hz are taken as the nominal frequency limits.

2.3 TRANSIENT RESPONSE

It was noted in Section 1.1.2 that ELF signals are predominantly transients generated by far-distant lightning flashes, with essentially a random-time distribution; steady-state sinusoidal inputs are the exception rather than the rule.

Unfortunately, for the faithful reproduction of transient signals, a limited system frequency response is the very thing that should be avoided. The limitations on the time-domain response, for various frequency-domain limitations, are well defined by the Laplace transforms, but some of the waveform distortions stemming from rather complicated transfer functions may not be intuitively obvious, and the generation of pass-band artifacts by certain types of input waveforms should be specifically noted.

Figure 2.3 displays some of the implications of a restricted low-frequency response and the artifacts generated by typical filters. Pulse inputs are shown in the top row (square waves at several frequencies), the second row shows the output after the signal has passed through a typical 2nd-order high-pass Butterworth filter with a 10-Hz lower-corner frequency, while the bottom row shows the further result of including a 60-Hz passive Twin-T notch filter in the signal path.

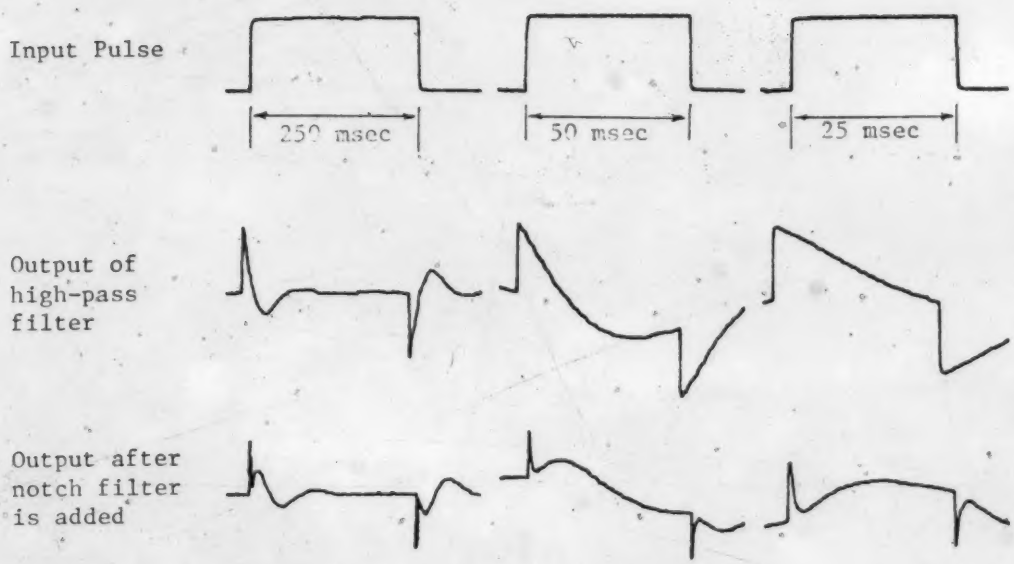

Fig. 2.3 Typical Signal Artifacts Due to Filter Transients

(see text for input-output conditions)

The above illustration of course, merely reminds one that low-frequency pulses have high-frequency edge components, that a high-pass filter will differentiate the edges of square waves, and that a Twin-T notch filter will compound the problem. In both cases, such circuits can generate signal "artifacts" which may seriously alter the waveforms of genuine pass-band signals.

We might note that the transient responses of standard filter types (Butterworth, Tchebycheff and Bessel) are well documented [52], [53] but in the communications field the steady-state frequency response is usually of more concern than such transient responses. For the

reception and recording of ELF signals, the reverse is true.

However, the willingness to tolerate a non-ideal frequency response does not really solve the problem. The attenuation at the low-frequency end of the pass-band (as noted in Section 2.2) must be greater than 20 dB/decade, which implies at least a 2nd-order high-pass filter. The most that can be done to minimize time-domain "ringing" is to ensure that only real poles exist in the filter transfer function. Figure 2.4 shows the limit of improvement by this route; waveform (b) shows the output of a 2nd-order Butterworth high-pass filter with a 10-Hz corner-frequency, and a 1-Hz square-wave input signal. The complex poles in the transfer function lead to excessive overshoot before baseline recovery. Waveform (c) is the output of a 2nd-order high-pass filter, with the same corner-frequency of 10 Hz but with only real poles in the transfer function. The reduction in signal overshoot is evident, but the major pass-band "artifacts" of course remain.

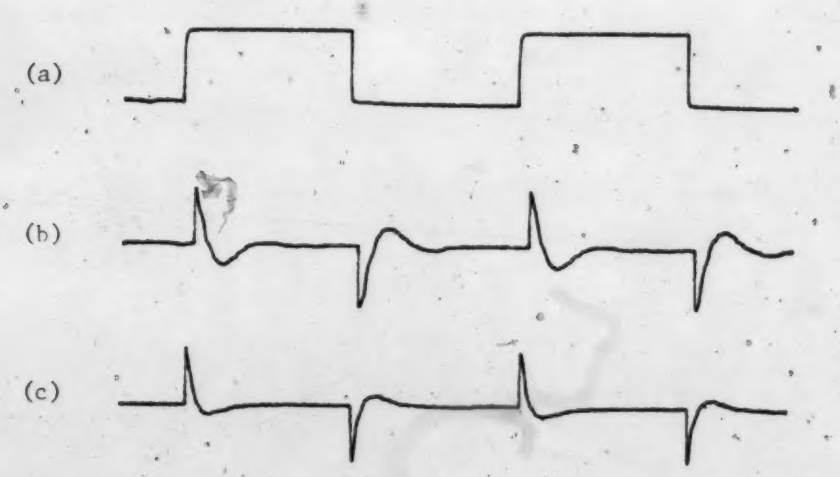

Fig 2.4 High-Pass Filter Transients
(see text for details)

The problem associated with the upper-frequency limit relates to the system impulse response. For input pulses with a period shorter than the filter time constant, the output will simply be some approximation to the system impulse response, regardless of the fact that the pulse "1/T frequency" may be far beyond the pass-band.

Again, complex poles in the transfer function controlling the high-frequency roll-off can lead to overshoot and ringing, while maintaining only real poles will minimize the problem. Figure 2.5 illustrates these points; waveform (b) shows the signal overshoot and ringing which constitutes the impulse response of a 2nd-order low-pass Butterworth filter, with a 500-Hz upper corner-frequency. Waveform (c) shows the improvement when a 2nd-order filter, with the same cut-off frequency but only real poles, handles the same input pulse.

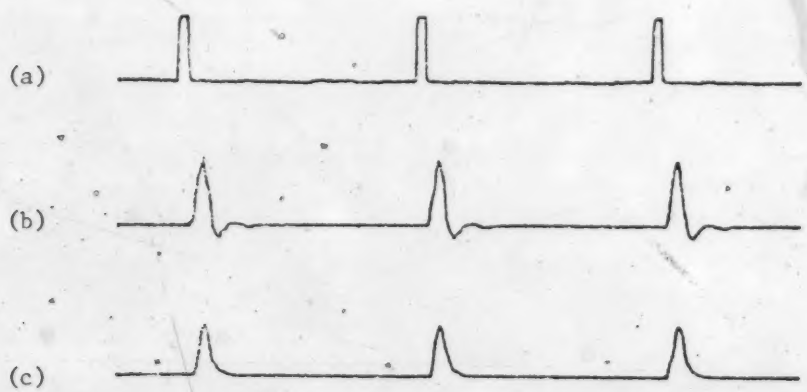

Fig. 2.5 Low-Pass Filter Impulse Response
(see text for details)

The transients introduced by the typical Twin-T notch filter can in fact be avoided. This is possible because the 60-Hz interference normally is steady state, and the notch filter steady-state response can be isolated from signal transients. Appendix A shows, in some detail, how a Twin-T notch filter can be modified to give a "clean" transient response, while Appendix B offers almost as effective a solution using a so-called "gyrator" notch filter.

From the foregoing comments, it is apparent that the general design philosophy must be to minimize system transients by using the lowest acceptable attenuation rates at the frequency-pass-band limits (although total avoidance of complex poles is not really practical) and by using a transient-free 60-Hz notch-filter system.

2.4 MAGNETIC-TAPE RECORDING

2.4.1 DIGITAL vs F.M. RECORDING

The decision to use a cassette-type portable magnetic-tape recorder for field recording of the ELF signals places immediate restrictions on the choice of recording methods and formats.

The magnetic-tape cassettes conform to international standards derived from the original Philips Corp. designs [54] which established the tape speed at 1 7/8 inches/sec.,(4.76 cm/sec). This provides an acceptable compromise between recording time and frequency response for domestic use, but such a low tape speed is an unfortunate restriction from a data-recording standpoint.

Direct analog recording of ELF signals down to 5 Hz is not

feasible with a magnetic-tape recorder because of the low-frequency limitations of the play-back head. The signal output level of a magnetic-tape "reproduce" head is proportional to the rate-of-change of the magnetic flux cutting the head windings, and this of course is a function of the frequency of the recorded signal, as well as the design of the head gap, core permeability and the number of turns of the coil winding [55]. The result is that the generated output voltage drops off with decreasing frequency at 20 dB/decade. With the available maximum tape retentivity of about 1000 gauss and the best available head design, the lowest useful recording and playback frequency is about 100 Hz, and at 10 Hz the recorded signal cannot usually be recovered from the background noise due to the magnetic-oxide and surface imperfections.

The use of digital-recording techniques is also ruled out by the 1 7/8 inch/sec tape speed, in this case due to high-frequency limitations. For digital sampling and a somewhat crude reproduction of a sine wave, as few as 5 samples/cycle may be tolerated, but even at such a low sampling rate, for a signal at 200 Hz and for an amplitude resolution of say 0.5% (8 binary bits per sample) this demands a serial recording "bit rate" of:

$$\text{Bit Rate} = 200 \times 5 \times 8 = 8{,}000 \text{ bits/sec.}$$

In recording digital data on magnetic tape, initially-sharp transitions between magnetization directions (corresponding to a binary 1 or 0) are blurred by self-demagnetization forces, so that the final transition is spread along a finite length of tape. As a result, the number of flux reversals per inch of tape which can be reliably recovered is not just a matter of reproduce-head gap resol-

ution but of tape bit-density capability as well. The theoretical limit for the highest-quality magnetic oxides is usually quoted as about 5,000 flux reversals per inch [56] but for the data-recovery reliability required by a digital system a recording density of about 1,000 bits/inch is a practical limit. At this bit density, a tape speed of 8 inches/sec. would be required for a serial data rate of 8,000 bits/second. Since the cassette tape-transport speed is a fixed 1 7/8 inch/sec. we would in fact be restricted to an upper signal frequency of:

$$f_{max} = \frac{1.875 \times 1000}{5 \times 8} = 46 \text{ Hz}$$

which is about one order of magnitude too low to be acceptable.

The above limitations therefore restrict the choice of recording methods to some form of frequency modulation. An F.M. recording technique permits the selection of an audio carrier frequency well within the record/reproduce range of the recorder to be used. The permissible modulation ranges from D.C. to perhaps 20% of the carrier centre frequency [57]. Such techniques have been widely used for many years, and linear voltage-to-frequency converters are available commercially or can be designed to specification using discrete components.

2.4.2 PULSE-DURATION MODULATION (PDM)

The direct use of a frequency-modulated sinusoidal carrier is in this case undesirable, since during playback spurious frequency shifts due to tape-transport speed variations can be generated, and

such frequency shifts cannot be distinguished from those due to the genuine modulation. Tape-transport speed variations of from 1% - 3% are typical in portable magnetic-tape recorders (due to the D.C. motor-speed control limitations and fluctuations in winding tension in the tape cassette) and would produce equivalent errors in the demodulated analog signal.

However, one type of pulse-width modulation offers a built-in monitor for such speed variations: the fixed-repetition-rate Pulse-Duration Modulation (PDM) with "trailing-edge" modulation [58]. This modulation method involves the following pulse waveforms:

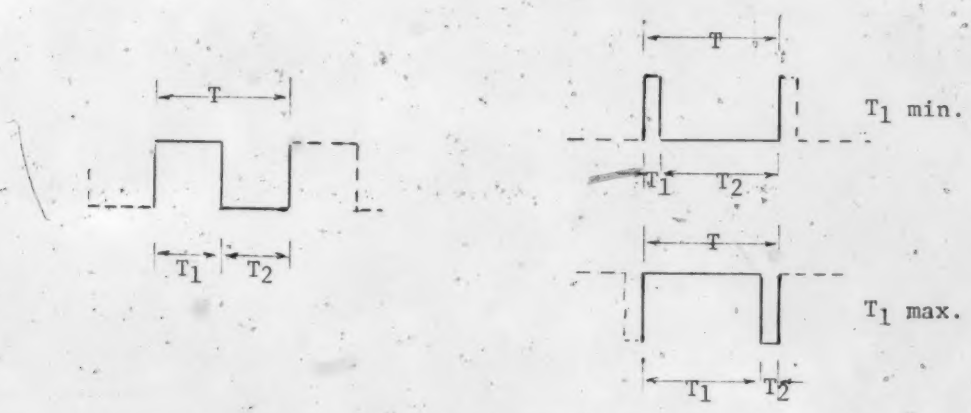

(a) Zero Modulation (b) Maximum Modulation

Fig. 2.6 Pulse-Duration-Modulation Waveforms

The "zero-modulation" waveform is shown in Fig. 2.6(a) and has a 50% duty cycle ($T_1 = T_2$). The repetition rate is held constant, while the relative durations of T_1 and T_2 are modulated as shown in Fig. 2.6(b),

i.e. $(T_1 + T_2) = T$ = a constant

and modulation of the transition time of the trailing edge of T_1 must be limited to prevent pulse "overlap", that is, T_1 or T_2 must never be reduced to zero duration, or modulation information will disappear, the basic repetition rate will be lost, and the demodulator output will be meaningless.

It was noted in Section 2.4.1 that for standard magnetic tape there is a theoretical resolution limit of about 5,000 flux reversals per inch. At a tape speed of 1 7/8 inches/sec. this implies a minimum pulse width of about 100 microseconds. With a portable tape-recorder upper-frequency limit of about 8 kHz, a reliable resolution of 150 microseconds with an uncertainty of a few microseconds appears to be a practical limit.

Recovery of the analog signal from the PDM waveform is effected by a demodulator whose output tracks the succeeding variations of ($T_1 - T_2$) with the durations of T_1 and T_2 measured each "cycle" by some form of sample-and-hold integrator. If a 5-sample approximation to a sine wave is again assumed to be "acceptable", then a 200 Hz maximum-modulation frequency requires 1,000 samples/second, which implies a PDM repetition rate of 1,000 pulses/second. This therefore defines the pulse widths of the PDM waveform as:

$$T = 1 \text{ millisecond}$$

$$T_1 = 500 \text{ μsec} \pm 350 \text{ μsec.}$$

$$= (150 \text{ μsec min., } 850 \text{ μsec max.})$$

$$T_2 = T - T_1$$

2.4.3 RECORD-PLAYBACK OF PDM WAVEFORMS

Although the pulse-duration modulation offers useful properties, the "transmission" medium in this case is a magnetic tape, and satisfactory recording and recovery of the PDM waveform remains a problem.

The modulation information of the PDM signal resides in the transition time of the trailing edge of T_1 relative to its leading edge. As already noted, a square-wave signal recorded on tape as an initially abrupt change in the direction of magnetization, does not retain its "squareness".

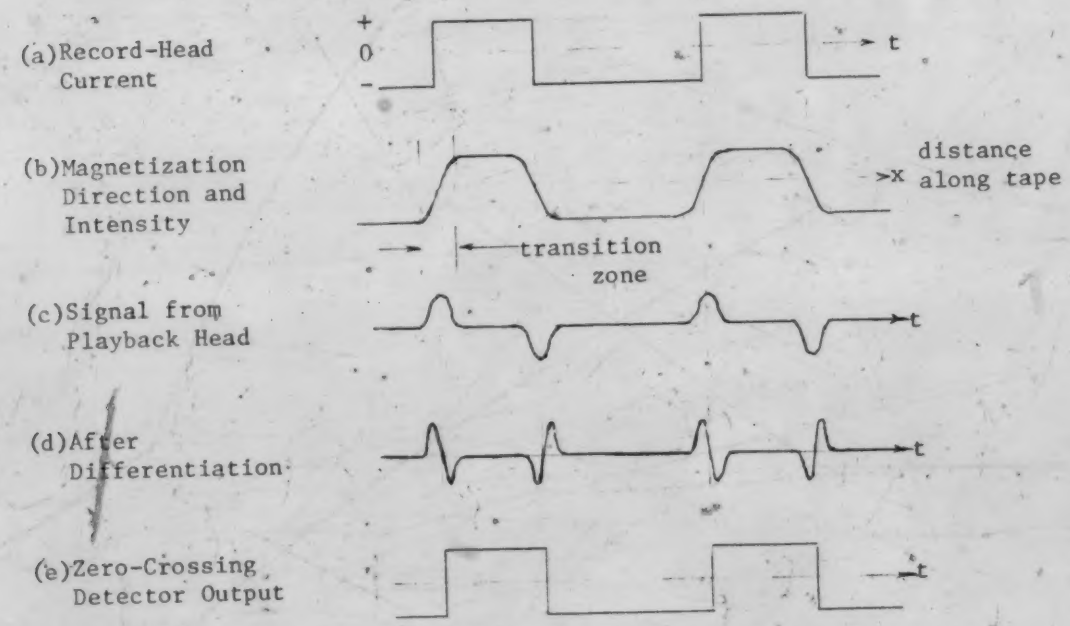

Fig. 2.7. Basic PDM Waveforms During Record-Playback

Figure 2.7(b) is a representation of how the linear distribution of tape magnetization is modified by the self-demagnetization forces, so that the original abrupt change imprinted by the record head reverts to a relatively-wide "transition zone", whose width is a function of the magnetic-oxide properties and its coating thickness.

The reproduce-head output voltage during tape playback is shown in Fig. 2.7(c), and this signal can then be differentiated to recover a signal whose "zero-crossing" points should represent the abrupt time transitions of the original recorded waveform. In theory, the zero-crossing detector could therefore be used to generate a replica of the original PDM waveform. In practice, this approach tends to result in a poor signal-to-noise ratio, since small amplitude variations of the playback signal and associated tape background noises are greatly accentuated by the differentiation, and a zero-crossing "time-jitter" results. In addition, for pulse periods much longer than the transition zones, the head output voltage has multiple regions of zero slope, which leads to ambiguous output signals from the differentiator, hence false zero-crossings and output-waveform errors. (The addition of hysteresis and some form of voltage-level logic can reduce these false zero crossings, but such methods tend to have critically-narrow tolerance margins for changing circuit parameters.)

A much more tolerant system results if the PDM signal is differentiated <u>before</u> it is recorded. As indicated in Figure 2.8(c), the tape-magnetization pattern will then have a continuously-decreasing intensity between each transition zone. The playback-head output voltage will

display a zero crossing which is actually related to the end of each transition zone, but since no added differentiation is involved, this zero crossing will be relatively stable in the presence of associated noise. In addition, the slowly-changing intensity of magnetization between transition zones provides a residual non-zero output signal of sufficient amplitude so that false zero crossings are avoided.

This method of recording and playback of the PDM waveform has therefore been used in the prototype system being described.

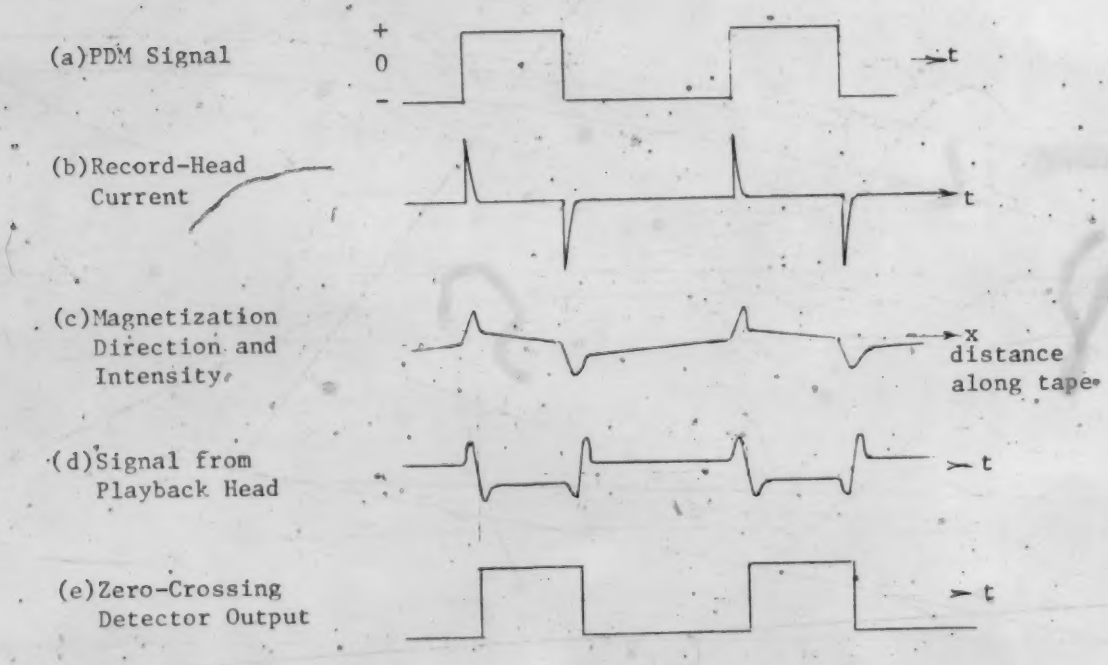

Fig. 2.8 Modified Record-Playback System Waveforms

2.4.4 COMPENSATION FOR TAPE-SPEED VARIATIONS

The demodulation of a PDM signal involves the generation of an output voltage of the form:

$$V_o = K(T_1 - T_2)$$

(with T_1 and T_2 as in Fig. 2.6) and involves a direct time-measurement demodulation. The signal-to-noise ratio of such a system will be related almost entirely to the "time-jitter" of the zero crossings of the recovered PDM waveform. In practice, the separation of the modulation from the PDM-carrier waveform is best achieved by a so-called "integrate-and-dump" system [59] which is one form of a synchronous detector.

Although the period T_1 is normally varied in response to modulation, it will also vary due to changing tape speed. However, any variation in the total period T must be due only to a tape-speed change. Therefore, if the output signal is normalized by a factor proportional to the total-period T, it is theoretically possible to make the output essentially immune to tape-speed variations.

i.e. if $V_o = \frac{K}{T}(T_1 - T_2)$

then a fractional change of tape speed will modify the time scale by a factor (α), so that

$$V_o = \frac{K}{\alpha T}(\alpha T_1 - \alpha T_2)$$

which remains $$= \frac{K}{T}(T_1 - T_2)$$

and hence no change in output voltage occurs. (The proviso of course is that the change in tape speed be slow relative to the sampling rate,

so that the same scale factor (α) will apply to T_1, T_2 and T. Since "wow-and-flutter" speed variations are usually at less than 10 Hz and since the sampling rate is the 1000/sec. pulse-repetition rate of the PDM carrier, the factor (α) will in fact be essentially constant.)

2.5 SYSTEM SENSITIVITY AND GAIN REQUIREMENTS

In a system design, it is of course necessary to have an estimate of the required input sensitivity. In the case of ELF signals this can be calculated from published data on the measured spectral density of ELF noise. From a number of sources [60],[61],[62] the average spectral density in the 5-Hz to 200-Hz range can be taken as about $0.05(mV/m)^2/Hz$ for the vertical E-field component, but peak or rms values are not simply related to the average values derived from spectral density data (due to the impulsive character of ELF signals). However, for design purposes the expected peak values can be taken as perhaps twice the "average" value.

For a nominal 200-Hz bandwidth, the peak values of background noise can therefore be estimated as

$$E_{(peak)} \approx 2\sqrt{\frac{0.05(mV/m)^2}{Hz} \times 200Hz} \approx 6\ mV/m$$

with regional lightning storms producing peak signals one or two orders of magnitude higher. Using these guidelines, the system requires a "full-scale" sensitivity of about 10 mV/m on the most sensitive range, and gain switching to allow for an attenuation of approximately 40 dB.

The amplifier-gain requirement is somewhat more difficult to

define, since it is dependent on the E-field sensor transfer characteristic, and on sensitivity of the pulse-duration-modulator circuit. The general requirement is simply that an ELF disturbance of 10 mV/m, whose frequency is within the pass band, must provide maximum modulation of the PDM-carrier waveform.

The required amplitude of output signal from the PDM modulator to the tape recorder is typically 1 Volt (peak) into the "AUX" input. However, the fact that the signal is in this case a differentiated pulse must be recognized. The automatic-gain-control circuits used in many portable recorders are designed to hold a proper recording level despite wide variations of the input-signal level, and are of course keyed to the average values of typical voice and music waveforms. With the low duty-cycle of voltage spikes generated by differentiating the PDM square waves, the automatic-level-control setting of the signal-amplifier gain can be excessive, leading to waveform clipping and an improper recording level. However, if the recorder is also equipped with a recording-level meter and a manual level control, satisfactory recording is readily accomplished by setting the indicated recording level about 10 dB below the level recommended for speech and music.

On playback, a signal from the "EARPHONE" jack of the magnetic-tape recorder is used to drive the PDM demodulator. The output amplitude is adjustable by the recorder "VOLUME" control, with a maximum of perhaps 3 Volts (peak) across a typical 10-ohm earphone load. (Note that in some recorder designs, a 10 to 50 ohm resistor may have to be provided as a nominal substitute load if the signal is taken from the earphone jack for use by high-input-resistance devices. Otherwise,

internal negative-feedback circuits may display instability, so that recorder-amplifier oscillations may occur.)

The demodulator output voltage is a matter of choice and design. In the system being described, the output has been scaled to ±5.0 volts full scale, for compatability with an available analog/digital computer input.

CHAPTER 3

DETAILED SYSTEM DESIGN

The general system configuration is shown below, in "block-diagram" form:

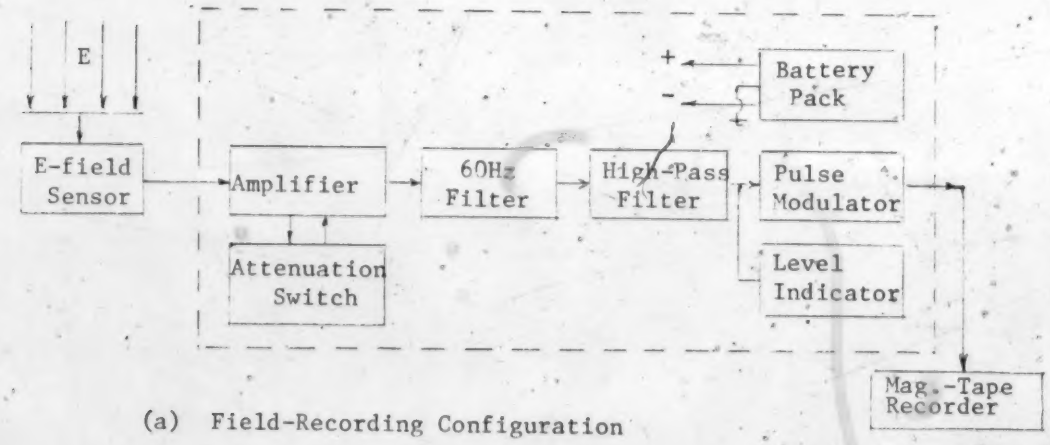

(a) Field-Recording Configuration

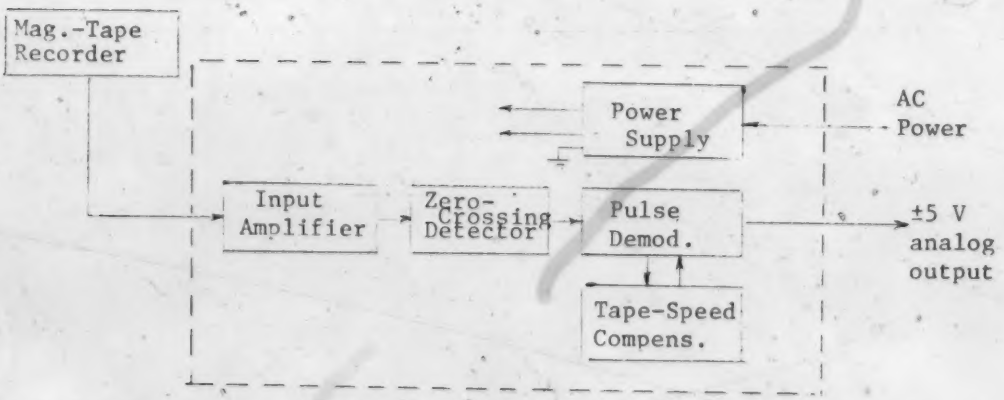

(b) Playback Configuration

Figure 3.1 System Block Diagram

The detailed design equations, circuit schematics and notes on circuit operation are included in the following sections. The discussion can be conveniently subdivided into four functional sections: the E-field sensor assembly, the signal amplifiers and filters, the PDM modulator, and the PDM demodulator.

It will be noted that recordings of system waveforms have been extensively used for illustrations. The ease with which such recordings could be made, with almost any desired time scaling, resulted from the fortunate availability of a Hewlett-Packard Model 5480A Signal Analyzer. This unit provides analog/digital sampling, with data memory-storage and playback facilities. A "recording" can be made consisting of 1,000 sequential samples at a choice of sampling rates from 2 samples/second to 100,000 samples/second, and "played back" at a much lower rate via digital/analog output facilities to a standard X-Y recorder.

3.1 THE E-FIELD SENSOR

For system portability, the usual E-field sensors mentioned in Section 1.2.2 are considered rather inconvenient. The following sub-sections cover the design of a "charge-induction" type of sensor, which appears to be a useful alternative to the whip antenna for measuring the vertical E-field component of ELF signals.

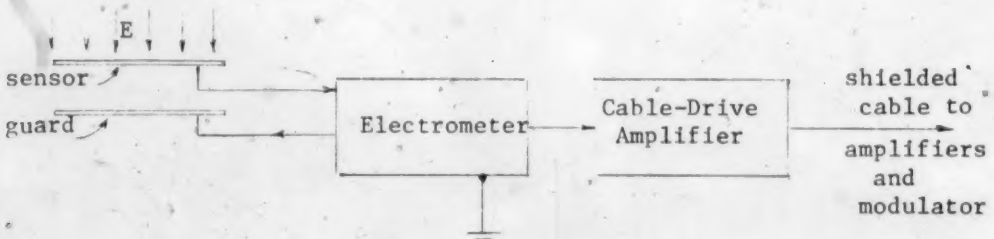

Fig. 3.2 The E-Field Sensor Block Diagram

3.1.1 THE CHARGE-INDUCTION PLATE

One of the simplest methods of measuring the vertical E-field at the Earth's surface is a "charge-induction-plate" method, which is basically the system used by Wilson in 1916 [63] to measure the Earth's surface-charge density.

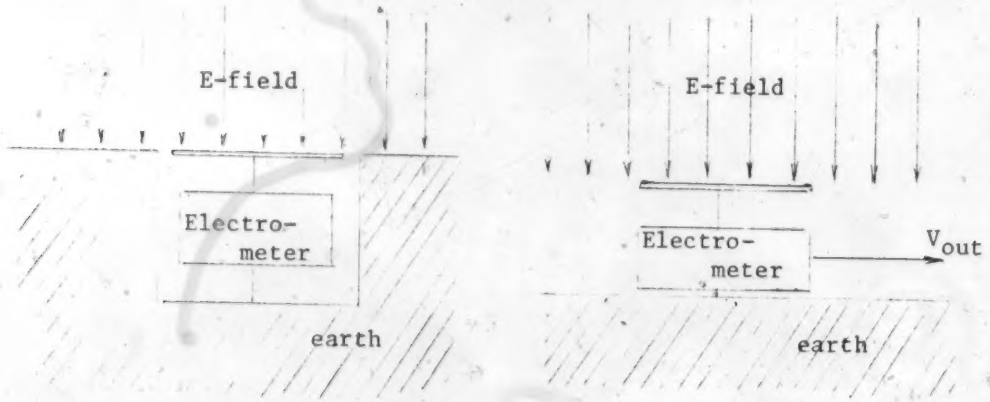

(a) The Wilson "Charge-Plate" (b) The Portable E-Field Sensor

Figure 3.3 The Charge-Induction Plate System

Wilson took great care to keep the charge plate flush with the Earth's surface, and used a null-balance method to prevent E-field distortion (since he was concerned with absolute charge-density measurements). For a portable system this is impractical, but as in Fig. 3.3(b) above, a shallow above-ground assembly has been used. This leads of course to some edge distortion of the incident E-field, but since the system can be calibrated in known fields, this distortion factor is of little concern. Note that the "guard" electrode is in this case used to reduce the effective mounting capacitance, not to eliminate electrode edge effects. (See Section 3.5 for the physical design details.)

3.1.2 THE SENSOR EQUATIONS

The signal voltage V_{in} available from the charge-induction plate for any incident E-field can be calculated from basic charge-capacity-voltage relationships.

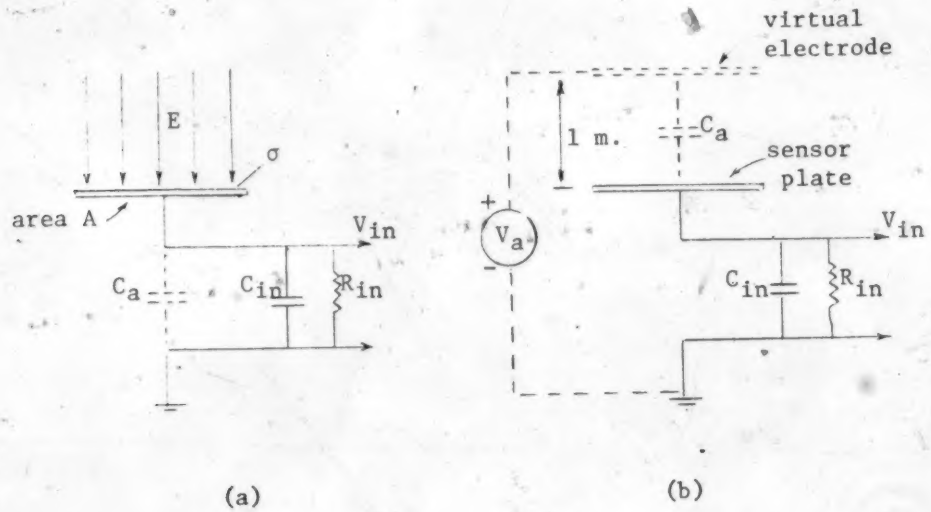

Figure 3.4 Equivalent Circuits For The E-Field Sensor

In Fig. 3.4(a) the normal incident E-field induces a surface-charge density of

$$\sigma = D = \varepsilon_o E$$

and for a plate area A, the total induced charge is simply

$$Q = \sigma A = \varepsilon_o EA$$

If C_a is the free-space capacity of the exposed plate, and C_{in} is the lumped capacity of the plate mounting, wiring, and electrometer input, then

$$V_{in} = \frac{Q}{C} = \frac{\varepsilon_o EA}{(C_a + C_{in})}$$

but the capacitance $C_a = \varepsilon_o A$, so that

$$V_{in} = E \cdot \frac{C_a}{C_a + C_{in}}$$

This instantaneous voltage will decay exponentially as the induced charge leaks off through associated leakage resistances represented in Fig. 3.4(b) by R_{in}.

For system analysis, the equivalent circuit of Fig. 3.4(b) is convenient. The incident vertical E-field can be viewed as the result of a voltage source V_a applied to a theoretical sheet-electrode located one metre above the sensor plate. The capacitance C_a remains valid and can be calculated directly as a parallel-plate condenser, and any E-field can be defined directly in volts/metre.

Using "standard" Laplace notation, the voltage transfer function can be written as

$$H(s) = \frac{V_{in}(s)}{V_a(s)} = \left(\frac{C_a}{C_a + C_{in}}\right)\left[\frac{s}{s + \frac{1}{R_{in}(C_a + C_{in})}}\right]$$

The charge-plate system is therefore a 1st-order high-pass filter, with a lower corner-frequency of

$$\omega_o = \frac{1}{R_{in}(C_a + C_{in})}$$

and for pass-band frequencies (for $\omega >> \omega_o$), the electrode system will appear as a simple capacitive voltage divider with

$$\frac{V_{in}}{V_a} = \left(\frac{C_a}{C_a + C_{in}}\right)$$

For the 10 inch by 6 inch charge-induction plate used, the value of C_a is approximately 0.33 picofarads, and the total input

capacitance of a typical electrometer circuit can be taken as approximately 10 picofarads. Therefore, for an E-field change of say 10 mV/m, the voltage signal available at the electrometer input will be

$$\Delta V_{in} = (\Delta V_a)\left(\frac{C_a}{C_a + C_{in}}\right) = (10\ \text{mV})\left(\frac{0.33}{10.33}\right) = 0.33\ \text{mV}.$$

(Greater sensitivity could of course be achieved by increasing the dimensions of the charge-induction plate, which would increase the value of C_a.)

If desired, the amplitude-response versus frequency can be calculated from

$$|H(j\omega)| = G(\omega) = \left(\frac{C_a}{C_a + C_{in}}\right)\left[\frac{1}{\sqrt{1 + (\omega_o/\omega)^2}}\right]$$

where $\omega_o = \dfrac{1}{R_{in}(C_a + C_{in})}$.

The transient response to a step input (such as the leading or trailing edge of a square wave) can be given in the time domain as

$$v(t) = \left(\frac{C_a}{C_a + C_{in}}\right) \exp[-t/R_{in}(C_a + C_{in})]$$

For a lower corner-frequency of say 1 Hz it is evident that R_{in} must be a very-high resistance, i.e.,

$$R_{in} = \frac{1}{\omega_o(C_a + C_{in})} = \frac{1}{(2\pi)(1)(10^{-11})} = 1.6 \times 10^{10}\ \text{ohms}$$

which is greater than 10,000 megohms, but is a realizable input resistance provided by many alternative electrometer circuits.

3.1.3 THE ELECTROMETER-AMPLIFIER CIRCUITS

As noted in Section 3.1.2, for the desired low-frequency response and the necessary voltage sensitivity of the E-field sensor, the following input conditions appear necessary:

$$(C_a + C_{in}) < 10 \text{ picofarad}$$

$$C_{in} \quad \text{minimize}$$

$$R_{in} > 10^{10} \text{ ohms}$$

The simplified schematic of the electrometer-input circuit is shown in Figure 3.5.

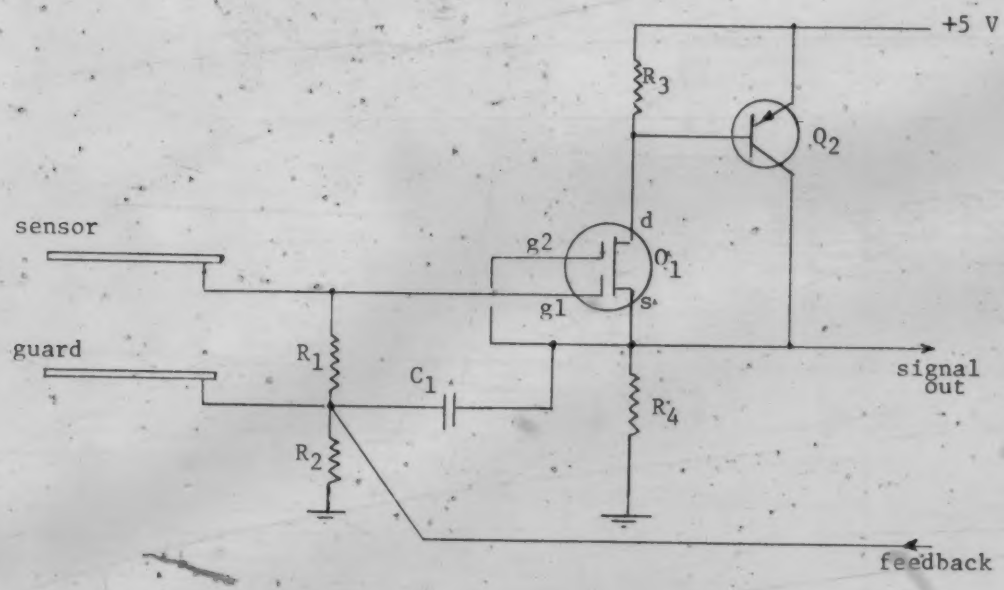

Figure 3.5 The Electrometer-Input Circuit

This configuration is essentially a unity-gain source follower, with a "bootstrapped" input resistor R_1. Since large electrostatic voltages can be encountered during handling and use of this "charge-induction"

type of sensor, gate protection of the input FET (field-effect transistor) is imperative. Input capacitance must be as low as possible, and the 1/f noise figure below 10 Hz is of concern. These considerations and component availability have led to a number of design compromises, although the electrometer performance remains adequate.

Transistor Q_1 is a dual-gate MOSFET (an RCA 40822, which has integral gate-protection diodes). This device retains a useful transconductance at the very-low drain current (100μA) used to minimize its noise figure, and the second gate provides isolation between the input gate and the drain, to reduce the effective input capacitance. Transistor Q_2 is a low-noise type 2N5087 PNP device, also operated at a low collector current (100μA) for reduced 1/f noise.

For such a circuit, the voltage gain is approximately

$$A_v = \frac{g_{m1} h_{fe2} R_4}{1 + g_{m1} h_{fe2} R_4}$$

and is therefore maximum for the maximum $g_{m1}R_4$ product. For the type 40822 MOSFET with zero voltage between gate 2 and the source, and with V_{ds} = 3 V, the best compromise between noise and gain appeared to be with I_d = 100μA and R_4 = 5K ohms. Under these conditions, $g_{m1} \approx 10^{-4}$mhos and with I_c = 100μA the 2N5087 has an h_{fe} = 100, so that actual gain of the "unity-gain" amplifier is approximately A_v = 0.98.

The R_2C_1 time constant of the "bootstrap" coupling network is kept greater than 1 second to ensure its low-frequency effectiveness to at least one decade below the nominal 5 Hz low-frequency cut-off of the over-all system response.

The input resistor R_1 is a Victoreen Corp., "Hi-Meg" electrometer resistor of 10^{10} ohms. With the "bootstrapping" arrangement, the effective input resistance will be

$$R_{eff} = \frac{R_{real}}{1 - A_v} = \frac{10^{10}}{1 - .98} = 5 \times 10^{11} \text{ ohms}$$

which is more than adequate in this application.

The electrometer section of Fig. 3.5 is A.C. coupled to a cable-drive amplifier, which is sketched in Fig. 3.6. This provides a nominal voltage gain of five, and provides a low-impedance cable drive to minimize noise pick up.

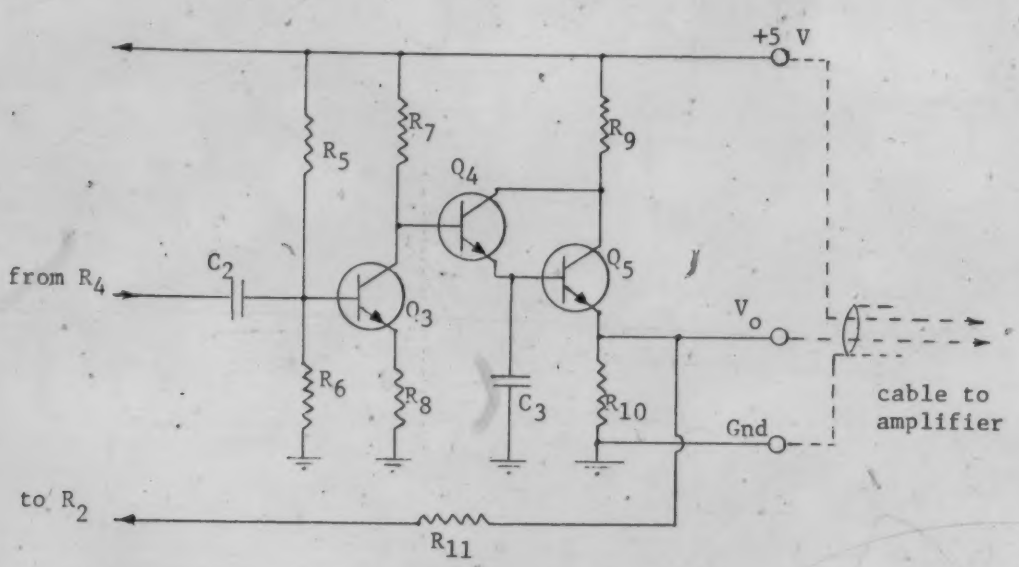

Figure 3.6 The Cable-Drive Amplifier.

Transistors Q_3, Q_4, Q_5 are all low-noise units, type 2N5210. For minimum 1/f noise at 10 Hz, Q_3 is operated at a collector current of 20 μA, and

and the optimum source resistance of 5K ohms (for minimum noise at this current level) is provided by the resistance of R_5 and R_6 in parallel. The emitter resistor R_8 provides bias stability, and is left unbypassed for flat low-frequency response.

With such a low collector current, the output resistance of Q_3 is fairly high, and the collector-load resistor R_7 must be high (120K ohms) to achieve an acceptable gain. Transistors Q_4 and Q_5 constitute a Darlington-connected emitter follower, which is necessary to minimize the loading on Q_3 and which provides the low source impedance for driving the shielded cable. Effective output impedance is approximately 10 ohms.

Capacitor C_3 provides an initial by-passing of radio-frequency and high audio-frequency noise, with the roll-off starting at about 2 kHz.

A direct-current feedback loop from output to input is provided by R_{11} to provide low-frequency stability, and sets the net voltage gain, from sensor plate to cable-drive amplifier output, at a nominal value of X5. (It might be noted that with higher gain, the single-shielded cable permits sufficient signal leakage back to the very-high-impedance sensor plate, so that low-frequency oscillations can occur in the 1-Hz to 10-Hz range. Double-shielded cable would presumably eliminate this problem.)

The detailed circuit schematic with component values used, is given as Figure 3.7.

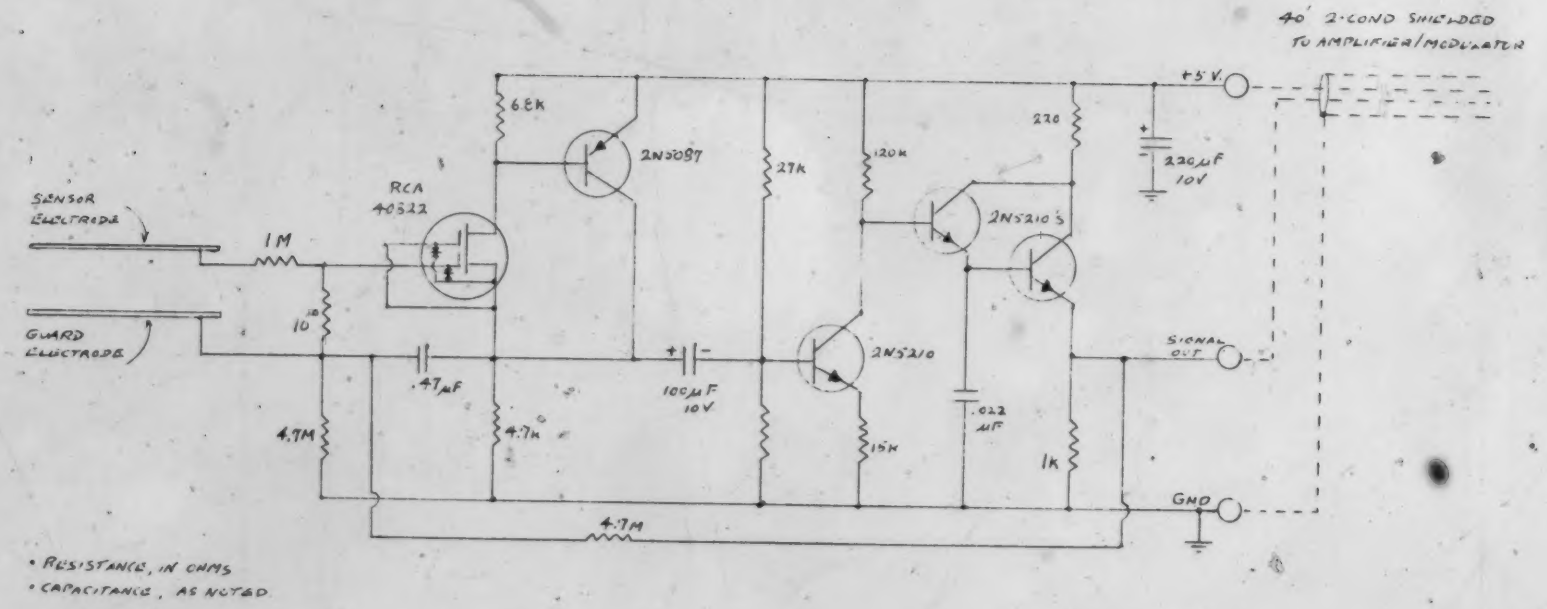

Figure 3.7 The E-Field Sensor Detailed Schematic

3.1.4 SENSOR CHARACTERISTICS

The characterization of the sensor assembly requires the measurement of R_{in} and C_{in}. This is effected by applying a square wave of known amplitude first to the sensor plate directly, and then to a sheet conductor supported a known distance above the sensor plate. The output-signal amplitude and waveform can then be used to calculate R_{in}, C_{in}, and the net gain from sensor plate to the output of the cable-drive amplifier. The guard-electrode extensions prevent distortion of the incident E-field, and are at D.C. ground potential.

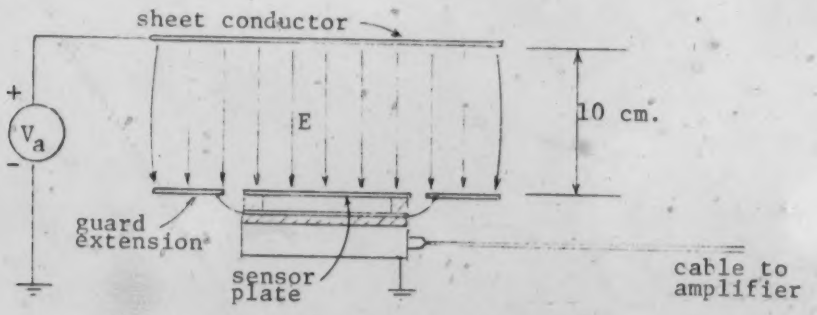

Figure 3.8 Sensor Calibration Arrangement

The results from such a series of tests are shown in Figure 3.9. The input 5-Hz square wave with an amplitude of 25 mV (p-p) is shown in Fig. 3.9(a). If this signal is connected directly to the sensor plate, the cable-drive amplifier output is as shown in Fig. 3.9(b), from which it is evident that the sensor assembly net voltage gain is

$$|A_v| = \left|\frac{V_o}{V_{in}}\right| = \frac{200\ mV}{25\ mV} = 8$$

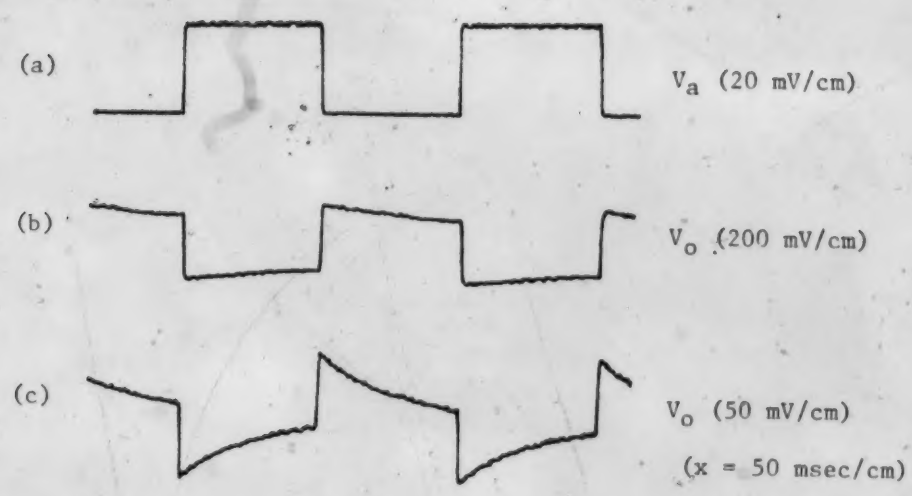

Figure 3.9 Sensor Calibration Waveforms (see text)

With a sheet conductor mounted 10 cm. above the sensor plate, the capacity C_a (of the equivalent circuit 3.4(b)) can be calculated assuming parallel sensor-plate areas, 10 cm. apart, giving C_a = 3.3 pF. If the input signal is connected to this overhead sheet as V_a, the measured output of the cable-drive amplifier is as shown in Fig. 3.9(c), from which V_o = 55 mV. From this, knowing the amplifier gain to be X 8

$$V_{in} = \frac{V_o}{8} = \frac{55 \text{ mV}}{8} = 7 \text{ mV}$$

Then, since $$V_{in} = V_a \frac{C_a}{C_a + C_{in}}$$

and rearranging, $$C_{in} = C_a \frac{(V_a - V_{in})}{V_{in}}$$

then $$C_{in} = (3.3)\frac{(25 - 7)}{7} = 8.5 \text{ pF}.$$

After the step response, the waveform of Fig. 3.9(c) shows an RC discharge curve due to the combined effects of the sensor time constant and the amplifier coupling-capacitor C_2 of Fig. 3.6. From the difference between the indicated time constants of Figures 3.9 (b) and (c), the exponential decay is estimated to be 0.44 of the step amplitude in 100 msec.

Then, since $e^{-0.1/RC} = 0.44$

$$RC = \frac{0.1}{\ln 2.3} = 0.12 \text{ sec.}$$

which is $R_{in}(C_a + C_{in}) = 0.12$ sec.

giving $$R_{in} = \frac{0.12}{(3.3 + 8.5)10^{-12}} = 10^{10} \text{ ohms.}$$

(It might be noted that although the effective resistance of the 10^{10} ohm input resistor should be about 5×10^{11} ohms due to the bootstrap circuit, this will be shunted by the leakage resistance of the gate-protection diodes in the 40822 MOSFET. The effective $R_{in} = 10^{10}$ ohms as calculated above, is therefore the resultant of these paralleled resistances.)

A noise figure for the sensor input system can be derived from the following test records:

(a) 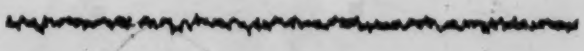 $R_{in} = 0$ ohms

(Hor. scale = 100 ms/cm)

(b) 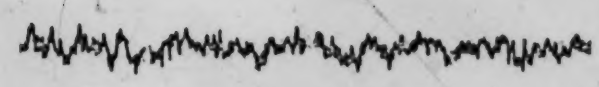 $R_{in} = 10^{10}$ ohms

Figure 3.10 Equivalent-Input Noise Records (see text)

Figure 3.10(a) shows the amplifier-output signal when the sensor plate is shorted to ground. The peak-to-peak amplitude of this noise is approximately 30 μV referred to the input (or approximately 7 μV rms for gaussian noise, assuming the 2σ level as the nominal peak value). With the electrode non-shorted but electrostatically shielded, the noise level is as shown in Figure 3.10(b), and is approximately 80 μV (p-p) or 20 μV rms, referred to the input.

The theoretical noise level can be calculated on the assumption that the dominant source will be the Johnson (thermal) noise in the 10^{10} ohm input resistance. The classical expression for Johnson noise is:

$$V_n = 2\sqrt{kTRB} \quad \text{Volts(rms)}$$

k = Boltzmann's constant
T = temperature, °K
R = resistance in ohms
B = bandwidth in Hz

In this case, the noise bandwidth is limited by the Thévenin-equivalent circuit:

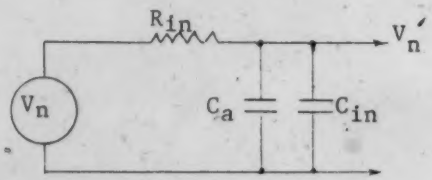

Figure 3.11 Thévenin-Equivalent Circuit for Input Noise

which sets an effective upper corner-frequency at approximately:

$$f_c = \frac{1}{2\pi R_{in}(C_a + C_{in})} = \frac{1}{2\pi(10^{10})(1.2 \times 10^{-11})} = 1.3 \text{ Hz}$$

The lower corner-frequency for the noise is at 0.3 Hz, set by the RC coupling network into transistor Q_3 of the cable-drive amplifier. The

effective noise bandwidth is therefore a nominal 1 Hz, and the expected thermal-noise level will be:

$$V_n = 2\sqrt{(1.38 \times 10^{-23})(2.98 \times 10^{2})(10^{10})(1)}$$

$$= 2\sqrt{41 \times 10^{-12}} = 13 \times 10^{-6} = 13\ \mu V\ (rms)$$

which is in reasonable agreement with the observed noise level of about 20 μV (rms).

A sensor noise figure can therefore be defined and calculated as:

$$NF \equiv 10 \log \left(\frac{\text{total noise-power output}}{\text{noise-power output due to } R_{in}} \right)$$

$$= 10 \log \left(\frac{20}{13} \right)^2 = 3.8\ dB$$

which indicates that the sensor noise level will be 3.8 dB greater than the theoretical noise level due to thermal noise in the very-high input resistance.

3.2 AMPLIFIERS AND FILTERS

As noted in the system block diagram of Figure 3.1(a), part of the field-recording system consists of the signal amplifiers, a 60-Hz notch filter and a high-pass filter with a lower corner-frequency of about 5 Hz. These are arranged as sketched in Figure 3.12 below, and will be discussed in detail in the following sections.

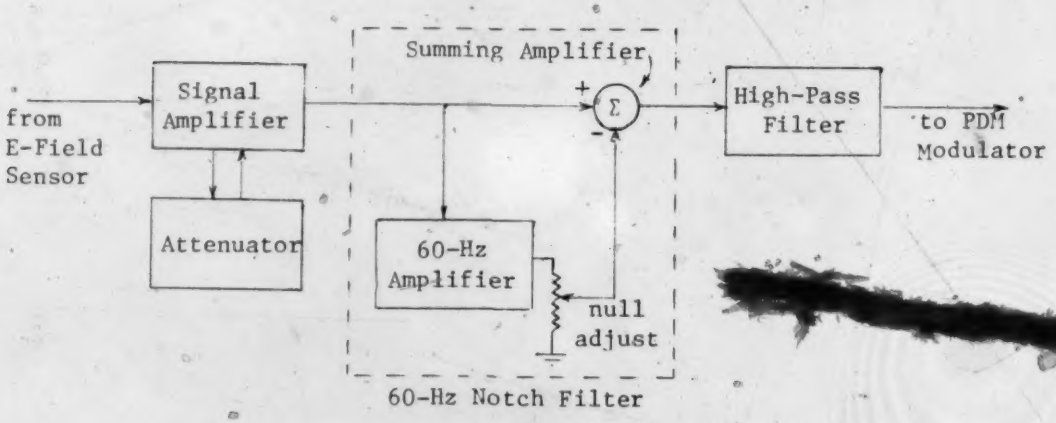

Figure 3.12 Amplifiers and Filters: Block Diagram

3.2.1 THE INPUT AND SUMMING AMPLIFIERS

The amplifiers are designed around integrated-circuit operational amplifiers. The simplified schematic is shown below:

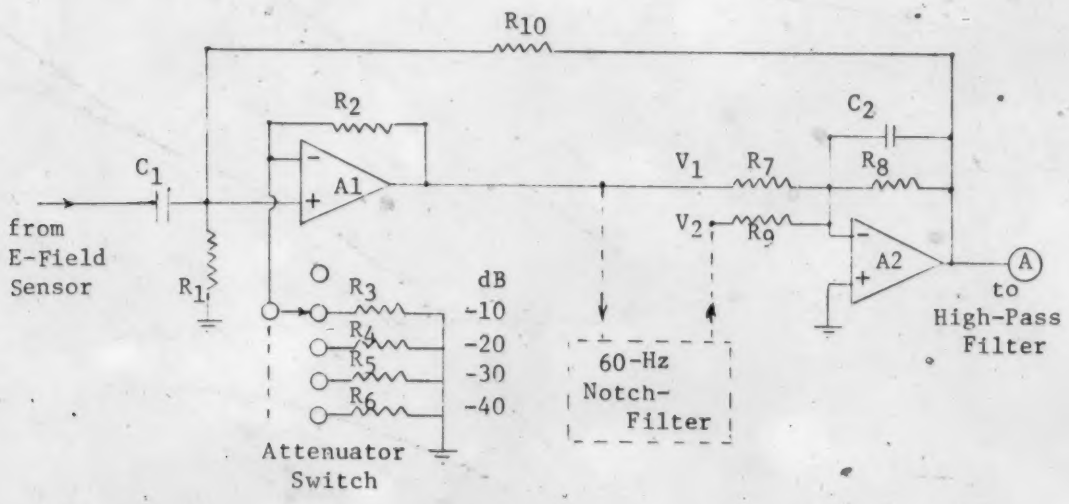

Figure 3.13 The Input and Summing Amplifiers

The effective input-coupling time constant R_1C_1 is selected so that its low-frequency roll-off starts at about 1 Hz, considerably below the 5 Hz dominant lower corner-frequency set by the high-pass filter (Section 3.2.3). Resistor R_1 is a relatively-low 22K ohms, so that the input-resistance changes of amplifier A1 due to attenuator switching will not materially alter the input time constant.

The gain switching of amplifier A1 is defined in terms of attenuation for system-application convenience. The resistance values of R_2, R_3, R_4, R_5, R_6 are selected so that voltage-gain changes are in 10 dB steps, as tabulated on the following page:

Attenuator Setting	Voltage Gain
0 dB	X 100
-10 dB	X 31
-20 dB	X 10
-30 dB	X 3
-40 dB	X 1

The voltage gain of amplifier A2 is set at X 2.5 by the resistance-ratio R_8/R_7. This amplifier also serves as a "summing" amplifier for the normal signal voltage V_1 and the out-of-phase 60-Hz signal V_2, so that the 60-Hz interference is effectively nulled out.

Capacitor C_2 across the feedback resistor of amplifier A2 provides the dominant high-frequency attenuation, with the roll-off starting at about 200 Hz. A small D.C. feedback is provided by resistor R_9 to minimize output D.C. shifts with different attenuator-switch settings.

3.2.2 THE 60-Hz NOTCH FILTER

It has already been noted that 60-Hz power-line interference is within the ELF pass band of interest (5 Hz - 200 Hz). Although system portability does offer the opportunity of selecting a recording site far removed from overhead power lines, the fact remains that 60-Hz interference can be so all pervasive that even in such locations a 60-Hz notch filter may still be required.

It was specifically mentioned in Section 2.3 that the transient response of the typical Twin-T notch filter can generate signal artifacts if the input waveform approaches the shape of a square-edged pulse. The

following notes offer a more detailed discussion of this problem.

The "standard" passive Twin-T RC notch filter is shown in Figure 3.14(a), in a symmetrical configuration. Figure 3.14(b) shows the filter transient response for various input pulse widths, for a notch frequency of 60 Hz.

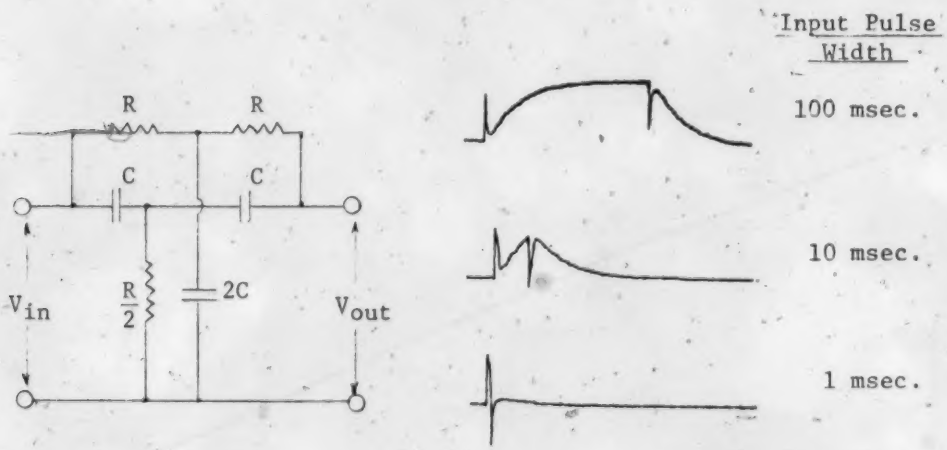

Schematic (a)

Transient Response (V_{out}) (b)

Figure 3.14 The Passive Twin-T RC Notch Filter

With the component symmetry noted in Fig. 3.14(a) and with no output loading, the voltage transfer function is

$$\frac{V_{out}}{V_{in}} = H(s) = \frac{s^2 + \omega_o^2}{s^2 + 4\omega_o s + \omega_o^2} \qquad (3.2.2.a)$$

where $\omega_o = 1/(RC)$.

From the above transfer function, it is evident that the Q of this configuration is only 0.25, so that for a 60-Hz notch frequency, the rejection-band width is 240 Hz (putting the -3 dB points at 16 Hz and

225 Hz). This notch width is of course unacceptable when the desired pass-band is 5 Hz to 200 Hz, and the signal artifacts of 3.14(b) are certainly undesirable.

Active network high-Q versions of the Twin-T notch filter are well known [64],[65] and can reduce the notch width to almost any desired value. However, the poor transient response remains and high-Q ringing can compound the problem.

The poor transient response as illustrated in Fig. 3.14(b) is related to the fact that the desirable notch in the frequency-response curve is a steady-state characteristic, while the transient response in the time domain is dominated by the RC-coupling configurations and their time constants. The input network (C and R/2) simply differentiates the edges of applied square waves or pulses.

Fortunately, in the present application, the steady-state response can be almost totally isolated from the transient response. In the modified notch-filter arrangement of Figure 3.15, the steady-state 60-Hz interference is isolated via a sharply peaked 60-Hz amplifier (the

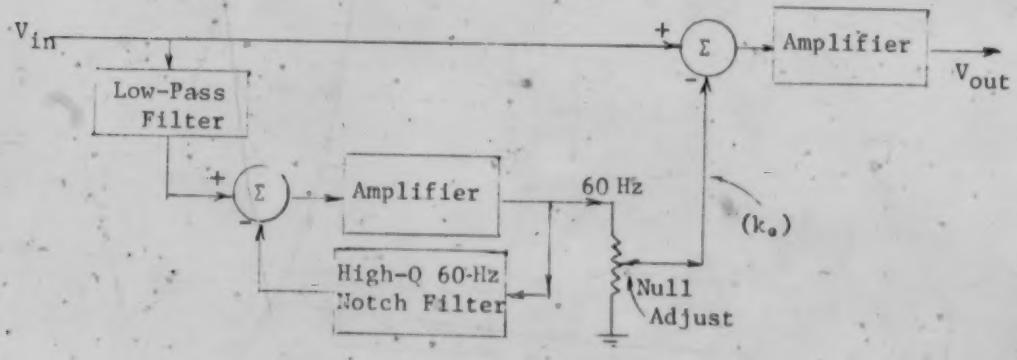

Figure 3.15 The Modified Notch Filter Block Diagram

high-Q notch filter is now located in the negative-feedback loop of an operational amplifier). This out-of-phase 60-Hz signal is then added to the original signal with its amplitude adjusted to "null out" the 60-Hz interference. The transient signals pass directly through, and never enter the twin-T network.

With typical component values as detailed in schematic Figure 3.21, this modified notch filter has the voltage transfer function:

$$H(s) \approx (1 - .13k_o)\left[\frac{s^2 + \left(\frac{.0045 - .045k_o}{1 - .13k_o}\right)\omega_o s + \left(\frac{1.01 - .175k_o}{1 - .13k_o}\right)\omega_o^2}{s^2 + .0045\omega_o s + 1.01\omega_o^2}\right]$$

where k_o is the fractional setting of the null-adjust potentiometer. It is evident that the second term of the bracketed numerator can be reduced to zero by adjusting the value of k_o (to about 0.1), leaving the transfer function as:

$$H(s) \approx .99\left(\frac{s^2 + 1.005\omega_o^2}{s^2 + .0045\omega_o s + 1.01\omega_o^2}\right) \qquad (3.2.2.b)$$

The steady-state zero has been reestablished, although a slight shift of frequency is necessary to restore the notch to precisely 60 Hz. (In practice, both the frequency and the null adjustements are made while observing the filter output with an oscilloscope, with a 60-Hz input signal derived from the power line.) The value of .0045 in the denominator of the transfer function indicates an effective Q of 1/.0045 ≈ 220, which gives a notch width of 60/Q = .27 Hz at the - 3 dB points.

The modified notch filter has a pulse response controlled by the characteristics of the summing amplifier, not by the twin-T network.

Only a residue of the high-Q ringing of the Twin-T network remains visible in the over all modified notch-filter response. The pulse response for the modified system is shown in Figure 3.16 below, for different input-pulse widths.

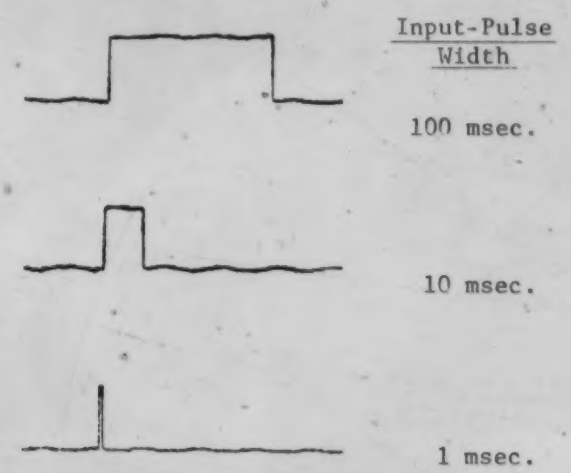

Figure 3.16 Pulse Response of the Modified Notch Filter

A much more complete discussion of the modified notch filter, its derivation, and the manipulation of the transfer-function poles, is given in Appendix A.

It should be noted that a so-called "gyrator" notch-filter circuit is often included in manufacturer's integrated-circuit application notes [66],[67] with no comment on its special characteristics. It does in fact have a transfer function similar to Eq'n (3.2.2.b) with a pulse response equal to that of Fig. 3.16. For medium and low-Q applications ($Q<20$) the gyrator would be preferred to the modified Twin-T system because of its circuit simplicity. For high-Q applications ($Q>20$)

undesirable capacitor ratios become necessary, which ruled out its use in the present ELF-receiver design. However, for completeness, a brief discussion of the gyrator notch filter is given in Appendix B.

3.2.3 THE HIGH-PASS FILTER

A basic second-order high-pass active filter is shown in Figure 3.17(a).

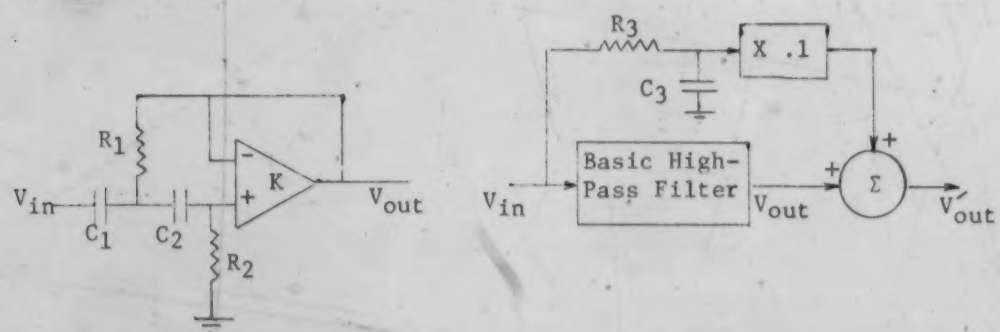

Basic High-Pass Filter (a)

Modified High-Pass Filter (b)

Figure 3.17 The High-Pass Filter Modification

The voltage transfer function of the basic high-pass filter is:

$$\frac{V_{out}(s)}{V_{in}(s)} = H_1(s) = \frac{s^2}{s^2 + [\omega_2 + 1/(C_1R_2) + (1 - K)\omega_1]s + (\omega_1\omega_2)}$$

where $\omega_1 = 1/(R_1C_1)$ and $\omega_2 = 1/(R_2C_2)$.

To retain only real poles in $H_1(s)$ (as suggested in Section 2.3 to reduce transient overshoot) component values can be chosen so that $R_1 = R_2$ and $C_1 = C_2$. Then for an amplifier gain factor of $K = +1$, the

transfer function would reduce to:

$$H_1(s) = \frac{s^2}{s^2 + 2\omega_o s + \omega_o^2} = \frac{s^2}{(s + \omega_o)^2}$$

where $\omega_o = 1/(R_1C_1) = 1/(R_2C_2)$, and the poles would both be real at $s = -\omega_o$. This would provide a low-frequency roll-off of 40 dB/decade, but for $f_o = 5$ Hz the response would only be down by about 28 dB at 1 Hz, which in practice is insufficient to maintain an acceptable base-line stability in the face of large E-field disturbances encountered at about this frequency.

The best approach appears to be the addition of a transmission zero around 1 Hz, which can be done effectively by the filter modification shown in Figure 3.17(b). For the desired frequency-response curve, complex poles must be tolerated ($R_1 = R_2/20$, $C_1 = 20C_2$) but the zero locations do provide some overshoot damping. (See Fig. 3.18 and Fig.3.20.)

The transfer function of the paralled low-pass network (R_3 and C_3 of Figure 3.17(b)) is:

$$H_2(s) = \frac{\omega_3}{s + \omega_3}$$

where $\omega_3 = 1/(R_3C_3) = \omega_o$. For the component values used (noted in Figure 3.21) and with the (X 0.1) scale factor provided by appropriate resistance values of the subsequent summing network, the resultant transfer function becomes;

$$\frac{V'_{out}(s)}{V_{in}(s)} = H(s) = H_1(s) + 0.1H_2(s)$$

$$= \left(\frac{s^2}{s^2 + (1.04\omega_o)s + \omega_o^2}\right) + \left(\frac{.1\omega_o}{s + \omega_o}\right)$$

or in factored form,

$$H(s) = \frac{(s + .17 + j9.2)(s + .17 - j9.2)(s + 33)}{(s + 15.8 + j25.8)(s + 15.8 - j25.8)(s + 30.3)}$$

These pole and zero locations can be graphically displayed as in Figure 3.18(b) to permit some visualization of their effect on the system frequency response.

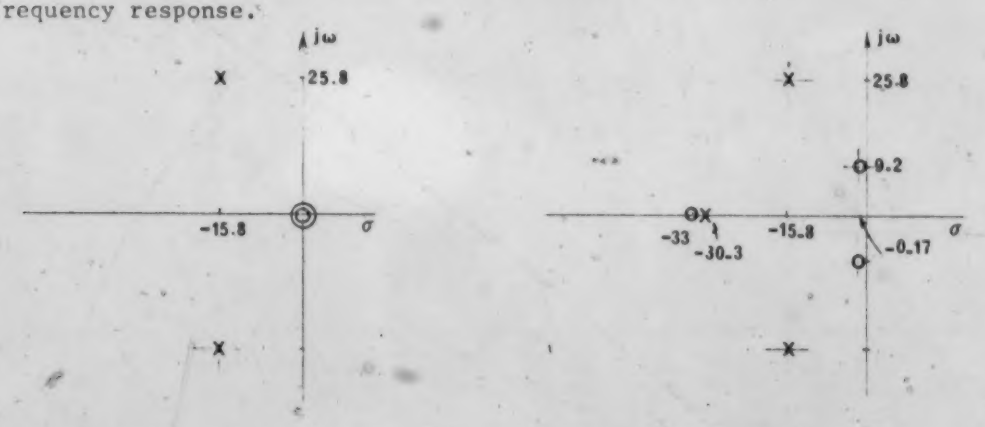

Basic High-Pass Section With Complex Poles

(a)

Pole-Zero Locations of the Modified High-Pass Filter

(b)

Figure 3.18 High-Pass Filter Pole-Zero Modifications

One penalty for securing the added attenuation rate just below 5 Hz in this manner, is the fact that a D.C. term has been added to the transfer function, $[0.1\omega_o/(s + \omega_o)]$ which for a notch depth of about -60 dB constitutes a zero-frequency leakage at the -20 dB level. (See Figure 3.19.)

Actually, this can be tolerated since the input coupling network provides a 20 dB/decade low-frequency roll-off, and the sensor

amplifier adds another 20 dB/decade attenuation from almost the same point. The effective low-frequency roll-off is indicated by the dotted curve in Figure 3.19.

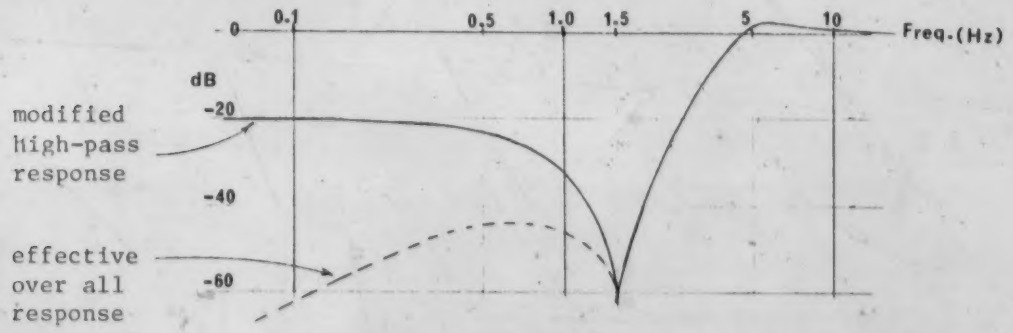

Figure 3.19 Frequency Response of the High-Pass Filter

The attenuation rate from 5 Hz down to 1.5 Hz is about 100 dB/decade, and provides an acceptable base-line stability, (as was indicated in Figure 2.1).

The transient response is of course somewhat degraded from that possible with only real poles, and is noted in Fig. 3.20 below.

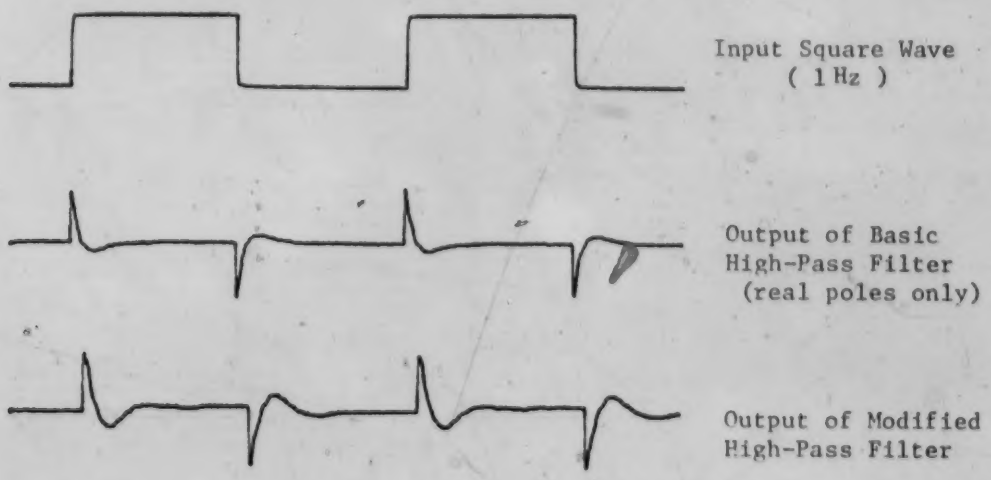

Figure 3.20 Transient Response of the Modified High-Pass Filter

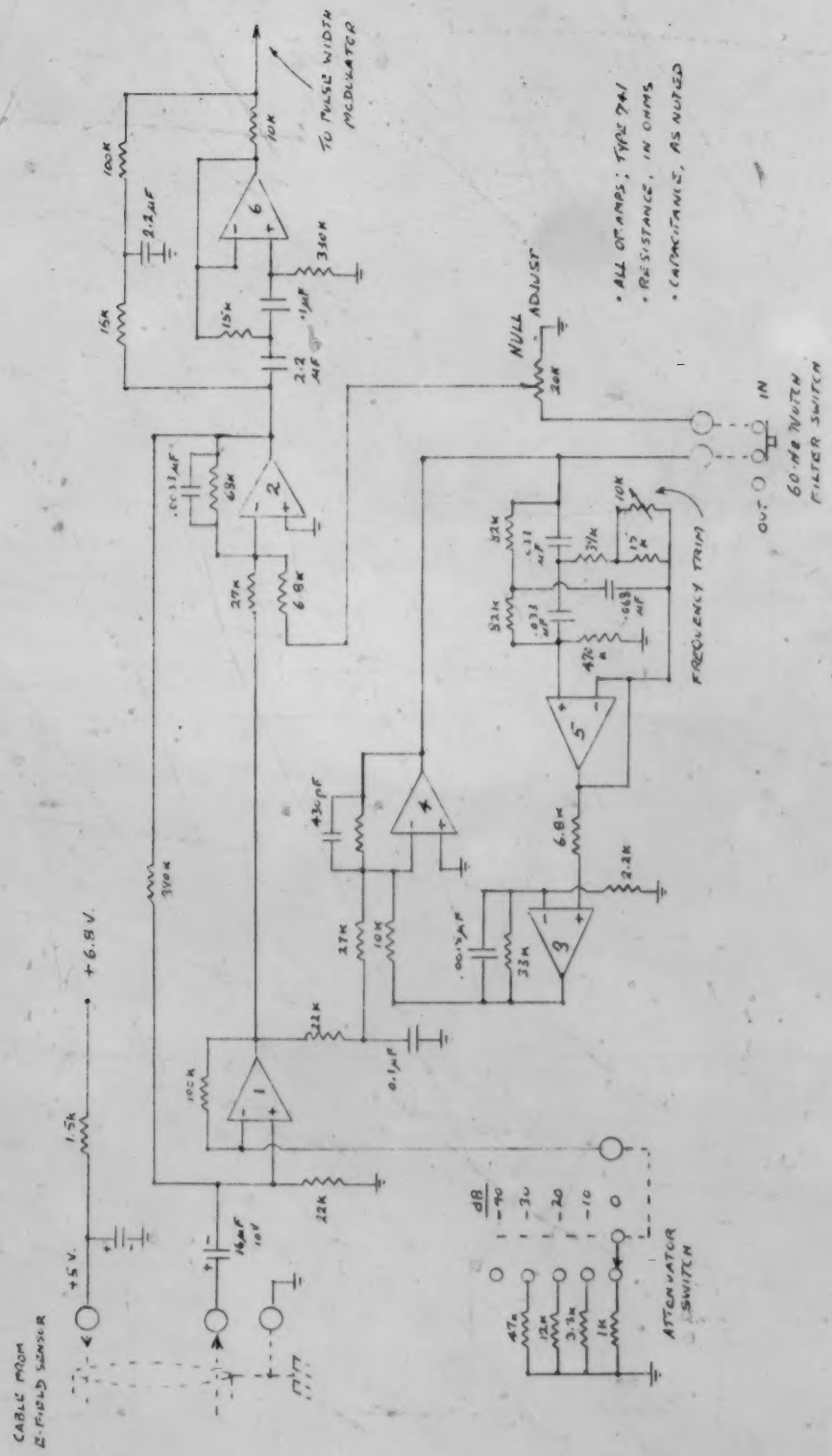

Figure 3.21 Detailed Schematic of the Amplifiers and Filters

3.3 THE PULSE-DURATION MODULATOR

The ouput of the modified high-pass filter network of Fig. 3.21 is the input signal to the pulse-duration modulator circuit. The operation of the modulator section can be conveniently discussed under a number of sub-sections, as outlined below in block-diagram form.

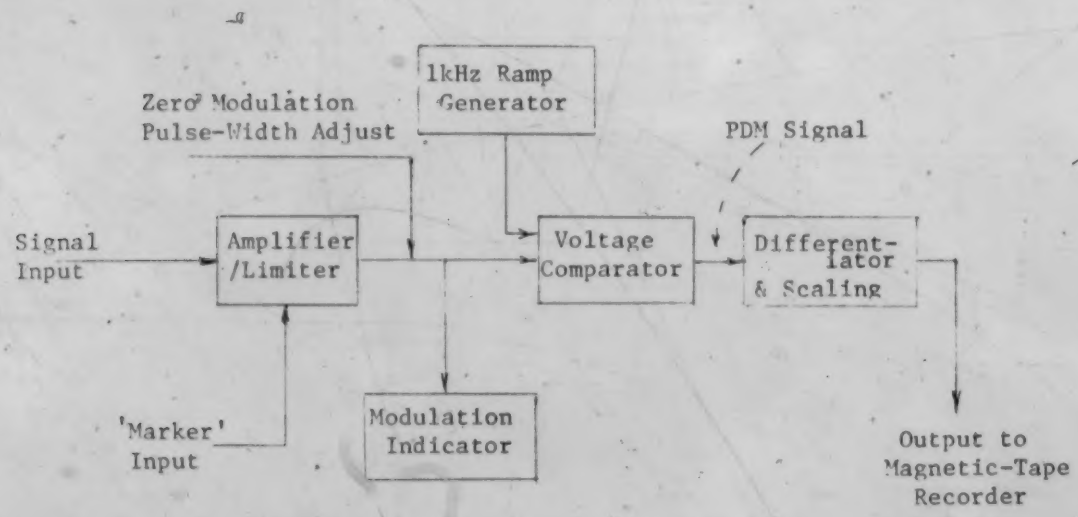

Figure 3.22 Pulse-Duration Modulator Block Diagram

The following sub-sections cover design details, schematics, and circuit operation.

3.3.1 BUFFER-LIMITER AMPLIFIER

A buffer-limiter amplifier is provided between the modified high-pass filter system (of Section 3.2.3) and the pulse-duration modulator. This amplifier performs several functions, and its general configuration is shown in Figure 3.23 below.

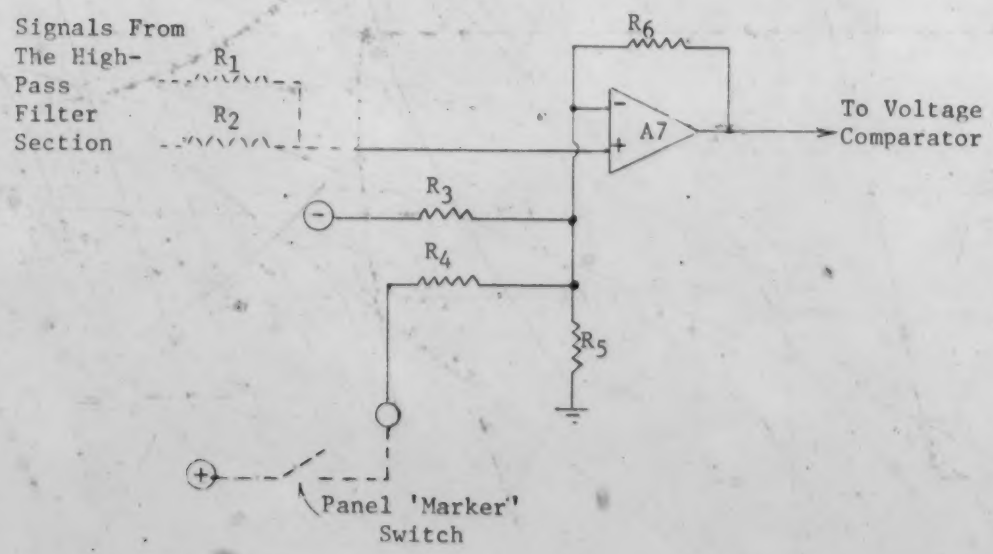

Figure 3.23 The Buffer-Limiter Amplifier

The signals from the low-pass shunt network and from the high-pass filter section are combined via scaling resistors R_1 and R_2, and become the signal input to the non-inverting amplifier A7.

A voltage gain of about X 13 is also provided by this amplifier (set by the resistance ratio $(R_5 + R_6)/R_5$). This final voltage gain is chosen so that an E-field disturbance of 10 mV/m at the sensor plate, with an attenuator-switch setting of 0 dB, will provide a voltage swing

of approximately 6 Volts at the output of amplifier A7. This constitutes a "full-scale" signal, which will be used to drive the pulse-duration modulator.

As noted in Section 2.4.2, a pulse-duration modulator should not be over modulated, or the basic pulse-repetition rate may be lost by "pulse overlap". Any danger of such over modulation is readily prevented by limiting the signal voltage at the ouput of amplifier A7, and since this limiting is non-critical, (it implies off-scale data), it is convenient to simply use the operational-amplifier saturation limits as an intrinsic signal-limiting system.

A panel MARKER switch is provided so that an "end-of-record" signal can be added to the data being recorded. This marker signal has been chosen as an off-scale signal (via R_4) of sufficient magnitude to over-ride any normal signal.

As noted in Section 3.2.3, traces of the D.C. offset voltages of operational amplifiers A1 and A2 will be passed through the low-pass shunting network of the modified high-pass filter system. In addition, the positive and negative clipping levels of amplifier A7 will differ by perhaps one-half volt. These combined offsets are trimmed out by a fixed-bias resistor R_3 during assembly and calibration. (This is effected by observing the output of amplifier A7 with an oscilloscope, while introducing an adjustable sine-wave signal into the system. The signal amplitude is adjusted so that a slight signal over-drive is observed at the output of amplifier A7, and resistor R_3 is then selected so that symmetrical peak clipping occurs.)

3.3.2 THE 1-kHz RAMP GENERATOR

The pulse-duration modulation scheme involves the use of a voltage "ramp", i.e., a voltage which rises linearly with time between predetermined limits. The voltage is "reset" to its initial value at the end of each millisecond, so that its repetition rate is 1 kHz. The simplified schematic is shown below.

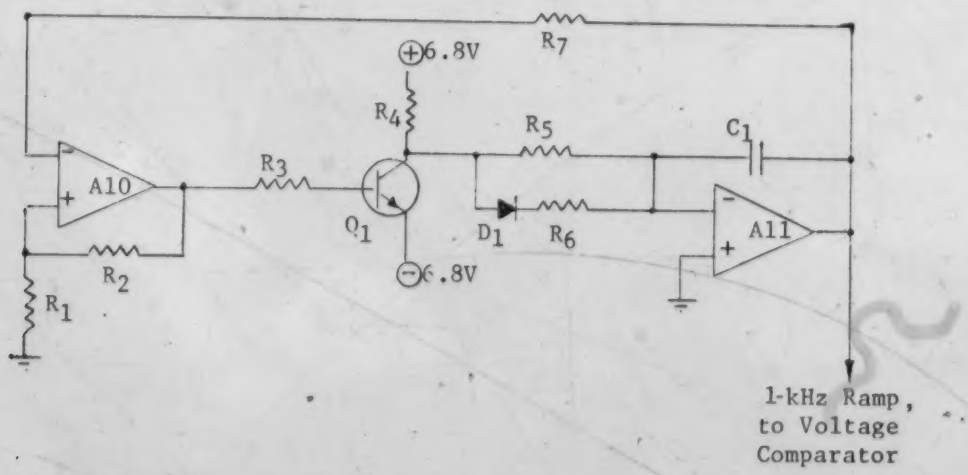

Figure 3.24 The 1-kHz Ramp Generator

Amplifier A11 is arranged as an integrator, with its output voltage being related to time by the expression:

$$V_o(t) = -\int \frac{V_{in}(t)}{C_1 R_5} dt + V_o(0) \qquad , t>0$$

Transistor Q_1 is normally conducting, so that the effective value of V_{in} is normally constant at the -6.5V saturation voltage of the collector of Q_1. The initial (reset) value of V_o at time t = 0, is approximately -4.9V, and using the component values noted in the detailed schematic

of Figure 3.29, the above equation can be evaluated as:

$$V_o(t) = -\left[\frac{(-6.5V)t}{(2.2\times10^{-9})(3\times10^{5})}\right] - (4.9V) \qquad , t>0$$

$$= (10^4 t - 4.9) \text{ Volts}$$

from which it is evident that $V_o(t)$ is a positive-going voltage ramp, rising at a constant rate of 10V/msec, and starting from an initial value of -4.9 Volts.

During this rise time, amplifier A10 is saturated with its output at approximately +6.5V. Resistors R_1 and R_2 scale this down to +4.7V which is then used as the reference voltage on the (+) input of A10. The (-) input of A10 is the ramp voltage $V_o(t)$, monitored via resistor R_7.

The ramp is terminated when $V_o(t)$ exceeds +4.7V, i.e, when the (-) input of amplifier A10 becomes positive with respect to the (+) input. When this occurs, the output of A10 switches abruptly from its positive-saturation level to the negative-saturation level of about -6.7V, (which switches the (+) input-reference value to -4.9V). The ramp duration is therefore the time required for V_o to rise from -4.9V to +4.7V at the rate of 10V/msec, or

$$T = \frac{(4.9 + 4.7)}{10} \text{ msec} = 960 \text{ microseconds}$$

When the output of amplifier A10 switches to its negative level, the base current for transistor Q_1 drops to zero, and its collector is no longer clamped to its -6.5V level. The RC time constant of the A11

integrator is now much reduced, since the diode D_1 conducts, and the effective V_{in} to the integrator is +6.8V through a resistance of only 17K ohms, $(R_4 + R_6)$. This generates a negative-going ramp, starting from an upper-switching level of +4.7V, with the relevant expression for $V_o(t)$ becoming:

$$V_o(t) = -\left[\frac{(+6.8V)t}{(2.2\times10^{-9})(1.7\times10^{4})}\right] + (4.7V) \quad , t>0$$

$$= (-1.8\times10^{5}t + 4.7) \text{ Volts}$$

Since this ramp voltage goes negative at the rate of 180V/msec, it reaches the -4.9V level (of the (+) reference input of the voltage-comparator A10) in the time

$$T_2 = \frac{(4.7 + 4.9) \text{ Volts}}{180\text{V/msec}} \approx 53 \text{ μsec.}$$

This constitutes the ramp "reset", after which amplifier A10 switches to its original state and the next voltage ramp begins.

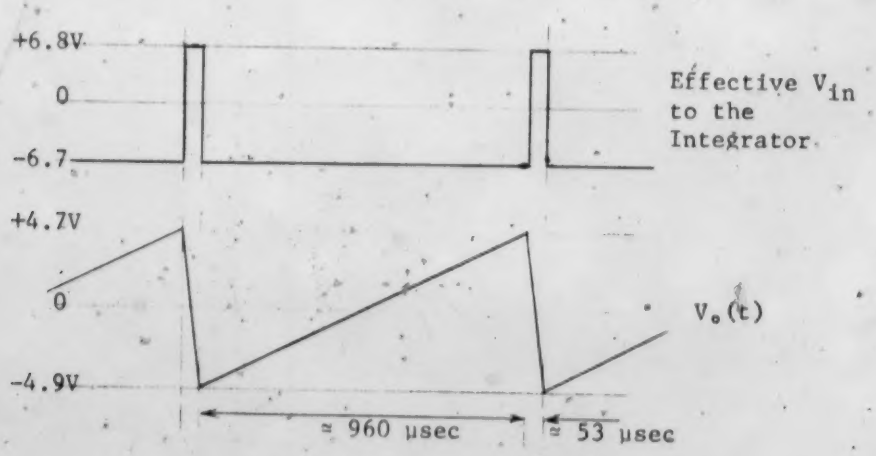

Figure 3.25 The 1-kHz Ramp-Voltage Waveform

3.3.3 THE VOLTAGE COMPARATOR

The required pulse-duration-modulated waveform is generated by the ouput switching of amplifier A9, which is arranged as a voltage comparator. The ouput-pulse duration is determined by the time taken for the linear ramp to rise from its initial value to the level of the modulating signal.

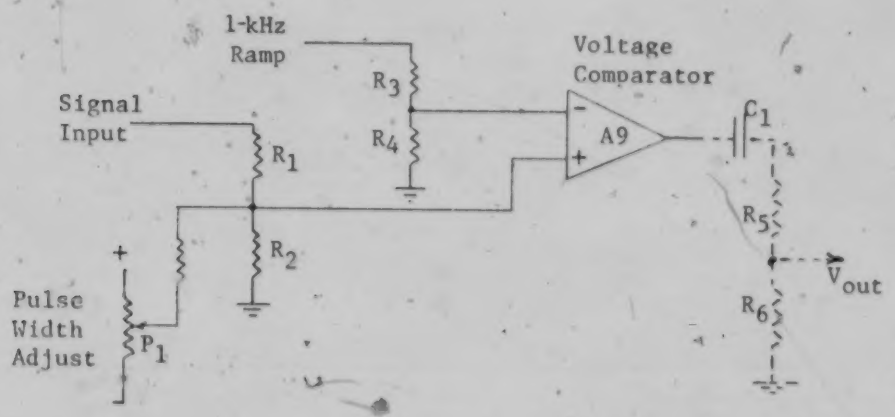

Figure 3.26 , The Voltage Comparator

The signal-input voltage (from the buffer-limiter amplifier) is scaled down to plus-or-minus 3 Volts maximum, by resistors R_1 and R_2 so that all voltage comparisons in amplifier A9 occur well within the linear common-mode range. The 1-kHz ramp signal from integrator A11 is also scaled down, by resistors R_3 and R_4, to +3.4V and -3.6V limits. This ensures that the ramp magnitude is always greater than the modulation signal, so that the basic pulse can never be reduced to zero duration. The ramp voltage therefore sweeps the (-) input of the voltage-

comparator from -3.6V up through the signal-voltage level present on the (+) input. When the ramp voltage exceeds the signal voltage, the (-) input becomes positive relative to the (+) input, and the output of amplifier A9 switches abruptly from its positive-saturation level to the negative-saturation level. The output reverts to the positive level when the ramp is "reset", and the (-) input of A9 reverts to the initial -3.6V level. The duration of the positive-output pulse is therefore linearly controllable by the signal level at the (+) input of voltage-comparator A9.

The time relationships of the various waveforms involved are sketched in Figure 3.27.

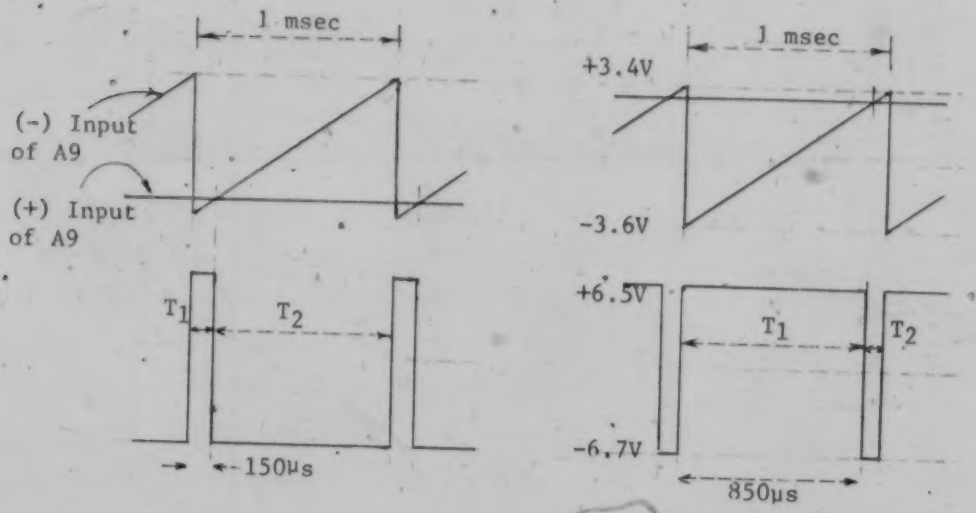

Figure 3.27 Pulse-Duration-Modulator Waveforms

It has already been noted that the positive and the negative saturation levels of the operational amplifiers are slightly different,

so that both the input signal (when adjusted for symmetrical clipping in the limiter) and the 1-kHz ramp voltage have slight D.C. components. The PULSE-WIDTH-ADJUST potentiometer P_1 (of Fig. 3.26) adds a selected bias voltage to the (+) input of the voltage-comparator A9, to control the "zero-modulation" switching time. This potentiometer is simply adjusted so that $T_1 = T_2$ with zero-input signal, as observed with an oscilloscope at the output of A9 or at the output to the tape recorder.

3.3.4 DIFFERENTIATION AND SCALING

The pulse waveform at the output of the voltage-comparator A9 is a true PDM waveform with trailing-edge modulation, but as noted in Section 2.4.3, an improved magnetic-tape record-reproduce characteristic is obtained if the pulse waveform is differentiated before use. The PDM waveform from the voltage comparator is therefore passed through an RC coupling network consisting of C_1 and $(R_5 + R_6)$, which has a very short time constant (relative to the minimum pulse width of T_1 or T_2). The resultant spike-exponentials, representing the transition times of the PDM waveform, are scaled by R_5 and R_6 to about ±1V peak, and are then fed to the output jack, ready for introduction into the typical "AUX" input of a cassette tape recorder.

3.3.5 THE MODULATION INDICATOR

The magnitude of the natural ELF signal varies with time, and in some cases with the recording site. Some indication of peak field-

strength is therefore required during the recording process, so that the best attenuator-switch setting can be selected for a reasonable PDM-modulation level.

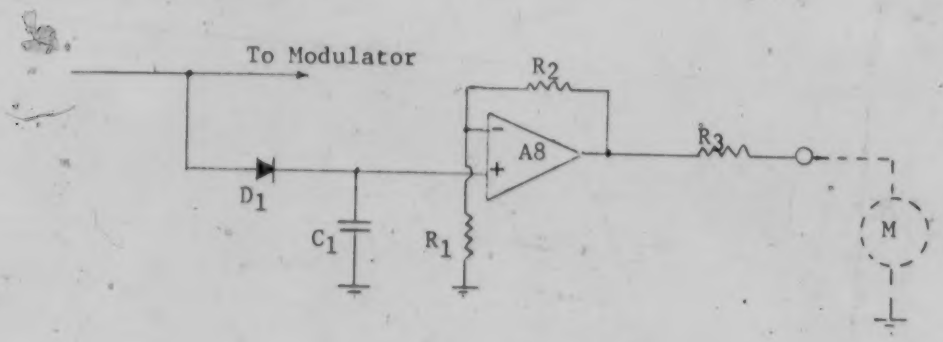

Figure 3.28 The Modulation-Level Indicator

Referring to the above schematic section, note that the signal being fed to the PDM modulator is "sampled" by diode D_1, with the positive peak values stored on C_1. The voltage on C_1 is continuously monitored by the high-input-impedance voltage follower A8, with a slow discharge rate via the input resistance of A8. The +3V maximum signal level to the modulator is restored to +6V maximum by a gain of two in the voltage-follower (set by the resistance ratio $(R_1 + R_2)/R_1$). The low-impedance output, via a calibration resistor R_3, drives a small panel-meter M, so that a full-scale E-field transient produces a full-scale meter deflection.

This indication of the modulation level is rather "crude", due to the random transient nature of the ELF signals. However, it has been observed that typical signals have reasonably equal positive and negative peaks (on the average), so that reading one polarity peak value is at least a useful guide. The discharge time constant of C_1 via the

input resistance of amplifier A8 (about 1 second) gives a rough indication of the average signal level.

3.3.6 THE PDM-MODULATOR TRANSFER CHARACTERISTIC

The transfer characteristic, from the voltage level at the (+) input of the buffer-limiter amplifier A7, to the pulse-duration modulation observed at the output of the voltage-comparator A9, is of interest from a system-calibration standpoint.

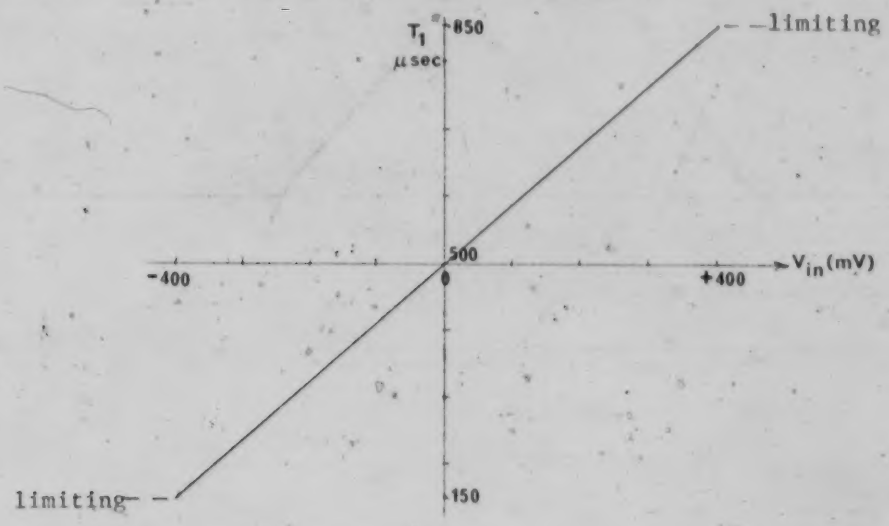

Figure 3.29 The PDM-Modulator Transfer Characteristic

The detailed circuit schematic, with component values, for the preceding sub-sections of Section 3, are combined in Figure 3.30 on the following page.

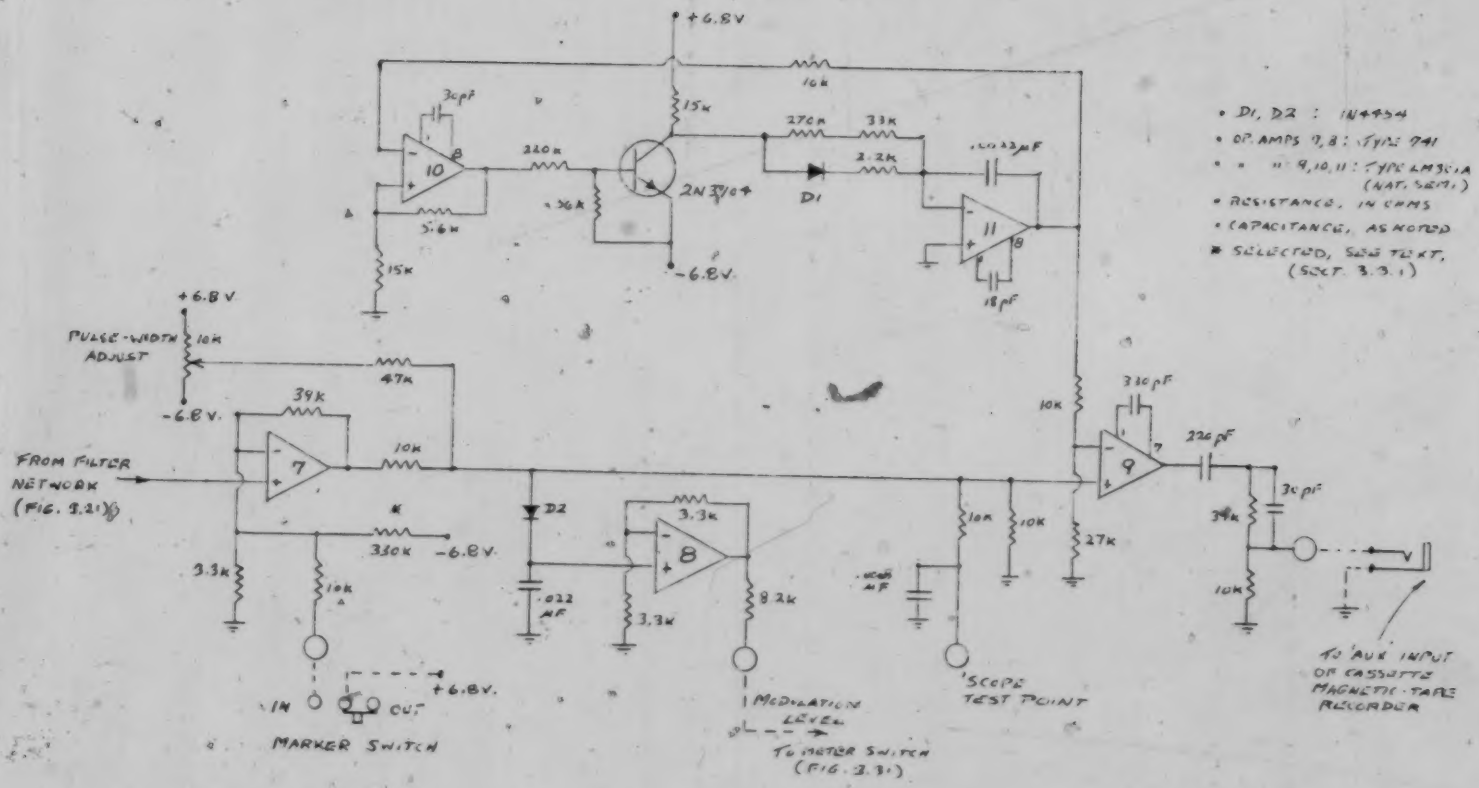

Figure 3.30 Detailed Schematic of the Pulse-Duration Modulator

3.3.7 THE BATTERY POWER SUPPLY

The detailed schematic of the battery power supply is given as Figure 3.31. The following notes cover the design and operating details.

For availability, weight, and cost considerations, standard-size "C" flashlight cells are used in the battery pack. Twelve cells are arranged to provide +9V and -9V relative to ground. Such cells are rated at 1200 mA-hours, intermittent use, to a nominal "end-voltage" of 1.2 Volts. The total current drain of the E-field sensor and the amplifier-filter-modulator system is approximately 26 mA, so that a useful battery life of about 45 hours can be expected. Alkaline-cell equivalents can of course be substituted for longer service life.

To retain constant operating voltages for some of the circuits (primarily the 1-kHz ramp generator), the battery voltages are reduced and stabilized at ±6.8V by simple Zener-diode/transistor voltage regulators. With the low collector-emitter voltages involved, and at the low current levels concerned, small-signal transistors (types 2N3904 and 2N3906) are adequate as series regulators without heat-sink precautions. Regulation is sufficient to hold operating voltages at ±6.8V ±.05V, for a battery-voltage run down from 9.5V to 7.4V.

A battery-test facility is included which makes use of the "modulation-level" panel meter. A Zener-diode type 1N5233B suppresses 6V of the battery voltage, to permit an expanded-scale reading in the 6V - 9V range of interest. The 5.6Kohm resistor sets meter deflection at approximately half-scale for the "end-of-life" indication. The +9V and the -9V battery packs may be checked individually by means of a panel-mounted selector switch.

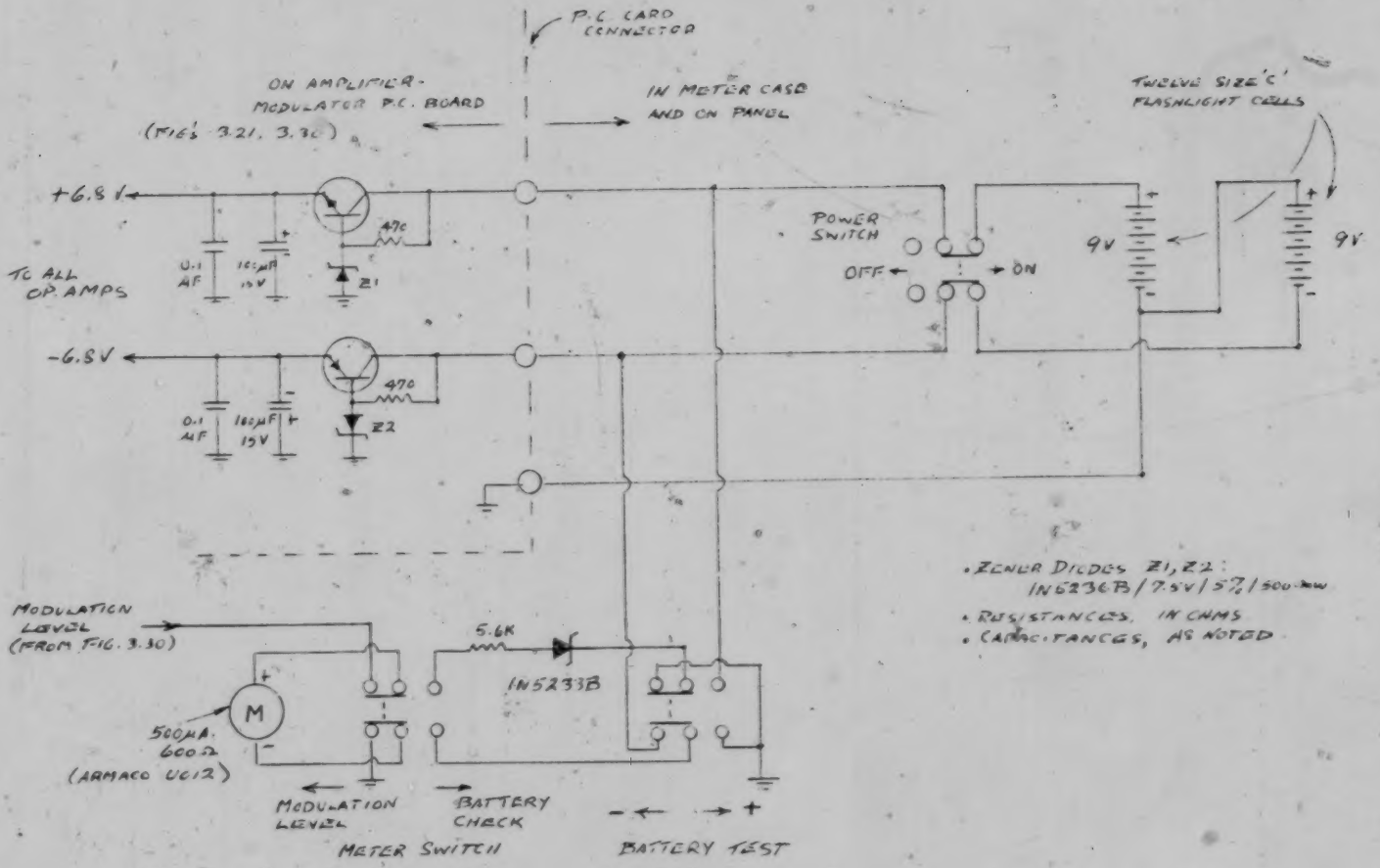

Figure 3.31 Battery Power Supply

3.4 THE PULSE-DURATION DEMODULATOR

During playback of a magnetic-tape recording, the PDM demodulation involves the following functional circuit blocks:

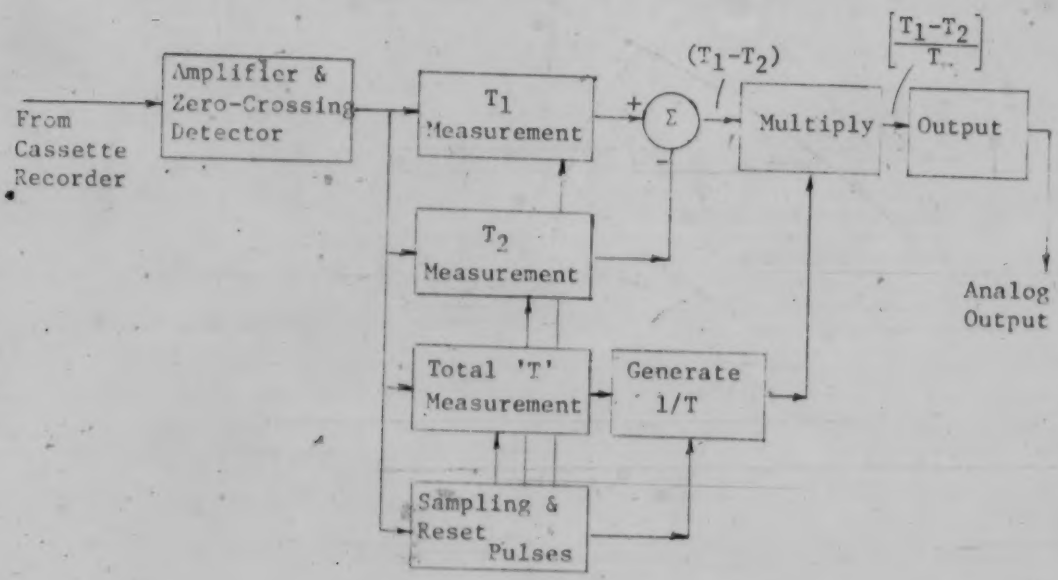

Figure 3.32 Demodulator Block Diagram

The design details and operation of these circuits are covered in the following sub-sections.

3.4.1 INPUT AMPLIFIER AND ZERO-CROSSING DETECTOR

The playback signal derived from the recorded differentiated PDM waveform has been sketched in Figure 2.8, but for use by the demodulator circuits, this amplitude-variable non-sinusoidal signal must be reformed into the best possible replica of the original PDM waveform. A simplified sketch of the circuits involved is shown in Figure 3.32.

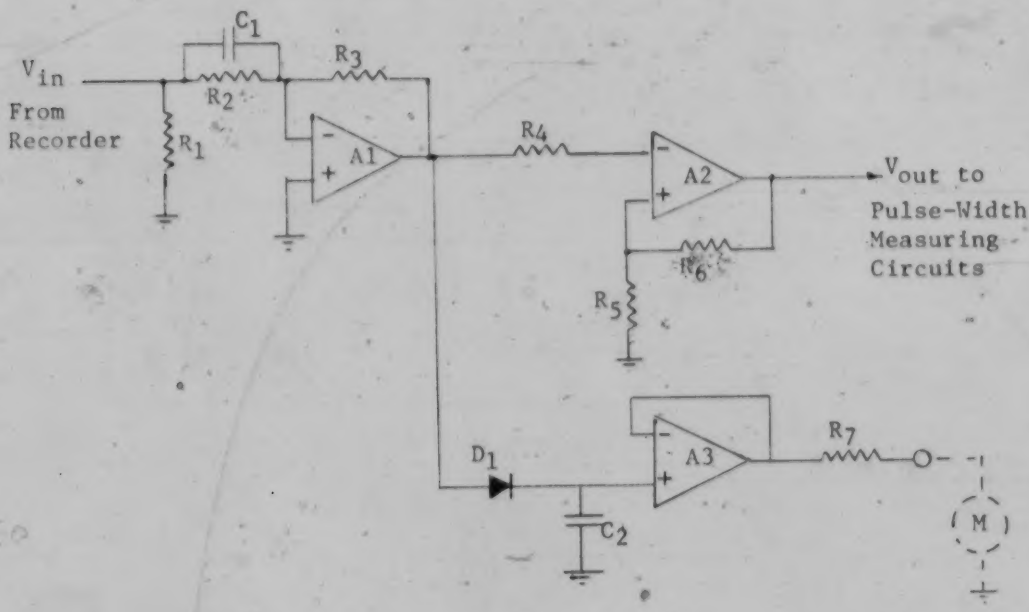

Figure 3.33 Input Amplifier and Zero-Crossing Detector

Referring to the above figure, the playback signal from the cassette tape recorder is developed across an input-load resistor R_1. This 10-ohm resistor provides the load equivalent of an earphone, and in the particular recorder used, it was noted that such a load resistor of

40 ohms or lower, was necessary to prevent recorder-amplifier oscillations. The typical portable recorder can produce a peak undistorted signal of about 3 Volts across such a load.

Amplifier A1 provides a voltage gain of five, set by the resistance ratio R_3/R_2, so that the ±3V peak signal input can slightly overdrive the amplifier output (about ±14V with the ±15V supply voltage). Since an output signal of about ±10V peak is normally used, full recorder output volume is not required, avoiding possible distortion from this source. Capacitor C_1 adds a slight high-frequency emphasis for somewhat sharper "zero crossings".

This precaution against waveform peak clipping in the input amplifier is necessary to ensure stability of the regenerated PDM waveform, since time displacements of the zero crossings can occur if the waveform is clipped and the duty cycle changes due to modulation. A small panel meter (M) is provided so that the peak signal level at the output of amplifier A1 can be conveniently set to a reference value during signal playback. Diode D_1 stores the peak (positive) value of the signal on capacitor C_2, and this voltage is "read out" by the high-input-impedance voltage-follower A3. Resistor R_7 provides the required meter calibration.

Amplifier A2 is the "zero-crossing" detector, which recreates the pulse-duration-modulated waveform, as sketched in Figure 3.34. This zero-crossing detection is simply achieved by operating amplifier A2 without a feedback resistor, so that its output is always at either the (+) or the (-) saturation limit. Acting as a voltage comparator, it switches state when the (-) input crosses through the nominal zero

voltage at the (+) input. In practice, a slight hysteresis is provided by resistors R_5 and R_6 to prevent false transitions due to minor noise fluctuations of the input signal. The polarity sense of periods T_1 and T_2 have been chosen for convenience in following circuits.

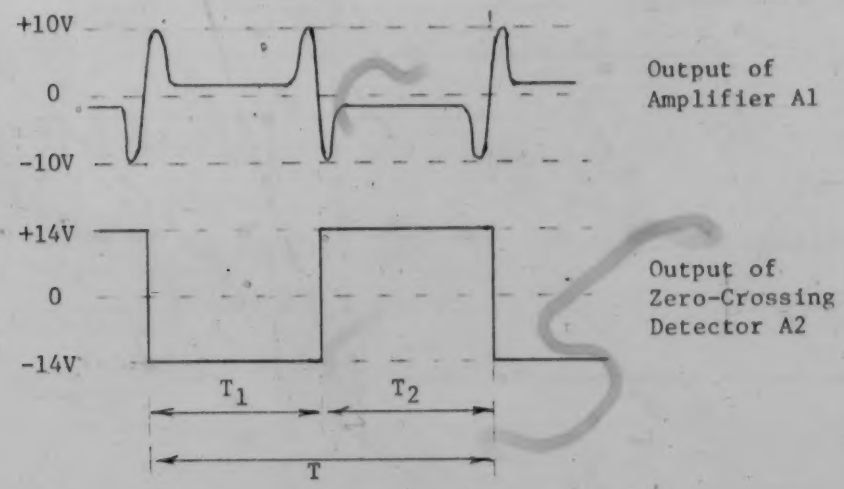

Figure 3.34 Zero-Crossing-Detector Waveforms

3.4.2 MEASUREMENT OF PERIODS T_1 AND T_2

Direct time measurements are made of the pulse-durations T_1 and T_2. With a pulse waveform available at the output of the zero-crossing detector, with constant-voltage positive and negative limits, an operational-amplifier voltage integrator can be used to make a very accurate pulse-duration measurement. The typical arrangement is shown in simplified form in Figure 3.35(a). Note that in this drawing, the integrator-reset and the sample-and-hold switches are sketched as

simple contact points, although as detailed in Figure 3.36, solid-state switches (junction field-effect transistors) are actually used.

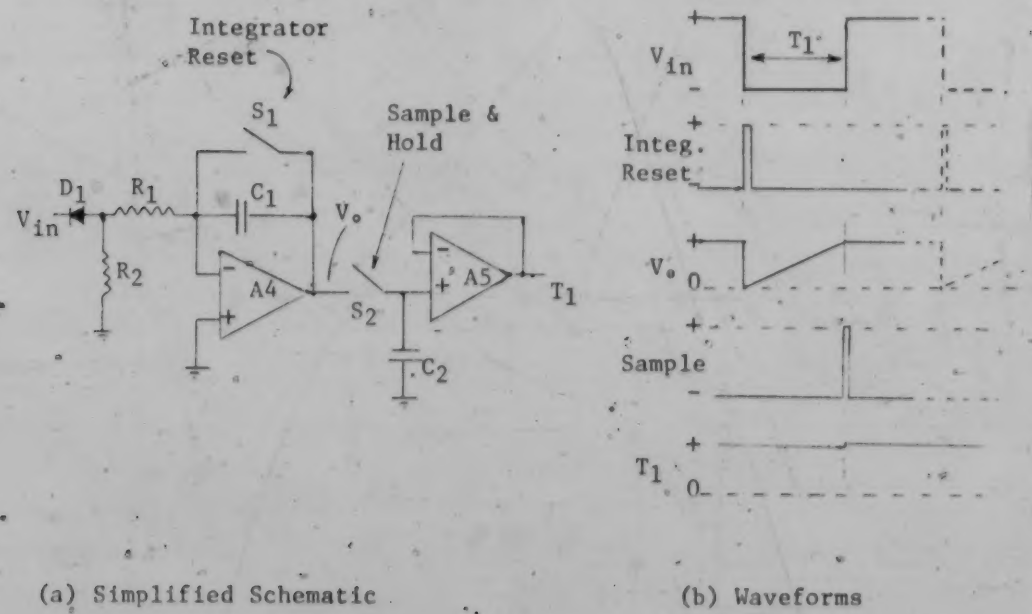

(a) Simplified Schematic (b) Waveforms

Figure 3.35 Typical Period Measurement

Referring to the above sketches, note that the negative transition of V_{in} (the output of the zero-crossing detector) is taken as the start of period T_1, and is used to generate an integrator-reset pulse. This pulse actuates switch S_1 (turns a FET switch ON) which "resets" the integrator by discharging capacitor C_1. The negative voltage level of V_{in} (via diode D_1 to ensure that only this portion of the waveform is related to the measurement of the period T_1) is integrated for the period T_1, and develops a positive ouput-voltage V_o. This integrator-output voltage is a linear function of time, since V_{in} is a constant, with the

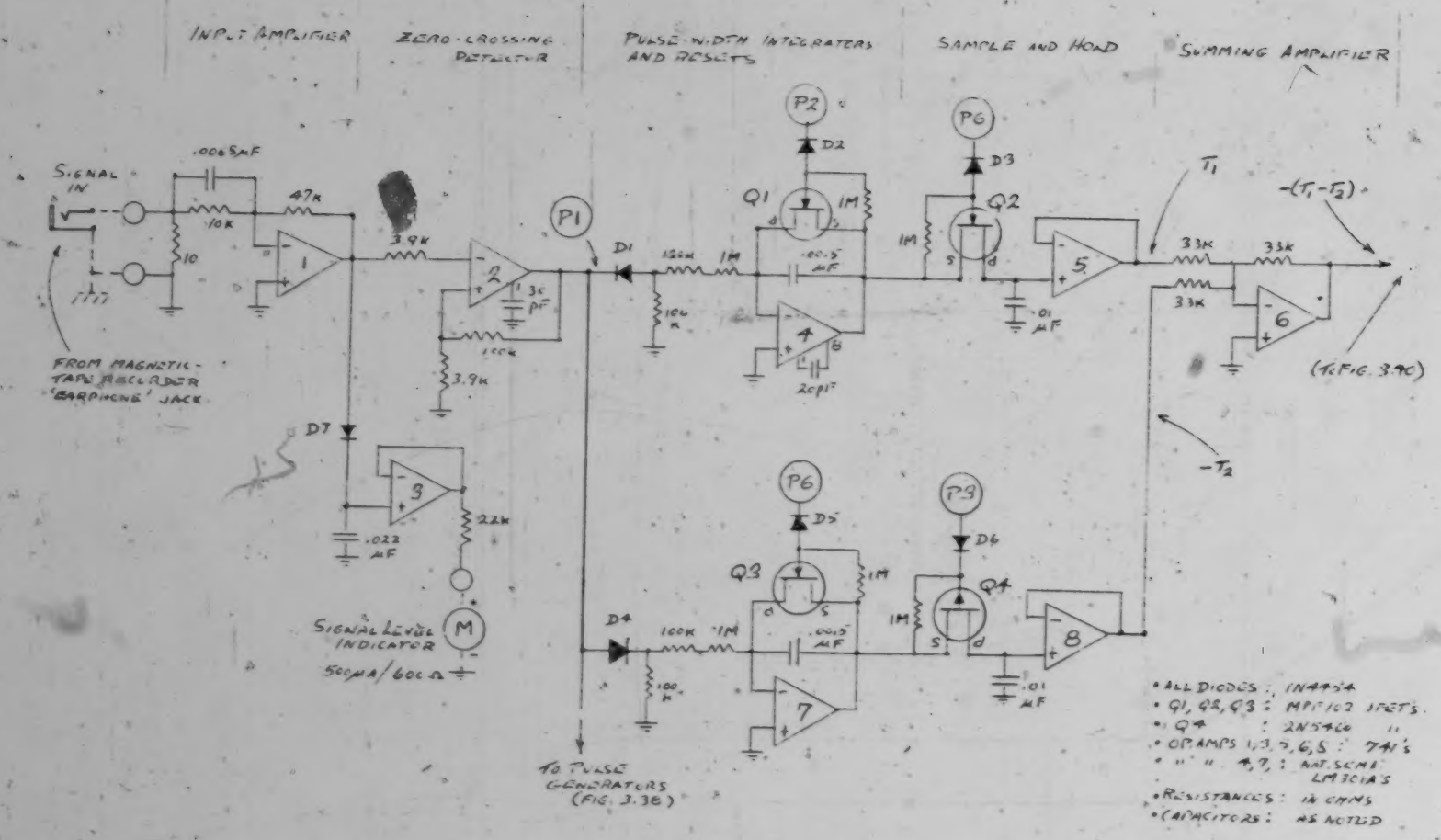

Figure 3.36 Schematic: Pulse-Duration Demodulator

value of V_o described by the relation:

$$V_o(T_1) = -(V_{in} - V_{diode})\frac{T_1}{R_1C_1} + V_o(0)$$

which for T_1 = 500 μsec, with typical RC component values as noted in Fig. 3.36, and with an ideal reset to $V_o(0) = 0$, can be evaluated as:

$$V_o \simeq \frac{(13.4)(5\times10^{-4})}{(1.12\times10^{6})(1.5\times10^{-9})} \simeq 4.0 \text{ Volts.}$$

Since this V_o is directly proportional to T_1, V_o becomes a linear voltage analog of the period T_1 as it varies from 150 μsec to 850 μsec.

The positive portion of V_{in} (which represents T_2) is effectively disconnected from this integrator by the diode D_1, leaving the integrator input voltage at zero via resistor R_2, so that the output V_o remains constant. The positive transition of V_{in} is used to generate a "sample-and-hold" pulse, which momentarily closes switch S_2, which charges capacitor C_2 to the voltage V_o. Note that the change in voltage on C_2 may only have to make up for the charge loss during the preceding period T, or it may be appreciably different if the value of V_o has been changed due to the modulation of period T_1. Amplifier A5 is arranged as a unity-gain voltage follower with its high-impedance input monitoring the voltage on capacitor C_2 with minimum charge loss during a period T.

This sequence of period T_1 measurement and the storage of its voltage analog on capacitor C_2 is repeated during each cycle of the PDM input waveform V_{in}, i.e., at the 1 kHz PDM repetition rate. The output of voltage-follower A5 is therefore essentially a "continuous" voltage

proportional to the pulse duration T_1. As the duration of T_1 changes in response to modulation, the output of amplifier A5 "tracks" its changing value as monitored by the 1000 samples/sec supplied by the integrator A4. A small 1-kHz ripple will of course be present on the signal at the output of amplifier A5 due to a trace of charge loss from capacitor C_2, and due to any ΔT_1 between succeeding samples.

Period T_2 is measured in a similar manner, but the decoupling diode is reversed so that only the positive periods of V_{in} are used by its voltage integrator.

The total period T is measured separately, and is discussed under Section 3.4.4.

It might be noted that this demodulation method is much more effective than the usual sharp-cut-off low-pass filter used for PDM demodulation, especially in terms of its transient response. The sample-and-hold ripple at 1 kHz is more than 70 dB down from its source magnitude as the PDM waveform V_{in}, and a full-scale modulation shift can be tracked in one or two samples, giving a rise time of 1 msec to 2 msec, with no waveform overshoot.

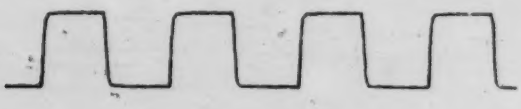

Reproduction at the Demodulator Output of a Recorded 10-Hz Square Wave.

Figure 3.37 Square-Wave Response of the PDM System

The above chart record shows a reproduced 10-Hz square wave, from modul-

ator input, via a magnetic-tape record, and back through the demodulator to a recorder.

Referring to the detailed schematic Figure 3.36, note that the $(+T_1)$ and the $(-T_2)$ voltages are summed by amplifier A6, whose output voltage therefore represents the signal $-(T_1 - T_2)$. Since the measurement channels for periods T_1 and T_2 are identical except for polarity, it is evident that if $T_1 = T_2$ representing zero modulation, then the output of amplifier A6 will be zero as required.

3.4.3 RESET AND SAMPLE PULSES

All reset and sample pulses are directly or indirectly derived from either the leading or the trailing edges of the PDM waveform, as regenerated by the zero-crossing detector A2.

As a specific group of functional circuits, these are detailed on a separate schematic Figure 3.38.

The duration of an integrator-reset or a sample-and-hold pulse is nominally 10 μsec, which is roughly determined by the time constant of the input RC coupling network (a 150 pF capacitor and a 68K resistor). Note that the pulses labelled (P4) and (P5) are derived from the trailing edges of the (P3) pulse, rather than directly from the (P1) waveform. This is necessary, since the functions controlled by pulses (P2) and (P3) must be completed before the functions controlled by pulses (P4) and (P5) can begin. All pulses have ±14V levels: the positive pulses are used to turn ON the type MPF-102 N-channel junction-FET gates, while the negative pulses are used to turn ON the type 2N5460 P-channel FET's.

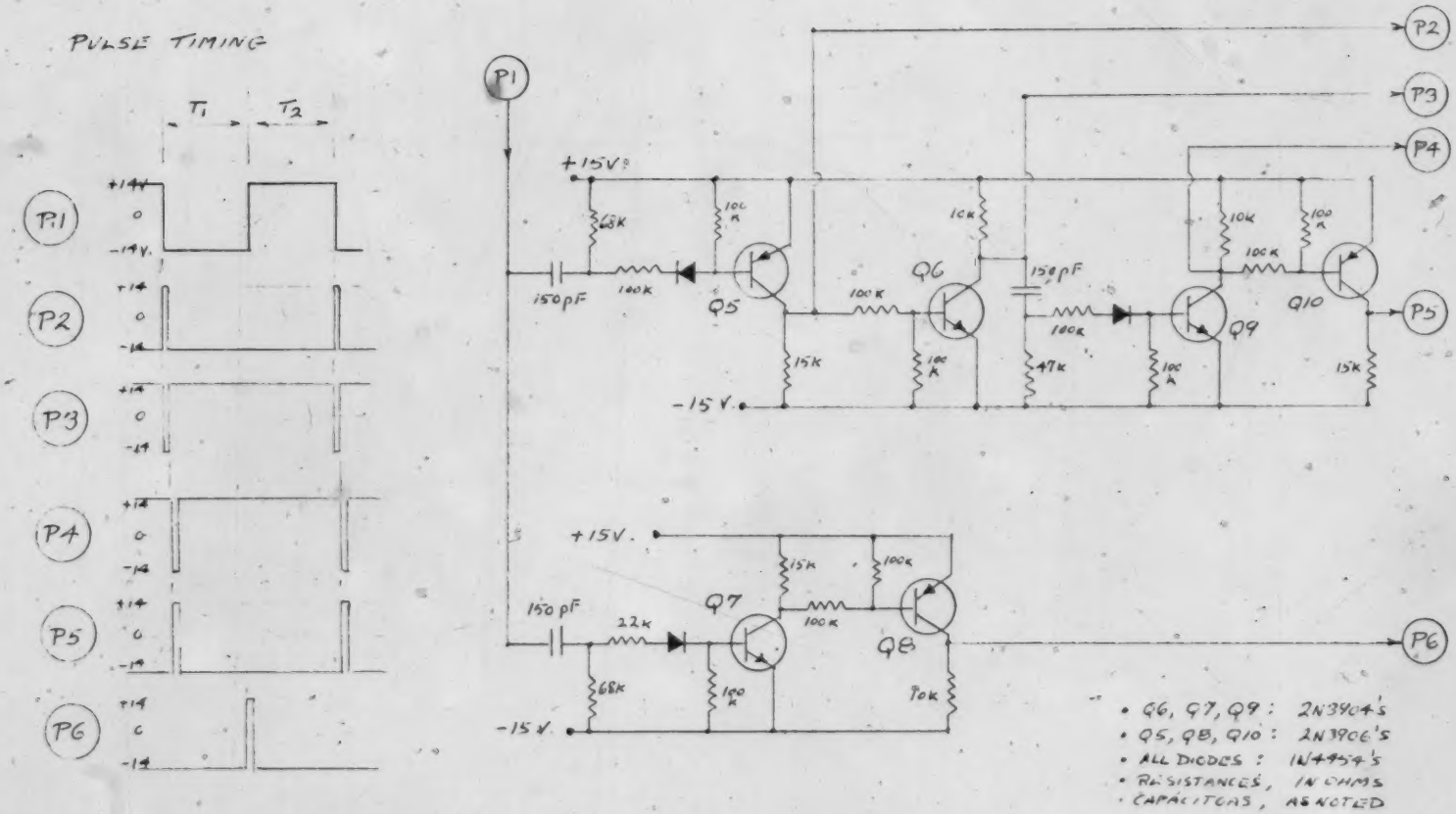

Figure 3.38 Schematic: Generation of Reset and Sampling Pulses

3.4.4 TAPE-SPEED COMPENSATION

The circuits detailed in Figure 3.40 provide the compensation for tape-speed variations, using the method discussed in Section 2.4.4 (the generation of a signal proportional to $(T_1-T_2)/T$). The basic waveform relationships are sketched below as Figure 3.39.

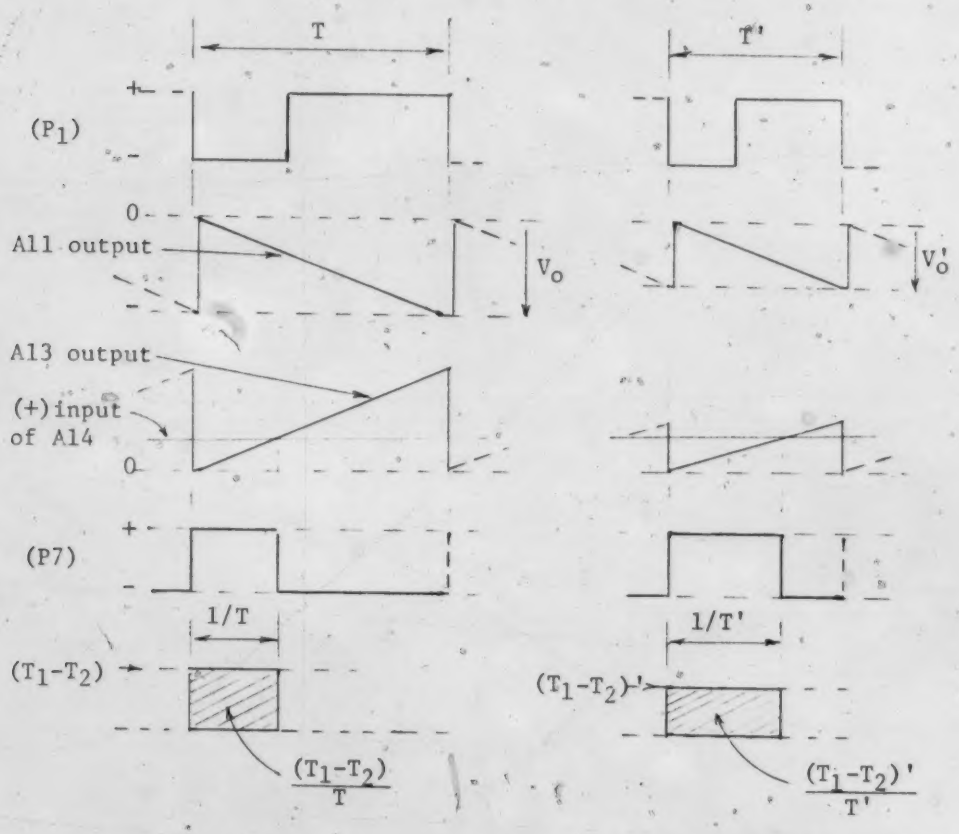

(a) "Normal" Tape Speed (b) Higher Tape Speed

Figure 3.39 Tape-Speed Compensator Waveforms
(refer to text for full discussion)

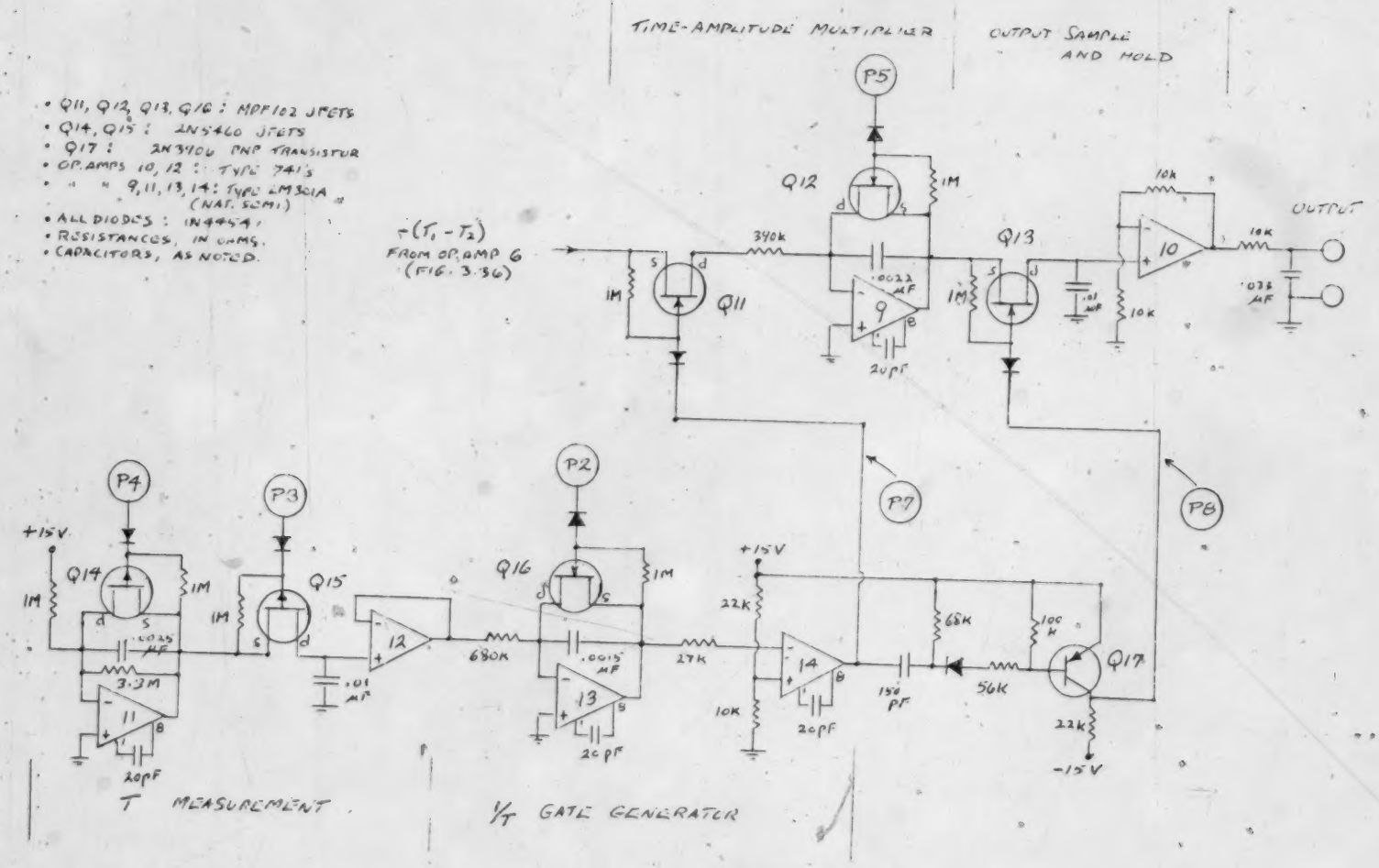

Figure 3.40 Schematic: Tape-Speed Compensator

The total-period T is measured independently of the T_1 and T_2 measurements. While it is true that T is already known implicitly as the sum of T_1 and T_2, the combined timing errors lead to a value of T which is not sufficiently stable to use in tape-speed compensation.

Referring to Fig. 3.40, amplifier A11 is arranged as a voltage integrator which produces a negative-going ramp of fixed slope. At the end of each period T, sample-pulse (P3) gates the value to a storage capacitor, with the voltage "read out" as V_o by voltage-follower A12. (Fig. 3.39, second row from the top, shows the relevant waveforms and their time relationship.) As soon as this sampling is complete, pulse (P4) resets the integrator to zero, and the measurement cycle repeats.

The "current" value of T (the voltage V_o) is the input to a second integrator A13, whose output is therefore a positive-going ramp whose slope is proportional to the period T (the longer the period T, the more negative is V_o, and the steeper is the output ramp from A13).

The ouput ramp from integrator A13 is applied as a sweep voltage to the (-) input of voltage-comparator A14; the (+) input is held at a fixed +5V. The output of A14 is therefore a waveform with the positive-pulse width related to the slope of the sweep voltage at its (-) input: the steeper the slope, the less time required for the sweep to rise from 0V to the +5V reference level, at which time the output changes state. If the period T increases, the pulse-width (P7) decreases and is proportional to 1/T (3rd and 4th row waveforms of Fig. 3.39).

The FET switch Q_{11} and the integrator A9, constitute a "time-amplitude" multiplier. In this case, the amplitude of the input voltage represents $-(T_1-T_2)$ and it is integrated for the time 1/T. The output

of integrator A9, at the end of the (P7) pulse, is therefore proportional to $(T_1-T_2)/T$ and this value is "sampled" by pulse (P8), stored on a hold capacitor, and read out by voltage-follower A10.

Figure 3.39(a) sketches this sequence for a "normal" period (T), with the output of integrator A9 being proportional to the area of the shaded rectangle (bottom row). Figure 3.39(b) represents the sequence during a tape-speed increase, which has slightly reduced the total period (T). However, the shaded rectangle now has longer duration but reduced amplitude, so that area is a constant (for this particular value of $T_1 - T_2$). The design performance is a very close approximation to:

$$\frac{T_1-T_2}{T} = \frac{(T_1-T_2)'}{T'}$$

This measurement and integration sequence is repeated for each cycle of the PDM waveform (P1), which as already noted, has a repetition rate of 1 kHz. The demodulated PDM signal is now a pseudo-continuous analog voltage at the output of amplifier A10. This output voltage can of course be scaled as desired by selecting the appropriate value of the feedback resistor (from the output of A10 to the (-) input). A simple output RC low-pass filter has been used to reduce the trace of 1-kHz "sampling" noise, since the recording system used was capable of reproducing it.

The effectiveness of such a tape-speed-variation compensation system can be demonstrated by introducing a "synthetic" PDM waveform as (P1) in place of the output of amplifier A2 (Fig. 3.36). This waveform was derived from a standard "function generator", which can provide

an asymmetrical pulse waveform, with a swept frequency; the equivalent of a regenerated PDM waveform from a tape recorder with a very bad tape-speed variation.

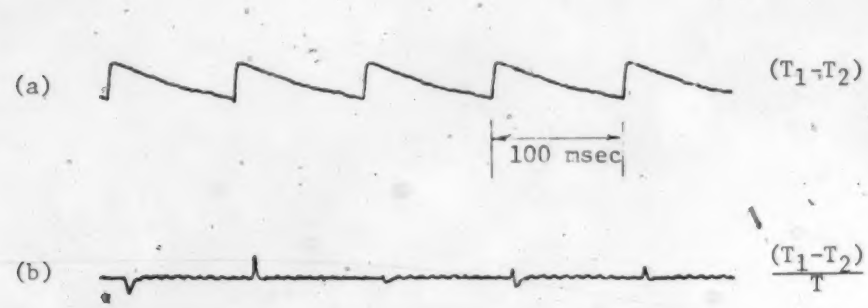

Figure 3.41 Tape-Speed-Variation Compensation

For the above test, the pulse ratio was set at $T_1 = 0.8\ T$, and the frequency sweep was from 1 kHz to 1.2 kHz in 100 msec; a 20% frequency shift. Figure 3.41(a) shows the expected change in the demodulated signal (T_1-T_2), (recorded from the output of amplifier A6, Fig.3.40, with the D.C. component suppressed). Figure 3.41(b) shows the "compensated" signal $(T_1-T_2)/T$ at the output of amplifier A10. The recorder gain for (b) was ten times that used for (a), to show the extent of the compensation. (The "spike" disturbances in the compensated signal of Fig. 3.41(b) occur during the frequency-sweep "flyback", which generates an equivalent tape acceleration which exceeds the compensator tracking rate. This is over 250 times the maximum tape acceleration expected in even a poor tape recorder, which might have a 2% speed change at a 10-Hz "flutter" rate.

It should be noted that this particular characteristic of pulse-duration modulation has long been recognized, and under other names (such as pulse-ratio modulation) has been used for various approaches to tape-speed "wow-and-flutter" compensation [68],[69].

3.4.5 POWER SUPPLY

The demodulator has been designed with an A.C. operated power-supply, on the assumption that playback of a signal tape and demodulation of the PDM signal can be done under "base-station" conditions where A.C. power is available.

The detailed schematic is given as Figure 3.42. This power supply provides +15V and -15V relative to a common ground, for use by integrated-circuit operational amplifiers. Since the load is essentially constant, adequate voltage regulation is provided by Zener diodes and series transistor regulators. FET current regulators are used to provide constant Zener currents, which improves the effective line regulation.

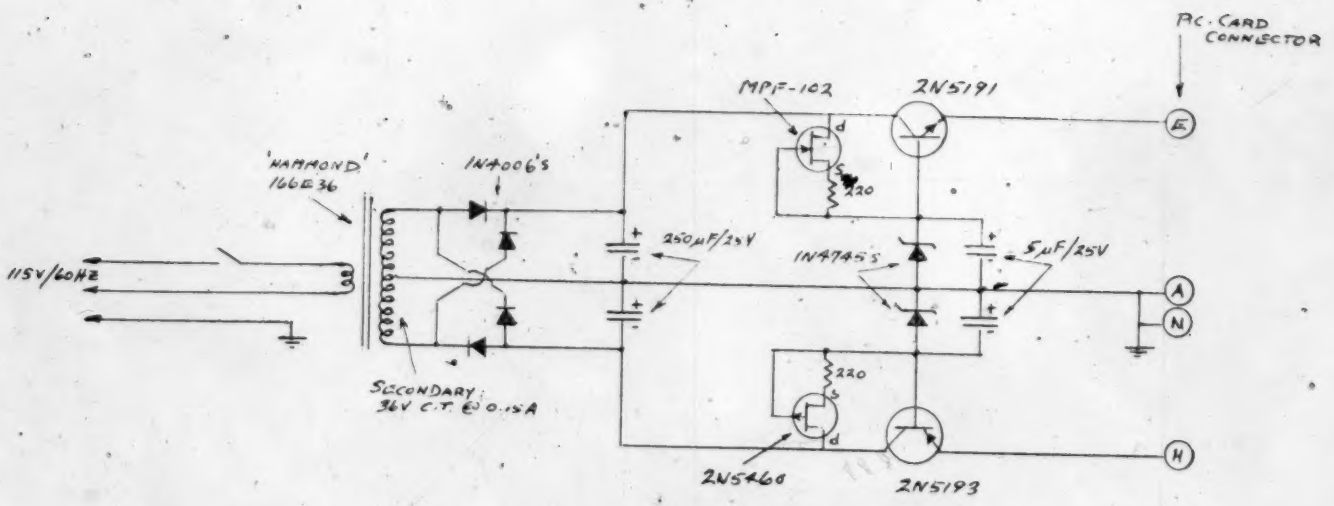

Ripple : <1 mV(p-p) @ 50 ma.

Line Reg: .08%/Volt

Load Reg: .13% for 0-50 ma load change.

Figure 3.42 Demodulator Power Supply

3.5 PHYSICAL-DESIGN DETAILS

The physical design of this prototype system has been largely dictated by the intended portability and component availability. For the sake of completeness, the following notes and sketches are included, but it should be appreciated that they relate only to this prototype system, which was intended to evaluate a number of design concepts. Many physical-design alternatives are of course possible, and could be equally acceptable.

(a) The E-FIELD SENSOR assembly is sketched in Figure 3.43. The physical dimensions were determined by the convenient size of the "Hammond"#1442-15 chassis (10"x6"x1"). This provides a sensor-plate area which is large enough to generate a useful signal voltage (a larger plate would improve the signal-to-noise ratio) and small enough to fit into an attache case.

(b) The AMPLIFIER-MODULATOR system was designed to fit into a standard black-phenolic "meter case" (6 3/4"x 5 1/4"x 2 15/16"). Figure 3.44 shows the panel arrangement used, the printed-circuit board location and the battery space. Some care is required to mount all of the components of Figure 3.21, 3.30, and 3.31 onto a single-sided PC board of the dimensions shown. The shield behind the PC board is imperative to prevent local pick up of 60-Hz interference by the high-impedance notch-filter circuits. Access holes must be drilled through this shield to permit frequency and null adjustments.

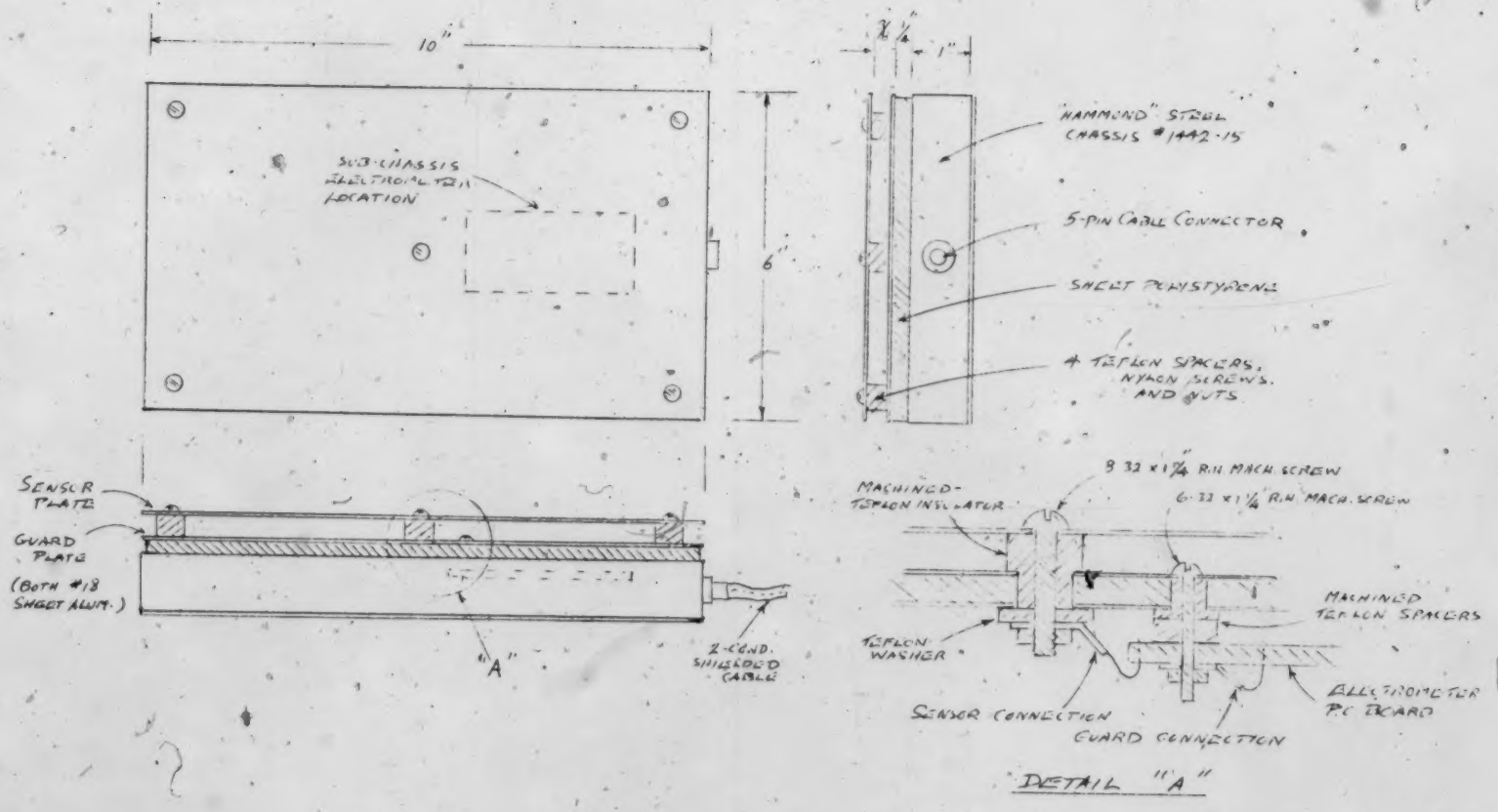

Figure 3.43 E-Field Sensor: Physical Design

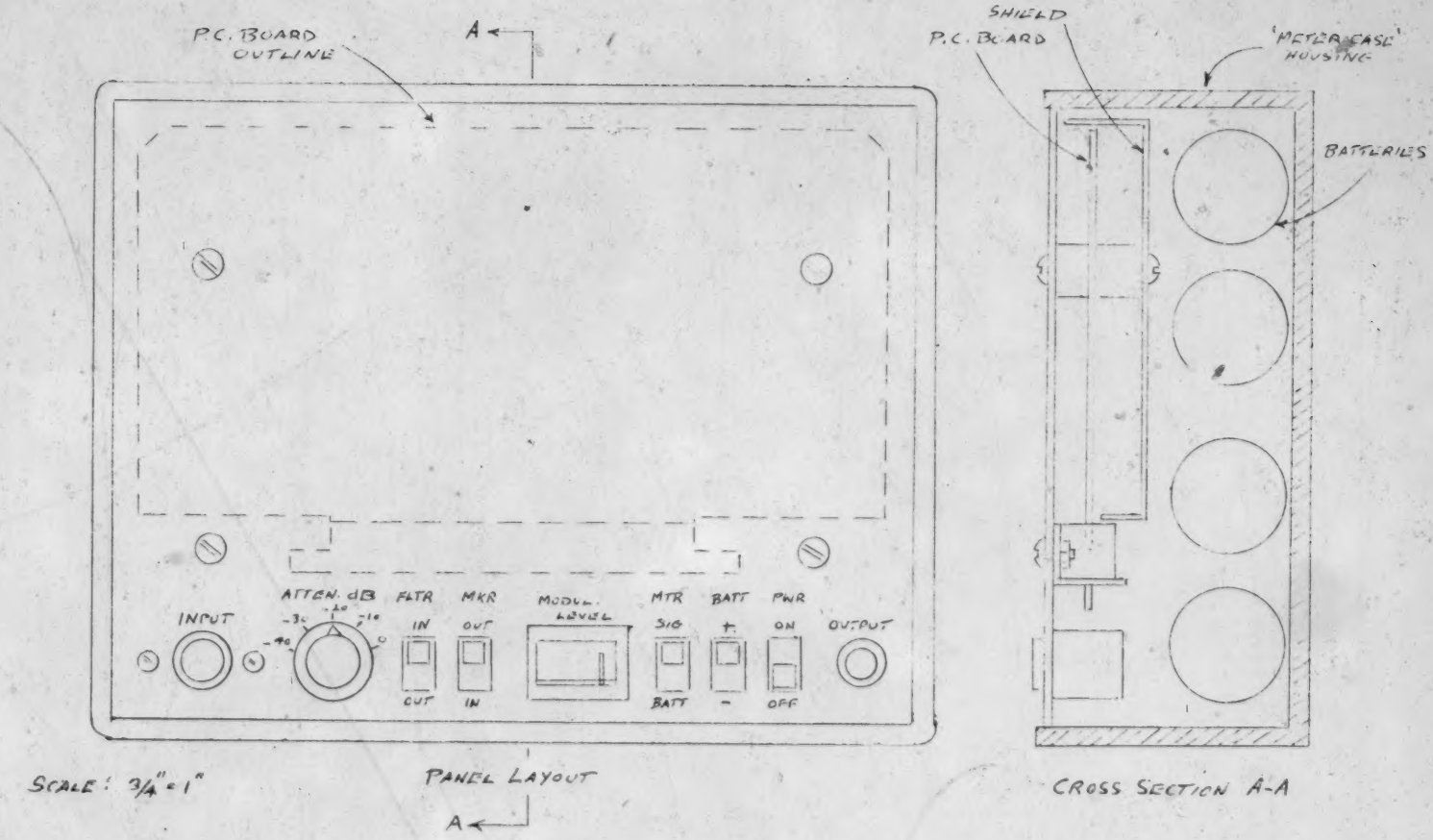

Figure 3.44 Amplifier-Modulator: Panel Layout

(c) The PDM DEMODULATOR system is also housed in a meter case, with the physical layout as shown in Figure 3.45. The circuit components of Figures 3.36, 3.38, and 3.40 are mounted on the plug-in printed-circuit board. The rectifier and regulator components of Figure 3.42 are mounted on a separate PC board secured to a sub-panel bracket. The output "banana jacks" are spaced to accept standard molded "General-Radio" twin-plug connectors.

The following are the nominal weights of the system sub-assemblies:

E-field sensor and 40' of cable	2.5	lbs
Amplifier-modulator (with batteries)	2.5	"
Portable tape recorder (with batteries)	4.5	"
Attache' case	3.5	"
Field-portable system	≈ 13	lbs
PDM demodulator	2.0	"

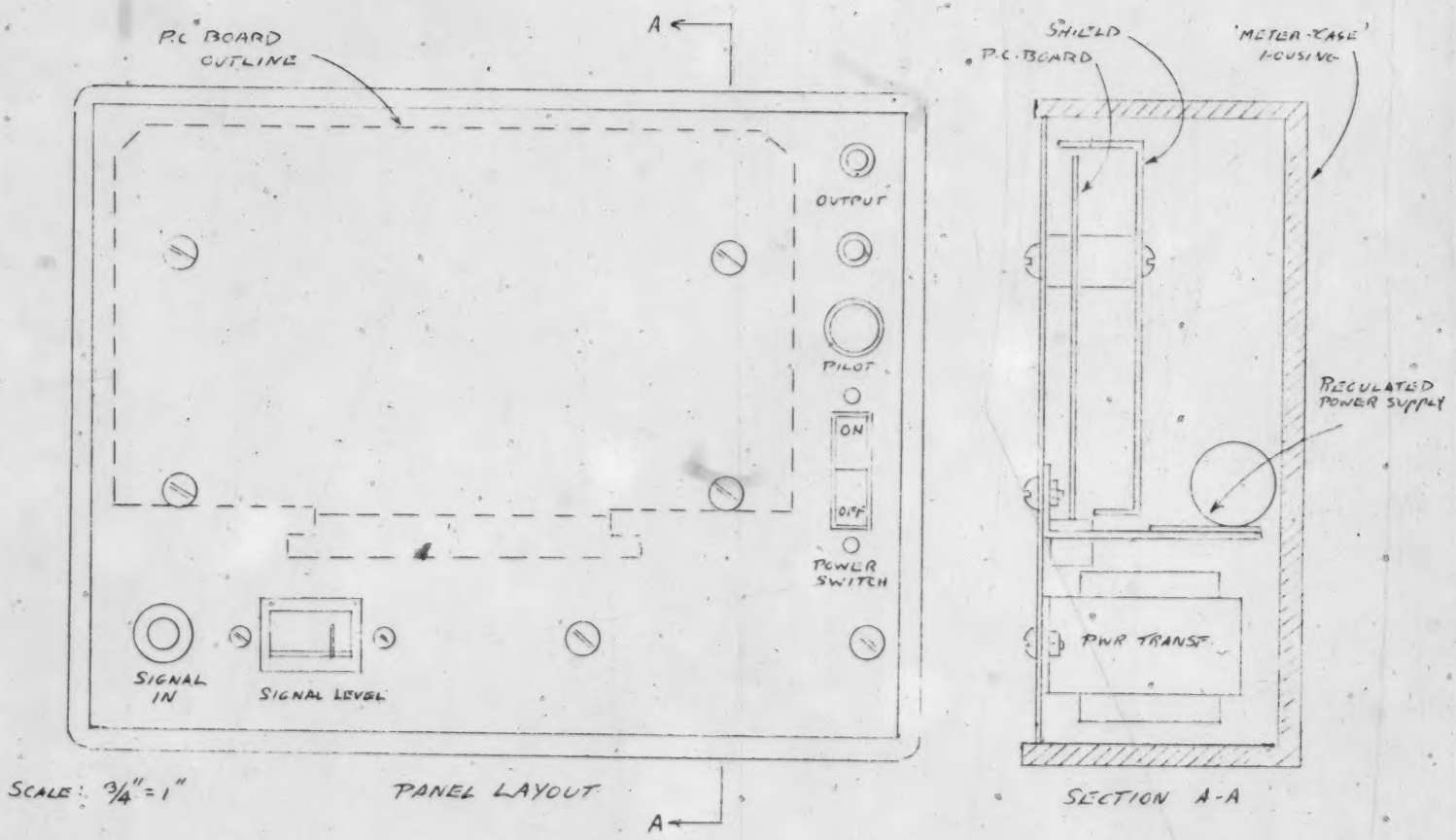

Figure 3.45 Demodulator: Panel Layout

3.6 THE MAGNETIC-TAPE RECORDER

The portable magnetic-tape recorder used with this system is a "Realistic" Model CTR-20 (listed as "Radio Shack" Cat. No. 14-873). The nominal frequency response is given as 60-10,000 Hz, and has been adequate for the required time resolution of the PDM pulse edges.

During recording, the output signal from the amplifier-modulator is introduced (via a shielded patch cord) into the "AUX" input of the tape recorder. The optimum recording level for the differentiated PDM signal appears to be at approximately -10 dB.

During playback, the recorder output signal is taken from the "EAR" jack, and introduced (again via a shielded patch cord) into the input jack of the PDM demodulator. Proper playback level (to prevent input-amplifier overload) is determined by observing the signal-level indicator on the demodulator panel.

As with all magnetic-tape systems, some problems related to signal "drop-outs" have been encountered. If proper zero crossings are not developed in the demodulator, valid T_1 and T_2 pulse widths cannot be established, and the output signal will be invalid for one or more samples. These effects are illustrated in Figure 3.46. The recording of Figure 3.46(a) originated from the first few feet of tape of a well-used cassette. A visual check showed small "crease" marks and "burnished" spots, which were presumably made by the drive-spindle rotation on a momentarily-stalled tape, probably during repeated replays and rewinds of this section. Figure 3.46(b) shows the signal derived from a later section of the tape, but with a somewhat low setting of the recorder volume control, leading to marginal control of the zero-crossing detector.

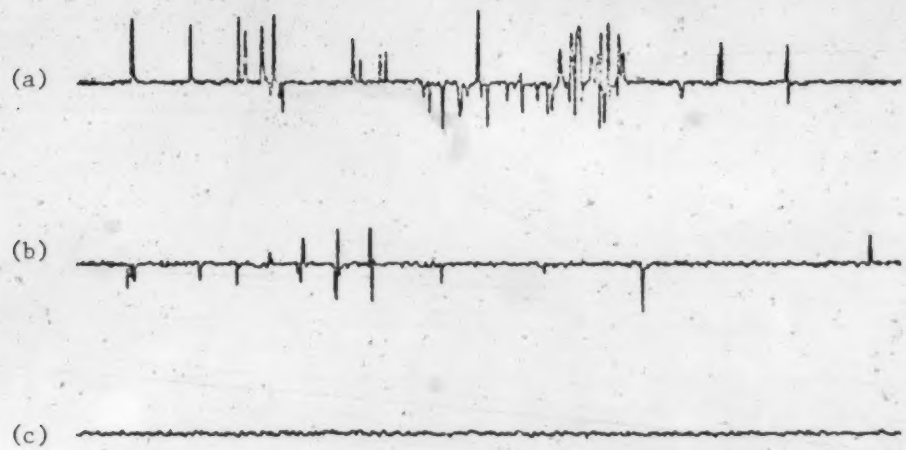

(a) Poor section of tape (worn spots).
(b) Good tape, but low playback volume.
(c) Good tape and proper playback volume.

Figure 3.46 Signal "Drop-Out" During Tape Playback

The recording of Fig. 3.46(c) was from the same section of tape as was Fig. 3.46(b), but with the volume-control setting increased until proper switching of the zero-crossing detector was observed.

Any good quality magnetic-tape cassette appears to be adequate, providing due care is exercised to prevent the physical blemishes noted above.

It should be noted that the presence of a few drop-outs in an otherwise good recording need not destroy the value of the record. The drop-outs rarely last for more than a few samples and typically produce output-signal discontinuities which are recognizable; the tape-signal

drop-out results in an immediate period-measurement error (of T_1, T_2 or T) which is sampled and produces an output-signal discontinuity which has a rise time limited only by the output RC filter and the recorder writing speed. The observed drop-out artifact is typically of several-volts magnitude and 2-4 msec rise time, which with a chart speed greater than a few inches/sec has a visually-different characteristic from normal ELF signals; thay can therefore be ignored, or the playback can be rechecked with different adjustments. If the signals are digitized for computer data reduction, such invalid drop-out spikes can be detected by a simple algorithm related to their excessive dV/dt, and the invalid points can be dropped and replaced in some acceptable manner (linear interpolation, a running average, etc.).

3.7 SYSTEM TRANSFER CHARACTERISTICS

The transfer characteristics of the system sub-assemblies have been noted in their respective sections. The following notes cover the over-all system characteristics, from incident E-field to the final demodulator output record.

The system frequency response is given in Figure 3.47. The 60-Hz notch width is less than 1 Hz, and the dotted response above 200 Hz is an indication that the effective amplitude response becomes difficult to define as the frequency approaches the 1 kHz PDM repetition-rate.

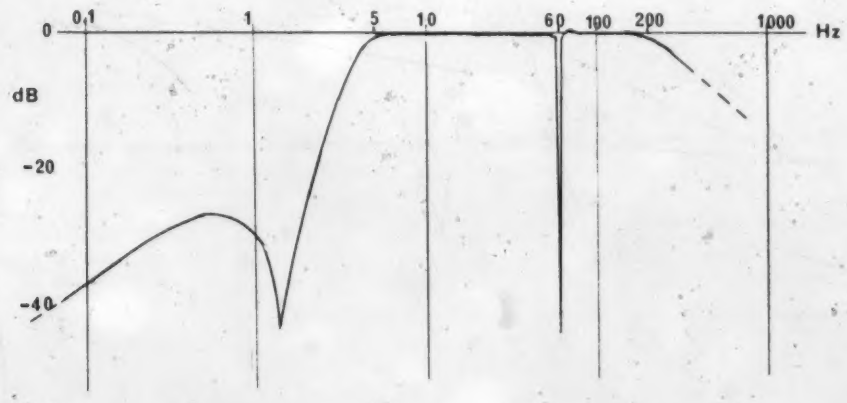

Figure 3.47 System Frequency Response

Although such a frequency-response curve implies a sinusoidal response, this is not true as waveform degradation occurs in a sampled-data system. Above 150 Hz, waveform reconstruction is dependent on the available number of samples per cycle provided by the PDM "carrier"

system. Figure 3.48 shows this loss of waveform reproduction as the number of samples per cycle drops from 10 samples/cycle at 100 Hz, to only 2 samples/cycle at 500 Hz. The output RC filter does provide a slight smoothing of the sampling steps without excessive slowing of the pulse rise time.

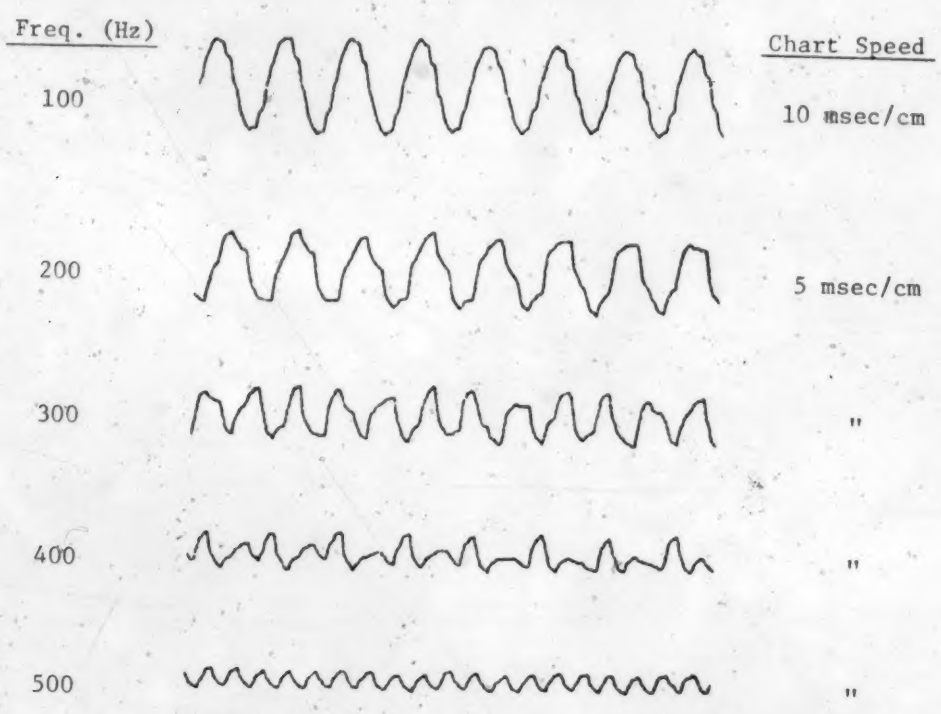

Figure 3.48 Sampling Rates and Waveform Reconstruction

The system pulse response is of course degraded by the low-frequency roll-off below 5 Hz, which in the time domain implies a time constant of about 30 milliseconds. Figure 3.49 shows the system pulse response from incident E-field signal, through the PDM-modulation process,

magnetic-tape recording and playback, to demodulation and chart recording.

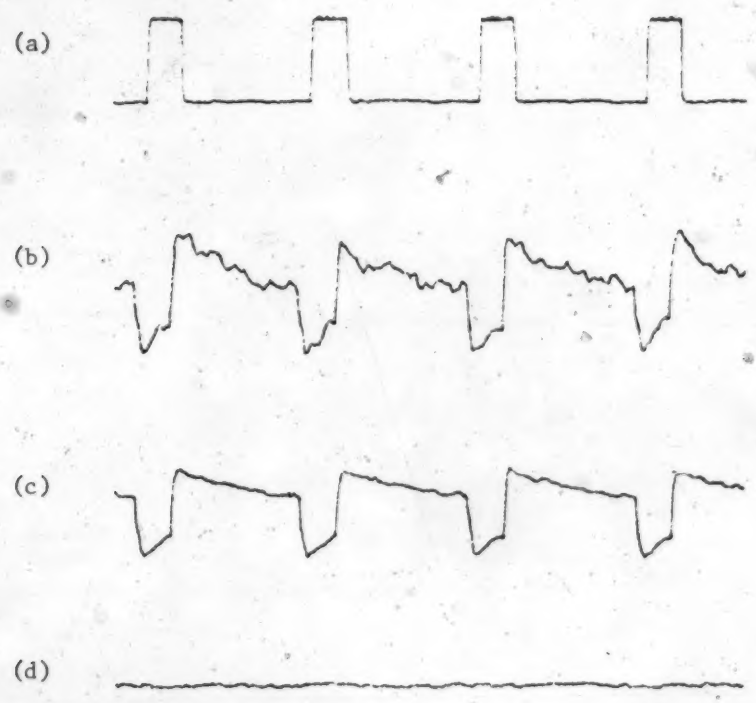

(a) Input waveform: 10 msec pulses.
(b) Demodulator output: vert.= 5V/cm, hor.= 20 msec/cm.
(Input E-field pulses = 10 mV/m; Atten. = 0 dB)
(c) Demodulator output (scale factors as in (b) above)
(Input E-field pulses = 100 mV/m; Atten. = -20 dB)
(d) Demodulator output (scale factors as in (b) above)
(Input sensor shielded; Atten. = -20 dB)

Figure 3.49 System Pulse Response

Figure 3.49(a) is the voltage waveform which establishes the incident E-field at the sensor plate. Figure 3.49(b) displays the full system sensitivity, with a 10 mV/m E-field pulse of 10 milliseconds duration recorded with 0 dB attenuation. Figure 3.49(c) reproduces a similar pulse but with an amplitude of 100 mV/m recorded at -20 dB attenuation. Figure 3.49(d) shows the system noise level, at an attenuator setting of -20 dB but with a zero input signal (an electrostatically-shielded sensor assembly). Note that with a positive voltage pulse applied to a calibrating plate mounted above the sensor plate, the incident E-field is negative. The system output has been arranged so that the strip-chart recording polarity agrees with the polarity of the incident E-field.

Figure 3.49 can also be used to calculate an over-all transfer characteristic, as shown in Figure 3.50.

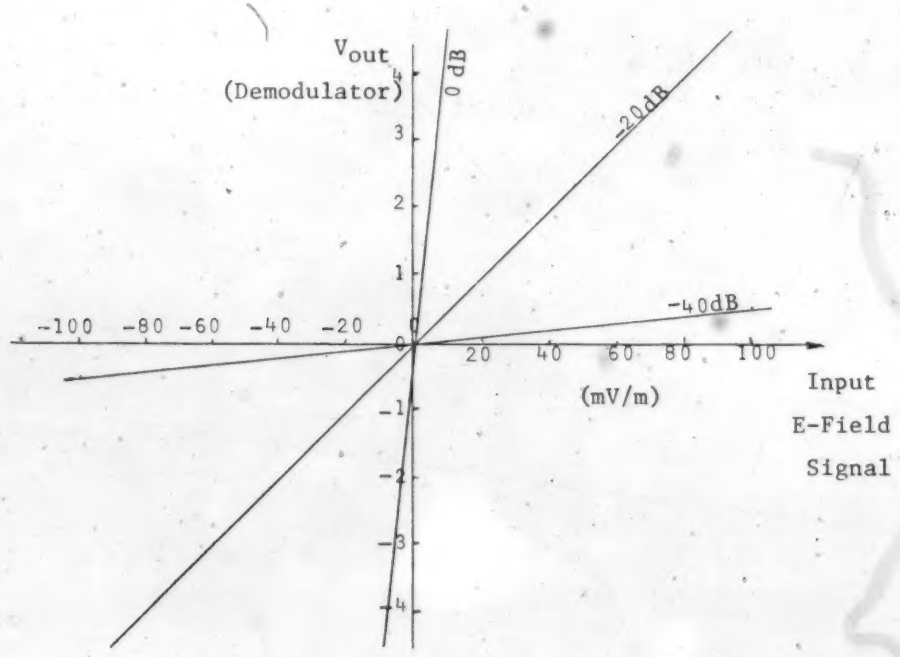

Figure 3.50 Input-Output Transfer Characteristics

Figure 3.50 provides an over-all system calibration: the demodulator output voltage versus the amplitude of the incident E-field signal (assuming the frequency is within the 5 Hz-200 Hz pass-band) for various settings of the amplifier-modulator attenuator switch.

CHAPTER 4

CONCLUSION

4.1 TYPICAL FIELD RECORDS OF ELF SIGNALS

As noted in the introduction to Chapter 3, the availability of a Hewlett-Packard Model 5480A Signal Analyzer has permitted the reproduction of field records with a wide choice of vertical sensitivity and horizontal time scaling. The resolution however is limited by the 1000 samples/scan, and in some of the following illustrations of expanded-scale X-Y recordings this may imply only 50 samples/cm. As a result, the apparent fine structure observable is in some cases simply quantization noise and must be interpreted with some caution.

The following pages show typical records of natural ELF signals. The vertical scale is given in terms of mV/m E-field amplitude, and the relevant horizontal time scaling is noted. A few features of interest have been marked, and selected sections have been repeated with an expanded time scale.

These particular records come from a series made at approximately 0800 hrs M.S.T. May 17, 1975, in Mayfair Park, Edmonton, Alberta. This is a river-valley municipal park, located close to the centre of the city, with the actual recording site being an open grassy area some 100 yards away from the nearest roadway and from lighting standards. The sky was cloudless and only a light breeze was blowing. No data are available regarding continental lightning activity for this period.

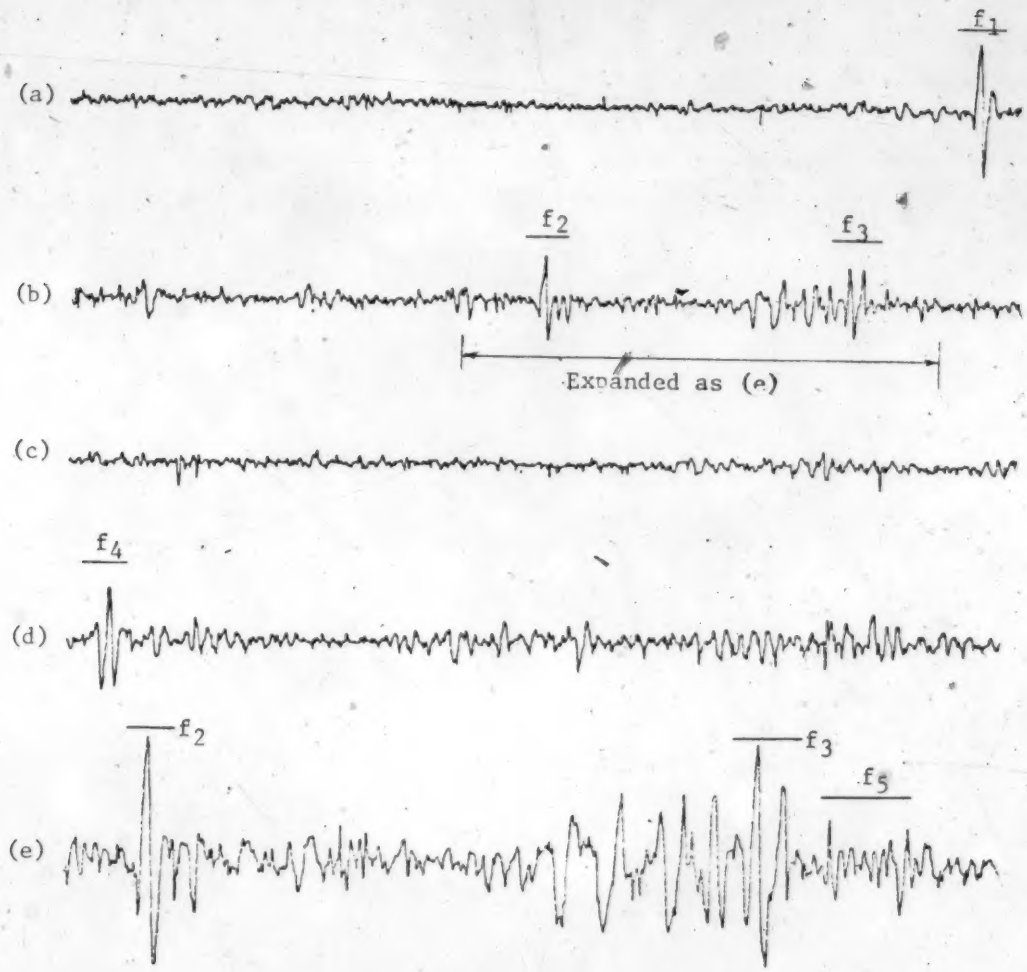

Scaling Data:

(a)	Vert: 40 mV/m/cm	Hor: 1 sec/cm
(b)(c)(d)	Vert: 30 mV/m/cm	Hor: 1 sec/cm
(e)	Vert: 12 mV/m/cm	Hor: 0.5 sec/cm

Features: f_1, f_2, f_3, f_4....typical bursts of 1 or 2 cycles, with a period of about 150 msec., initial deflection may be either positive or negative.

f_5....a burst of oscillations at about 13 Hz, presumably related to the n=2 mode of the Schumann resonances.

Figure 4.1 Typical ELF Field Recordings (Sample #1)

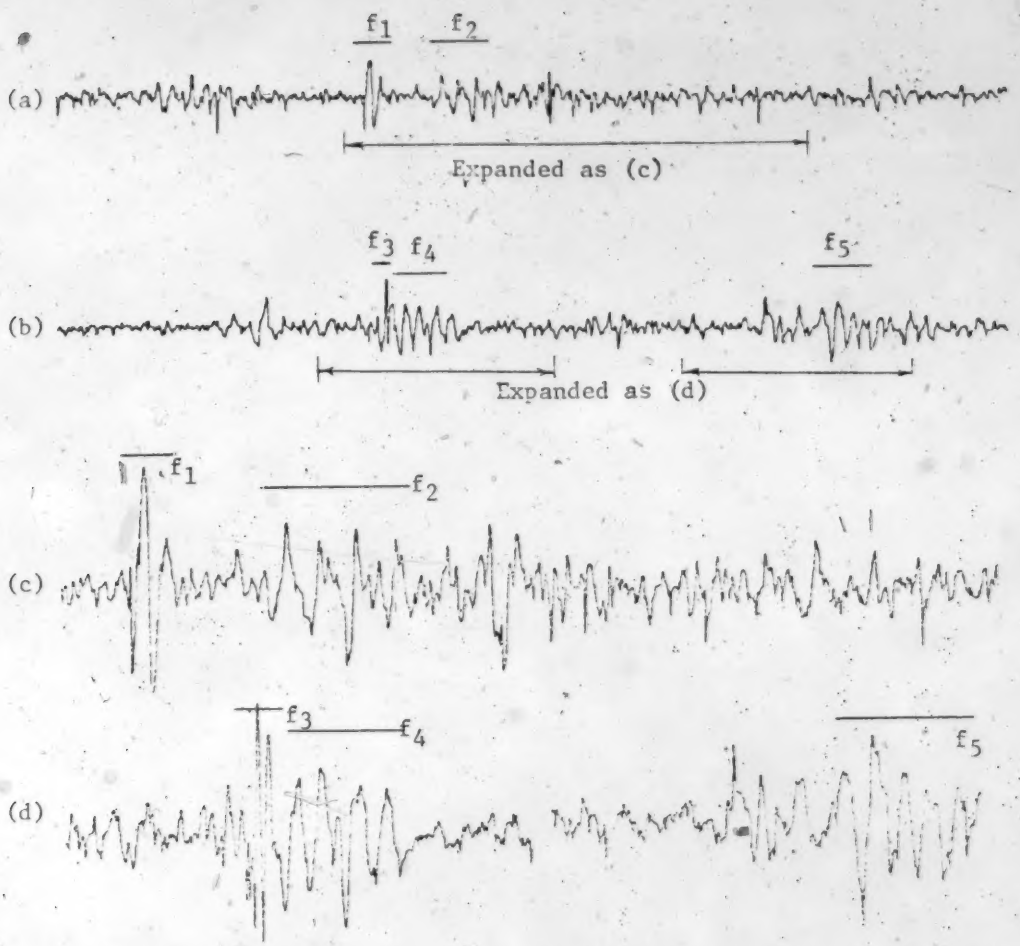

Scaling Data: (a)(b) Vert: 30 mV/m/cm Hor: 1 sec/cm
(c)(d) Vert: 12 mV/m/cm Hor: 0.5 Sec/cm

Features: f_1....short burst similar to f_1,f_2 of Fig. 4.1, at 7 Hz.
f_2...."sawtooth" pattern at about 4 Hz, also noted in other portions of this record.
f_3....short burst similar to f_1, but at about 13 Hz.
f_4,f_5....bursts of several cycles at about 5 Hz.

Figure 4.2 Typical ELF Field Recordings (Sample #2)

The preceding ELF recordings (Figures 4.1 and 4.2) have of course been selected because of their "features" of interest. Minute-to-minute changes in the character of the ELF signals are evident, primarily as changes from relatively-quiet periods (such as in Figures 4.1(a) and (b)) to periods displaying various types of noise-burst activity (such as in Figure 4.2(b)).

The noise bursts recorded in Figures 4.2(c) and 4.2(d) display several characteristics which might be noted. Features such as (f_1) are frequently observed; typically little more than one cycle with a period of about 150 msec (≈6.7 Hz) and presumably related to the n=1 mode of the Schumann resonances. Feature (f_3) is a similar burst but at about 13 Hz (presumably the n=2 mode). In each case, the resonant-mode oscillation is abruptly terminated by an "over-riding" signal having a distinctly different characteristic; in the case of (f_3) the new signal (f_4) consists of several cycles of a damped 5 Hz oscillation. Feature (f_2) is a rough "saw-tooth" waveform with a fundamental frequency of about 4 Hz, and this tendency towards a saw-tooth pattern is noticeable in other parts of the same recording.

The recording samples on the following pages (Figures 4.3, 4.4 and 4.5) were made at the same Mayfair-Park site as those of Figures 4.1 and 4.2, but several months later; at 1300 hrs M.S.T. September 26,1975. Some of the noise bursts on these later records have a greater complexity and generally a somewhat greater amplitude than those of the earlier recordings. There has been insufficient monitoring to offer any comments as to whether these are diurnal or seasonal differences.

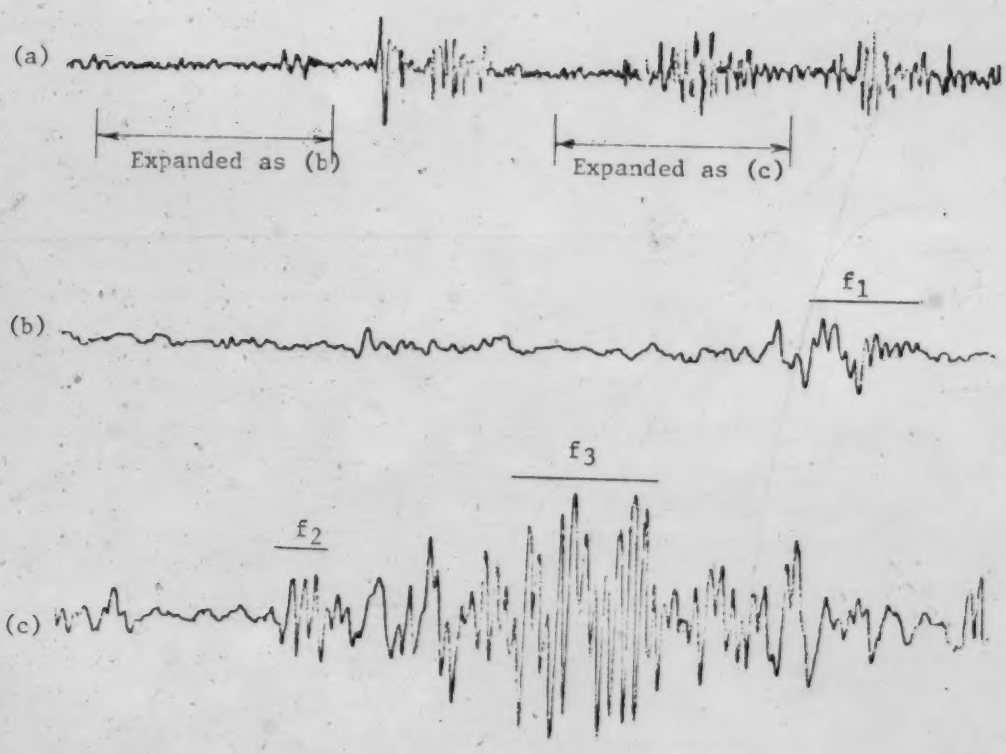

Scaling Data: (a) Vert: 30 mV/m/cm Hor: 1 sec/cm
(b)(c) Vert: 12 mV/m/cm Hor: 0.25 sec/cm

Features: f_1....oscillations at approximately 27 Hz, superimposed on a low-frequency (5 Hz) disturbance.
f_2....several oscillations at about 22 Hz.
f_3....oscillations at about 22 Hz, superimposed on other disturbances.

Figure 4.3 Typical ELF Field Recordings (Sample #3)

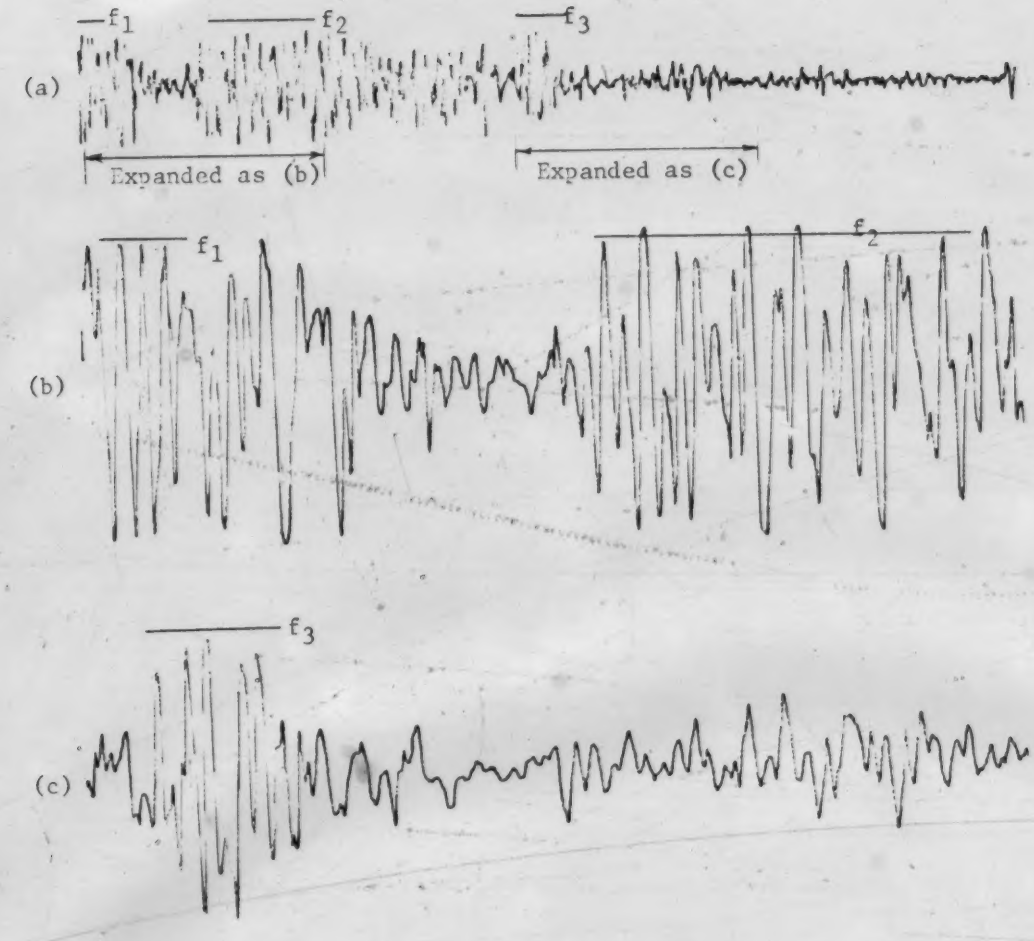

Scaling Data: (a) Vert: 30 mV/m/cm Hor: 1 sec/cm
(b)(c) Vert: 12 mV/m/cm Hor: 0.25 sec/cm

Features: f_1....oscillations at about 13 Hz.
f_2....disturbances with components at 5.7 Hz, 7.3 Hz, 13 Hz, and 20 Hz.
f_3....disturbances at about 13 Hz, but less coherent than the burst noted as f_1.

Figure 4.4 Typical ELF Field Recordings (Sample #4)

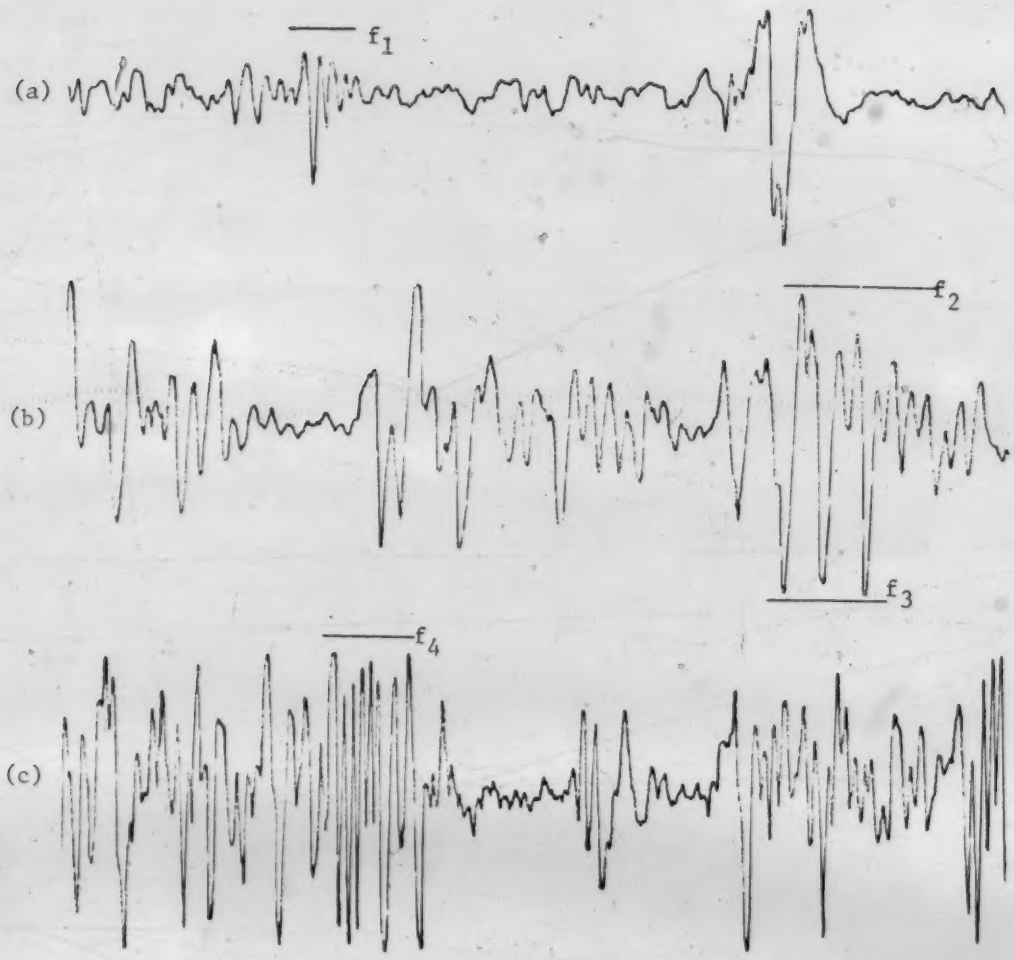

Scaling Data: (a)(b)(c) Vert: 12 mV/m/cm Hor: 0.25 sec/cm

Features: f_1....damped oscillations at about 21 Hz.
f_2....oscillations at 15 Hz superimposed on other disturbances.
f_3....negative impulses at a 6.7 Hz repetition rate.
f_4....oscillations at about 32 Hz.

Figure 4.5 Typical ELF Field Recordings (Sample #5)

In Figure 4.3(b), feature (f_1) appears to be a lightly-damped burst of oscillations at 27 Hz (the n = 4 mode of the Schumann resonances) superimposed on a few cycles of a 5 Hz disturbance. A common excitation source might be presumed because of their time juxtaposition. In Figure 4.3(c), feature (f_2) consists of damped oscillations at about 22 Hz (perhaps the n = 3 mode), and feature (f_3) is a longer burst at 22 Hz superimposed on a low-frequency disturbance, and building up to a higher amplitude for a few cycles.

In Figure 4.4(b) feature (f_1) consists of a burst of damped oscillations at about 13 Hz (the n = 2 mode). Similar components can be seen in feature (f_2) of the same recording but incoherently mixed with disturbances at several other frequencies. Further traces of the 13 Hz oscillation are evident in recording-strip (c) feature (f_3).

In Figure 4.5(a), feature (f_1) is a damped oscillation at about 21 Hz (the n = 3 mode). In recording-strip (b), feature (f_2) consists of 15 Hz oscillations apparently excited by the larger negative impulses which occur at a repetition rate of about 6.7 Hz. These impulses do not appear to be fundamental-mode oscillations since they are not sinusoidal, but the uniformity of spacing and the similarity of their amplitude and shape would imply a common origin. Recording-strip (c) includes bursts of oscillations (such as feature (f_4)) at about 32 Hz (the n = 5 mode).

4.2 COMMENTS

Several comments should be added to the material covered in the preceding chapters, and these comments relate to two specific themes: circuit design details which have been tolerated in the prototype system but are quite evidently not optimum, and secondly the problem of system transient responses and possible signal artifacts.

From the standpoint of further circuit development, the relevant points might be itemized as follows:

(a) The newer high-grade low-noise FET operational amplifiers (such as the Burr-Brown 3523 series, or the Teledyne-Philbrick 1421 series) should be evaluated for use as the electrometer/cable-drive amplifier in the E-field sensor assembly.

(b) The battery drain of the amplifier-modulator module could be considerably reduced by the use of low-current-drain operational amplifiers (such as the RCA CA-6078A) in several locations. Such units could be used in the linear-amplifier stages although their slew-rate limitations would probably rule out their use in the pulse circuits.

(c) The temperature stability of the prototype system has not been evaluated. Voltage-offset drifts are a minor concern since the closed-loop gains are relatively low, and integrator drifts lead only to D.C. shifts which are zeroed out during playback and the generation of a chart recording. The system has been used in the field over a temperature range of 0°C - 25°C with no evidence of trouble except an occasional sign of null shift in the 60-Hz

notch filter. Metallized-film polycarbonate capacitors with a temperature coefficient of less than 100ppm/°C were used in obviously critical circuits, but a complete review of the system temperature stability would be useful.

(d) It would be interesting to explore the added capabilities of a "stereo" portable recorder. A second signal with a pass band from 200 Hz - 10 kHz could be extracted from the electrometer amplifier, and this could be directly recorded as an analog signal on the second recorder channel. On playback, time-correlated ELF and VLF signals would then be available for recording on a 2-pen system.

With regard to system transients and potential signal artifacts, the general problem has already been discussed in Section 2.3, together with examples of pass-band transients generated by filter step and impulse responses. However, a comment should be added in regard to the apparent lack of concern by investigators in the ELF field regarding such instrumentation problems.

In reviewing the rather extensive literature on ELF investigations, it was noted that there was no documentation of instrumentation step or impulse responses, no mention of the type or order of the low and high-pass filters used, only an occasional sketch of the frequency response of a system and never a full Bode plot of magnitude and phase versus frequency. Only a single mention was found of the possible degradation of waveforms by notch filters [70]. This lack of concern regarding system transient response is all the more surprising in view of the

impulsive nature of typical ELF signals, and the fact that some aspects of theoretical work have been based on the analysis of waveshapes of recorded transients.

Figure 4.6 is an illustration of this point.

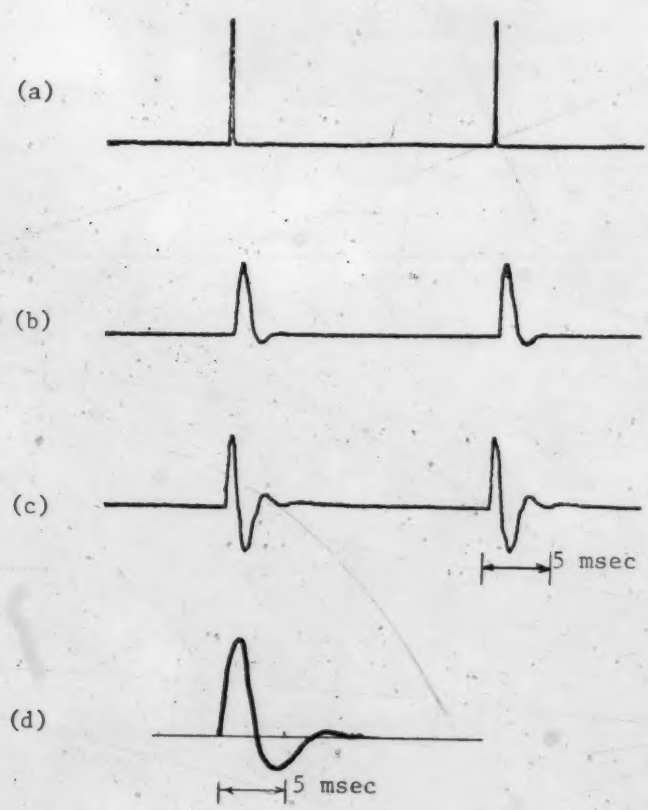

Figure 4.6 Filter Artifacts and a "Slow-Tail" Waveform

In the above Figure, waveform (a) is a 250 μsec input pulse, waveform (b) is the resultant output from a 2nd-order Butterworth low-pass filter which has a 500-Hz upper corner-frequency, and waveform (c)

shows the added distortion if a passive Twin-T 60-Hz notch filter is included in the signal path. Waveform (d) is a sketch of a typical ELF "slow-tail" waveform used in the study of far-distant lightning discharges [71],[72]. It is evident that one needs only select the proper order low-pass filter with an appropriate corner-frequency, and the filter impulse response would match the "slow-tail" waveform.

A somewhat related concern pertains to published recordings such as those reproduced in Figure 4.7.

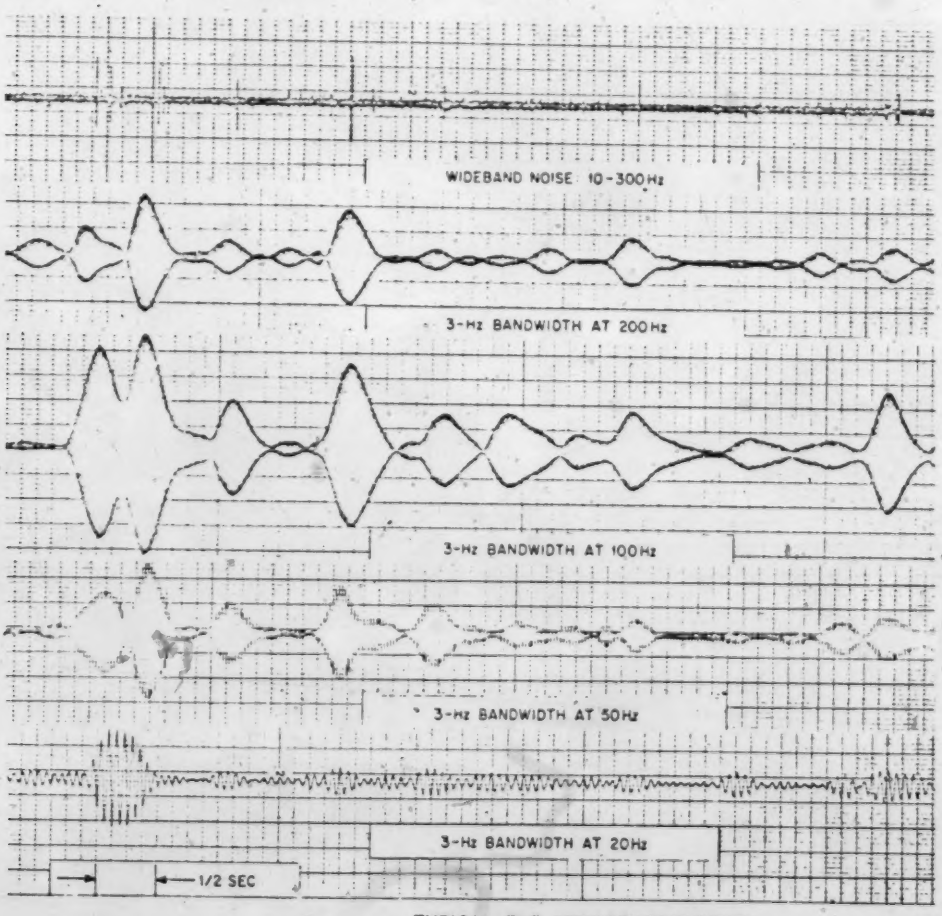
WIDEBAND NOISE 10-300Hz
3-Hz BANDWIDTH AT 200Hz
3-Hz BANDWIDTH AT 100Hz
3-Hz BANDWIDTH AT 50Hz
3-Hz BANDWIDTH AT 20Hz
1/2 SEC
TYPICAL ELF ATMOSPHERIC NOISE
Wide-band and narrow-band ELF noise from Florida (Feb. 1968).

Figure 4.7 Typical ELF Atmospheric Noise (Evans and Griffiths [73])

The implication is that the wideband noise contains the narrow-band components illustrated. However, the impulsive nature of the wideband record is evident, and a transient pulse a few milliseconds in duration obviously does not have a 1/2-sec train of 20-Hz oscillations as a component. The further implication that low-frequency components maintain phase coherency over dozens of cycles is also unfortunate, and does not agree with reality; waveform coherency for more than 4 or 5 cycles is rarely observed. The narrow-band recordings of Figure 4.7 simply portray the impulse responses of the high-Q sharply-tuned filters. Any attempt to use such equipment in making estimates of spectral densities would seem to be rather futile.

An additional point in this regard is that published spectral-density estimates [15],[17],[22] have probably been based on the classical method which compensates for the instrument frequency response after the time-domain data has been transformed to the frequency domain, since multiplication is then involved instead of convolution. Unfortunately, there is no evidence that anything except the steady-state frequency response of the system is ever used for this correction. From a circuit-theory standpoint, it has been pointed out [74] that a short-burst of oscillations is equivalent to multiplying a steady-state sinusoid by a gating pulse. In the frequency domain, this requires the convolution of the instrument's steady-state response with some sinc function, to derive its "impulse" frequency response. Since this transient frequency response may be considerably different from the steady-state response, the published spectral-density estimates may be considerably in error.

4.3 SUMMARY

The Extremely-Low-Frequency (ELF) spectrum of electromagnetic waves (3 Hz – 3 kHz) has a number of special characteristics. The background noise in this range is generated primarily by global lightning activity, and the resultant disturbances may propagate to great distances in the Earth-ionosphere cavity (via a TEM guided-wave mode) since the attenuation at such low frequencies may be less than 1 dB/1000 Km. Cavity resonances are identifiable at about 8 Hz, 14 Hz, 20 Hz, ... , the so-called Schumann resonances. The extensive earth penetration at ELF wavelengths has been used for geophysical prospecting, and penetration is sufficient even in sea water to permit signal transmissions to submerged submarines.

Measuring and recording systems for ELF signals are typically semi-permanent large-scale facilities. Directional H-field sensors are heavy, bulky and must be specially installed to be free of vibration in the Earth's natural magnetic field. Vertical E-field components are usually monitored by omni-directional elevated-whip or ball antennae. Extensive back-up instrumentation is typically required, with signals being recorded on computer-grade magnetic-tape systems for subsequent analysis.

This thesis is concerned with the system design of a portable receiver-recorder for special field investigations. The nominal pass-band is 5 Hz – 200 Hz to cover all Schumann-resonance phenomena with acceptable waveform reproduction. Battery operation and portability has been a prime consideration (13 lbs total weight) and a cassette

magnetic-tape recorder provides the data-storage medium.

The system design has been given in detail, with all relevant design equations and circuit schematics for:

1) A "charge-induction" type of E-field sensor, with an electrometer input and a cable-drive amplifier.

2) A semi-remote (40 ft from the E-field sensor) variable-gain amplifier system. The frequency response is shaped to minimize pulse-waveform distortion, and a modified 60-Hz notch filter has been included which does not generate pulse transients. A Pulse-Duration-Modulation (PDM) system is included to permit the recording of ELF signals on magnetic tape.

3) A PDM demodulator system permits recovery of the ELF signals from the magnetic tape. Special circuits are included to compensate for tape-speed variations during playback. Output of the regenerated ELF signal is at a suitable voltage level for chart recording or analog/digital conversion.

Reproductions are included of typical field-recorded ELF signals, and these records are at least equal in quality to those in the published literature on ELF research. It is noted that signal artifacts are especially likely in ELF instrumentation, due to the impulsive nature of ELF signals and the usual transient responses of signal filters.

The detailed derivation of the modified 60-Hz notch filter is given in Appendix A, and illustrates how transient and steady-state responses can be separated to ensure a good pulse response.

REFERENCES

[1] A.D.Watt, VLF Engineering, London, Pergamon Press, 1967.

[2] A.D.Watt, R.W.Plush, W.W.Brown, and A.H.Morgan, "Worldwide VLF Standard Frequency and Time Signal Broadcasting," J. of Res. of the N.B.S., vol. 65D, pp. 617-627, Nov.-Dec. 1961.

[3] E.R.Swanson and C.P.Kugel, "VLF Timing: Conventional and Modern Techniques Including Omega," Proc. IEEE, vol. 60, pp. 540-551, May 1972.

[4] F.W.Chapman, D. Llanwyn Jones, J.D.W.Todd, and R.A.Challinor, "Observations on the Propagation Constant of the Earth-Ionosphere Waveguide in the Frequency Band 8 c/s to 16 Kc/s," Radio Science, New Series, vol. 1, pp. 1273-1282, Nov. 1966.

[5] Nikola Tesla, "Art of Transmitting Electrical Energy Through the Natural Mediums," U.S.Patent 787412, April 18, 1905.

[6] Nikola Tesla: Lectures Patents and Articles, Pub. by Nikola Tesla Museum, Belgrade, 1956.

[7] H. Barkhausen, Phys. Zeits., pp. 401-403, 1919.

[8] H. Barkhausen, "Whistling Tones From The Earth," Proc. IRE, vol. 18, pp. 1155-1159, July 1930.

[9] T.L.Eckersley, "Musical Atmospherics," Nature, 135, pp. 104-105, Jan. 19, 1935.

[10] L.R.O.Storey, "An Investigation of Whistling Atmospherics," Trans. Roy. Soc. (London), 246, pp. 113-141, 1953.

[11] J.Katsufrakis, "Whistlers and VLF Emissions," Natural Electromagnetic Phenomena Below 30 Kc/s, ed. D.F.Bleil, New York, Plenum Press, pp. 261-286, 1964.

[12] W.O.Schumann, Z.Naturforschg., 7a, pp. 149-154, 1952.

[13] Ibid., pp. 250-252.

[14] W.O.Schumann and H.Konig, Z. Naturwissenschaften, vol. 41, pp. 183-184, 1951.

[15] M.Balser and C.A.Wagner, "Observations of Earth-Ionosphere Cavity Resonances," Nature, vol. 188, pp. 638-641, Nov. 19, 1960.

[16] J.Galejs, Terrestrial Propagation of Long Electromagnetic Waves, New York, Pergamon Press, pp. 295-298, 1972.

[17] D.L.Jones, "Extremely Low Frequency (ELF) Ionospheric Radio Propagation Studies Using Natural Sources," IEEE Trans. on Comm., vol. COM-22, pp. 477-484, April 1974.

[18] J.R.Wait, "The Guest Editor's Past Interest in Extremely Low Frequency (ELF) Electromagnetics," IEEE Trans. on Comm., vol. COM-22, pp. 587-588, April 1974.

[19] H.E.Rowe, "Extremely Low Frequency (ELF) Communications To Submarines," IEEE Trans. on Comm., vol. COM-22, pp. 371-385, April 1974.

[20] M.H.Benedick and B.Greenberg, "The Sanguine Biological-Ecological Research Program," IEEE Trans. on Comm., vol. COM-22, pp. 570-577, April 1974.

[21] M.McClintok, P.Ressman, and A.Scott, "Talking To Ourselves," Environment, vol. 13, pp. 16-43, Sept. 1971.

[22] F.W.Chapman and D.L.Jones, "Earth-Ionosphere Cavity Resonances and the Propagation of Extremely Long Radio Waves," Nature, vol. 202, pp. 654-657, May 16, 1964.

[23] J.R.Wait, "Earth-Ionosphere Cavity Resonances and the Propagation of ELF Radio Waves," Radio Science: J. of Res. of NBS, vol. 69D, pp. 1057-1070, August 1965.

[24] F.W.Chapman, D.Llanwyn Jones, J.D.W.Todd, and R.A.Challinor, "Observations on the Propagation Constant of the Earth-Ionosphere Waveguide in the Frequency Band 8 c/s to 16 Kc/s," Radio Science, New Series, vol. 1, pp. 1273-1282, Nov. 1966.

[25] W.L.Taylor and A.G.Jean, "Very-Low-Frequency Radiation Spectra of Lightning Discharges," J. of Res. of NBS, vol. 63D, pp. 199-204, Sept.-Oct. 1959.

[26] A.D.Watt, "ELF Electric Fields From Thunderstorms," J. of Res. of NBS, vol. 64D, pp. 425-433, Sept.-Oct. 1960.

[27] H.R.Arnold and E.T.Pierce, "Leader and Junction Processes in the Lightning Discharge as a Source of V.L.F. Atmospherics," Radio Science: J. of Res. of NBS, vol. 68D, pp. 771-776, July 1964.

[28] H.L.Jones, R.L.Calkins and W.L.Hughes, "A Review of the Frequency Spectrum of Cloud-to-Cloud and Cloud-to- Ground Lightning," IEEE Trans. on Geos. Electr., vol. GE-5, pp. 26-30, March 1967.

[29] C.Polk, "Relation of ELF Noise and Schumann Resonances to Thunderstorm Activity," Planetary Electrodynamics, (Vol. 2), New York, Gordon and Breach Science Pub., pp. 55-83, 1969.

[30] E.L.Maxwell, "Atmospheric Noise from 20 Hz to 30 kHz," Radio Science, New Series, vol. 2, pp. 637-644, June 1967.

[31] P.Beckmann, "Amplitude-Probability Distribution of Atmospheric Radio Noise," Radio Science: J. of Res. of NBS, vol. 68D, pp. 723-736, June 1964.

[32] M.J. Rycroft, "Resonances of the Earth-Ionosphere Cavity Observed at Cambridge, England," Radio Science: J. of Res. of NBS, vol. 69D, pp. 1071-1081, August 1965.

[33] E.L.Maxwell and D.L.Stone, "Natural Noise Fields from 1 cps to 100 kc," IEEE Trans. on Ant. and Prop., pp. 339-343, May 1963.

[34] J.A.Shand, "Some Quantitative Characteristics of the Schumann-ELF Natural Electromagnetic Background," Can. J. of Phys., vol. 44, pp. 449-459, March 1966.

[35] S.L.Bernstein, et al., "Long Range Communications at Extremely Low Frequencies," Proc. of IEEE, vol. 62, pp. 292-312, March 1974.

[36] H.G.Hughes, "Differences Between Pulse Trains of ELF Atmospherics at Widely Separated Locations," J. of Geoph. Res., vol. 76, pp. 2116-2125, March 1971.

[37] T.Ogawa, Y.Tanaka, T.Miura, and M.Yasuhara, "Observations of Natural ELF and VLF Electromagnetic Noises by Using Ball Antennas," J. of Geomag. and Geoelec., vol. 18, pp. 443-454, 1966.

[38] T.R.Larsen and A.Egeland, "Fine Structure of the Earth-Ionosphere Cavity Resonances," J. of Geophys. Res., vol. 73, pp. 4986-4989, 1968.

[39] J.E.Lokken, "Instrumentation For Receiving Electromagnetic Noise Below 3000 cps," Natural Eelectromagnetic Phenomena Below 30 Kc/s," ed. D.F.Bleil, New York, Plenum Press, pp. 373-428, 1964.

[40] J.A.Slankis and A.Becker, "Telluric and Magnetic-Telluric Measurements at 8 Hz," Trans. of AIME, pp. 237-244, June 1969.

[41] J.A.Slankis, W.M.Telford, and A.Becker, "8-Hz Telluric and Magnetotelluric Prospecting," Geophy., vol. 37, pp. 862-878, Oct. 1972.

[42] E.L.Maxwell, "Atmospheric Noise From 20 Hz to 30 kHz," Radio Science, New Series, vol. 2, pp. 637-644, June 1967.

[43] H.G.Hughes, "On The Directional Dependency of 'Slow-Tail' Extremely Low Frequency Atmospheric Waveforms," J. Atm. and Terr. Phys., pp. 545-552, 1967.

[44] M.D.Clayton, C.Polk, H.Etzold, and W.W.Cooper, "Absolute Calibration of Antennas at Extremely Low Frequencies," IEEE Trans. on Ant. and Prop., vol. AP-21, pp. 514-523, July 1973.

[45] D.L.Jones and D.T.Kemp, "Experimental and Theoretical Observations on the Transient Excitation of Schumann Resonances," J. Atm. and Terr. Phys., vol. 32, pp. 1095-1108, 1970.

[46] T.Ogawa, Y.Tanaka T.Miura, and M.Yasuhara, "Observations of Natural ELF and VLF Electromagnetic Noises by Using Ball Antennas," J. of Geomag. and Geoelec., vol. 18, pp. 443-454, 1966.

[47] A.D.Watt, VLF Engineering, London, Pergamon Press, p. 409, 1967.

[48] R.S.Dahlberg, "An Investigation of Natural Earth Currents," Geophy., vol. 10, pp. 494-506, 1945.

[49] J.A.Slankis and A.Becker, loc. cit.

[50] J.A.Slankis, W.M.Telford, and A. Becker, loc. cit.

[51] C.T.Fessenden and D.H.S.Cheng, "Development of a Trailing-Wire E-Field Submarine Antenna for Extremely Low Frequency (ELF) Reception," IEEE Trans. on Comm., vol. COM-22, pp. 428-437, April 1974.

[52] K.W.Henderson and W.H.Kautz, "Transient Responses of Conventional Filters," IRE Trans. on Circ. Theory, vol. CT-5, pp. 333-347, December 1958.

[53] G.A.Beck, "Comments on 'Transient Responses of Conventional Filters'," IRE Trans. on Circ. Theory, vol. CT-8, pp. 166-167, June 1961.

[54] E.R.Hanson, "A Tape Cassette Standard," J. Aud. Eng. Soc., vol. 16, pp. 430-435, October 1968.

[55] C.E.Lowman, Magnetic Recording, New York, McGraw-Hill, 1972.

[56] J.C.Mallinson, "Theoretical Limit to Digital Pulse Resolution in Saturation Recording," IEEE Trans. on Magn., vol. MAG-5, pp. 91-97, June 1969.

[57] C.B.Pear, Magnetic Recording, New York, Reinhold Pub., 1967.

[58] H.E.Rowe, "Pulse Modulation Systems," Signals and Noise in Communications Systems, New York, D. VanNostrand, Chapter V., 1965.

[59] A.B.Carlson, Communication Systems: An Introduction to Signals and Noise in Electrical Communication, New York, McGraw-Hill, pp. 406-409, 1968.

[60] E.L.Maxwell, "Atmospheric Noise From 20 Hz to 30 kHz," Radio Science, New Series, vol. 2, pp. 637-644, June 1967.

[61] E.L.Maxwell and D.L.Stone, "Natural Noise Fields from 1 cps to 100 kc/s," IEEE Trans. on Ant. and Prop., pp. 339-343, May 1963.

[62] J.A.Shand, "Some Quantitative Characteristics of the Schumann-ELF Natural Electro-Magnetic Background," Can. J. of Phys., vol. 44, pp. 449-459, March 1966.

[63] C.T.R.Wilson, "On Some Determinations of the Sign and Magnitude of Electric Discharges in Lightning Flashes," Proc. Roy. Soc. Lond., Series A, vol. 92, pp. 555-574, 1961.

[64] T.Mollinga, "Active Parallel-T Networks, Part 1," EEE: Circuit Design Engineering, pp. 93-98, April 1966.

[65] R.Dobkin, "High-Q Active Twin-T," EEE: Circ. Des. Eng., pp. 46-48, September 1969.

[66] R.C.Dobkin, "Op-Amp Circuit Collection," National Semiconductor Corp. Application Note, AN-31, p. 14, Feb. 1970.

[67] Fairchild Linear Integrated Circuits Data Catalog, p. 113, Nov. 1971.

[68] I.P.Ivanov, "Pulse-Ratio Modulation in Magnetic Recorders," Biomedical Sciences Instrumentation, (Proc. 9th Ann. Biomed. Sc. Instr. Symp.,) vol. 8, pp. 44-47, 1971.

[69] B.H.Brown, "Magnetic Tape Recorders for Low Frequency Biological Signals," Bio. Med. Eng., pp. 348-357, August 1971.

[70] J.O.Sinneger, "An ELF Wide-Band Noise Receiver," IEEE Trans. Geosc. Elect., vol. GE-10, pp. 113-118, April 1972.

[71] H.G.Hughes, "On The Directional Dependency of 'Slow-Tail' Extremely Low Frequency Atmospheric Waveforms," J. Atm. and Terr. Phys., vol. 29, pp. 545-552, 1967.

[72] D.L.Jones, "Propagation of ELF Pulses in the Earth-Ionosphere Cavity and Application to Slow-Tail Atmospherics," Radio Science, vol. 5, pp. 1153-1162, Aug.-Sept. 1970.

[73] J.E.Evans and A.S.Griffiths, "Design of a Sanguine Noise Processor Based Upon World-Wide Extremely-Low-Frequency (ELF) Recordings," IEEE Trans. on Comm., vol. COM-22, pp. 528-539, April 1974.

[74] R.J.LaSpisa and D.N.Arden, "Filter Design for Optimal Transient Performance," IEEE Trans. on Circ. Theory, vol. CT-18, pp. 532-538, Sept. 1971.

APPENDIX A

THE MODIFIED TWIN-T 60-HZ NOTCH FILTER

A.1 THE PASSIVE TWIN-T NOTCH FILTER

A typical twin-T network, with symmetrical elements and a resistive load is shown in Figure A.1(a), and its frequency response is sketched in Figure A.1(b).

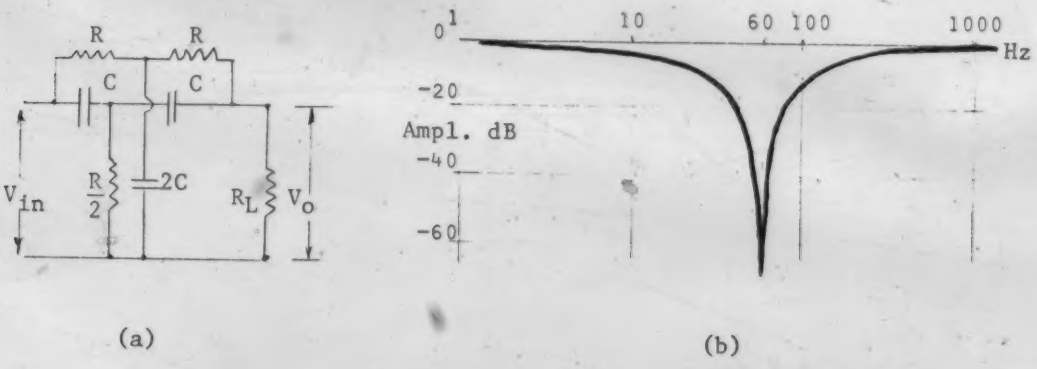

Figure A.1 The Passive RC Twin-T Notch Filter

The voltage transfer function for Figure A.1(a) can be written, in standard Laplace notation, as:

$$\frac{V_o(s)}{V_{in}(s)} = H_o(s) = \frac{s^2 + \omega_o^2}{s^2 + 2(2 + R/R_L)\omega_o s + (2R/R_L + 1)\omega_o^2}$$

where $\omega_o = 1/(RC)$. With negligible loading on the filter output, e.g., if the notch filter feeds into a high-impedance voltage follower, $R_L \to \infty$ and the transfer function reverts to:

$$H_o(s) = \frac{s^2 + \omega_o^2}{s^2 + 4\omega_o s + \omega_o^2} \qquad \text{(A-1)}$$

The Q of such a filter is low (.25) and for a 60-Hz notch frequency this leads to a 3-dB-down notch width of 240 Hz.

The poles of this filter are real, and the pole-zero locations are sketched in Figure A.2.

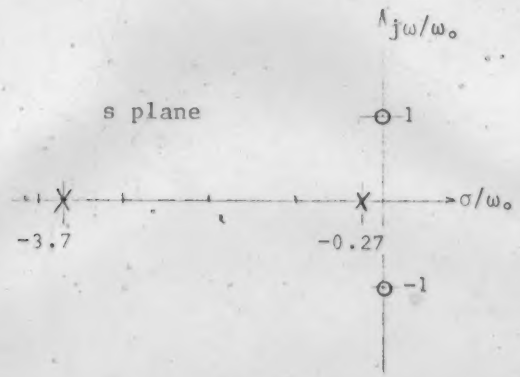

Figure A.2 Poles and Zeros of the Passive Twin-T Filter

The impulse response of the passive twin-T notch filter can be derived from Eqn. (A-1):

$$H_o(s) = \frac{s^2 + \omega_o^2}{s^2 + 4\omega_o s + \omega_o^2}$$

$$\approx 1 + \frac{.31\omega_o}{s + .27\omega_o} - \frac{4.3\omega_o}{s + 3.7\omega_o}$$

and returning to the time domain via the inverse Laplace transforms, gives the impulse response:

$$h_o(t) = [\ \delta(t) + .31\omega_o e^{-.27\omega_o t} - 4.3\omega_o e^{-3.7\omega_o t}\ ]u(t)$$

which for f_o = 60 Hz, $t > 0_+$, and t = milliseconds, gives:

$$h_o(t) = 117e^{-0.1t} - 1625e^{-1.41t} \qquad (t=\text{msec}) \qquad (A\text{-}2)$$

The form of this impulse response is sketched in Figure A.3:

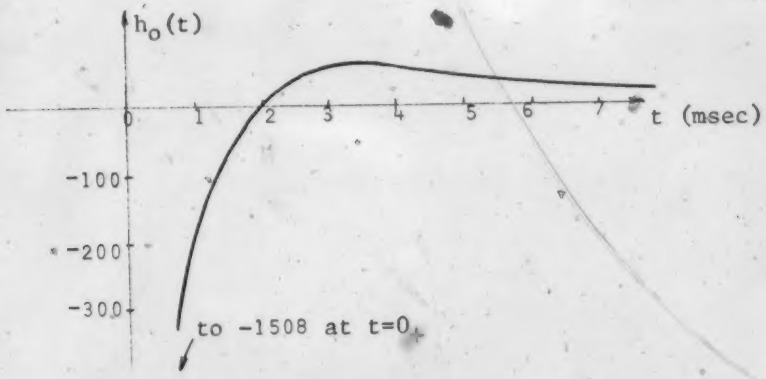

Figure A.3 Impulse Response of the Passive Twin-T Filter

The pulse response can be evaluated by using a unit-amplitude input pulse of width (τ):

$$x(t) = u(t) - u(t-\tau)$$

giving,
$$X(s) = \frac{(1-e^{-\tau s})}{s}$$

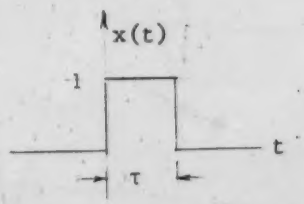

The ouput response of the passive twin-T filter with this input pulse, is:

$$Y_o(s) = X(s)H_o(s)$$

$$= \frac{(1-e^{-\tau s})}{s} \left(\frac{s^2 + \omega_o^2}{s^2 + 4\omega_o s + \omega_o^2} \right)$$

$$= (1-e^{-\tau s}) \left(\frac{1}{s} - \frac{1.16}{s + .27\omega_o} + \frac{1.16}{s + 3.7\omega_o} \right)$$

and reverting to the time domain, with f_o=60 Hz, and t=msec, the pulse response is given by:

$$y_o(t) = [1 + 1.16(e^{-1.4t} - e^{-0.1t})]u(t) - [1 + 1.16(e^{-1.4(t-\tau)} - e^{-0.1(t-\tau)}]u(t-\tau)$$

which produces the following waveforms for typical values of the pulse width (τ):

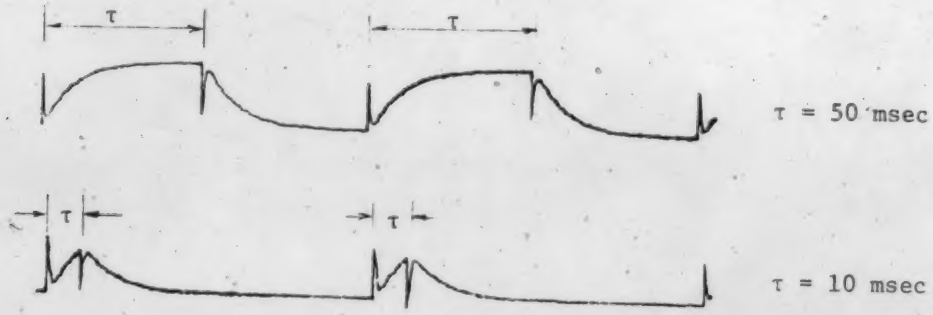

Figure A.4 Pulse Response of the Passive Twin-T Filter

A.2 THE HIGH-Q TWIN-T NOTCH FILTER

To increase the effective Q of a twin-T notch filter, an active-network version can be arranged as shown in Figure A.5(a), with its typical frequency response shown in Figure A.5(b).

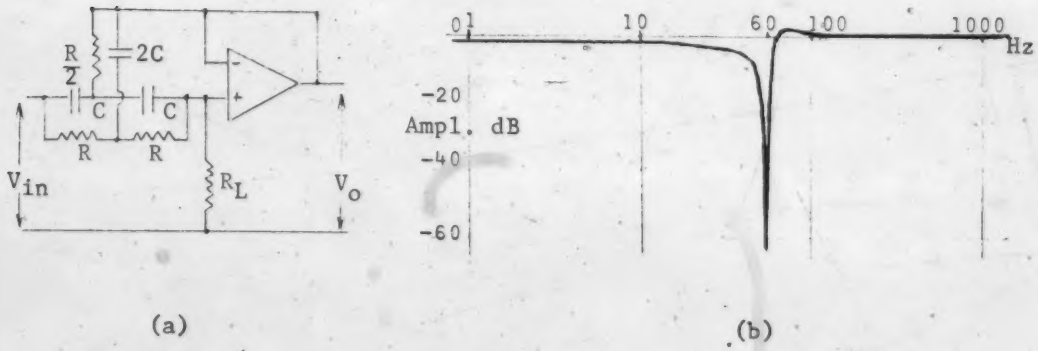

Figure A.5 High-Q Active Twin-T Notch Filter

In this case, if the voltage-follower gain is very close to unity, some deliberate network loading by resistor R_L is usually necessary to reduce the gain and maintain stability at the high Q value desired.

The voltage transfer function for the circuit of Fig. A.5(a), assuming a voltage-follower gain of unity, will be:

$$\frac{V_o(s)}{V_{in}(s)} = H_1(s) = \frac{s^2 + \omega_o^2}{s^2 + 2(R/R_L)\omega_o s + (2R/R_L + 1)\omega_o^2} \qquad \text{(A-3)}$$

and for the resistance $R_L \to \infty$ the poles and zeros coincide on the $j\omega$ axis.

For typical values of components for f_o=60 Hz. ($\omega_o = 2\pi f_o$), e.g., let R=80Kohms, C=.033μF in Fig. A.5(a) above, the gain is readily cont-

rolled by varying the resistance of R_L, which can therefore be used to control the Q and hence the notch width.

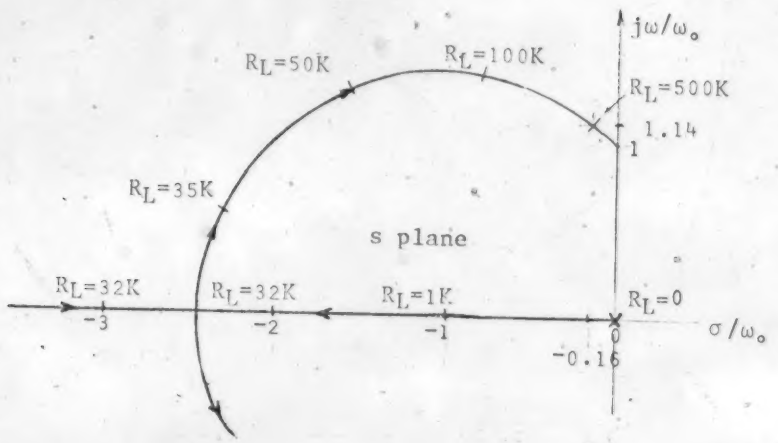

Figure A.6 Root Locus for the High-Q Twin-T Notch Filter

The locus of the positive complex root is shown in Figure A.6, as the gain is varied in terms of the load resistor R_L; the poles become complex for R_L>33Kohms. From Eqn. (A-3) the Q can now be expressed in terms of this loading resistor R_L as:

$$Q = \frac{R_L}{2R} = \frac{R_L}{160\text{Kohms}}$$

e.g., with R_L = 500Kohms (and R = 80Kohms as already noted), the filter Q = 500/160 = 3.1, so that for f_o = 60 Hz the notch width has been reduced to 60/3.1 ≈ 20 Hz. This notch characteristic is sketched in Figure A.5(b); the presence of the pole is evident on the high-frequency side of f_o.

The impulse response will now reflect the presence of the complex poles. From Eqn. (A-3),

$$H_1(s) = \frac{s^2 + \omega_o^2}{s^2 + 2(R/R_L)\omega_o s + (2R/R_L + 1)\omega_o^2}$$

which for R_L = 470Kohms (the closest standard resistor value to the 500Kohms), gives in terms of partial fractions:

$$H_1(s) = 1 - 132\left[\frac{s + .17\omega_o}{(s + .17\omega_o)^2 + (1.15\omega_o)^2} + \frac{(.86)(1.15\omega_o)}{(s + .17\omega_o)^2 + (1.15\omega_o)^2}\right]$$

and for f_o = 60 Hz, t = milliseconds, and t>0, the time-domain impulse response becomes:

$$h_1(t) = -e^{-0.06t}\,(132\cos.43t + 114\sin.43t) \qquad \text{(A-4)}$$

Figure A.7 The Impulse Response of a High-Q Twin-T Filter

The pulse response can be derived by using the same approach as for the passive twin-T filter, i,e., the input pulse is assumed to be of unit amplitude with a duration τ, giving:

$$Y_1(s) = X(s)H_1(s)$$

$$= \frac{(1-e^{-\tau s})}{s} \cdot \frac{s^2 + \omega_o^2}{s^2 + 2(R/R_L)\omega_o s + (2R/R_L + 1)\omega_o^2}$$

and again with resistor R_L = 470Kohms, the output in terms of a partial fraction expansion becomes:

$$Y_1(s) = (1-e^{-\tau s})\left[\frac{.74}{s} + \frac{.258(s + .17\omega_o)}{(s + .17\omega_o)^2 + (1.15\omega_o)^2} - \frac{.264(1.15\omega_o)}{(s + .17\omega_o)^2 + (1.15\omega_o)^2}\right]$$

Returning to the time domain, with f_o = 60 Hz and t = milliseconds, gives the pulse response as:

$$y_1(t) = \left[.74 + e^{-.06t}\ (.258\cos.43t - .264\sin.43t)\right] u(t)$$
$$- \left[.74 + e^{-.06(t-\tau)}\ [.258\cos.43(t-\tau) - .264\sin.43(t-\tau)]\right] u(t-\tau)$$

....(A-5)

which produces the following waveforms for typical values of pulse width:

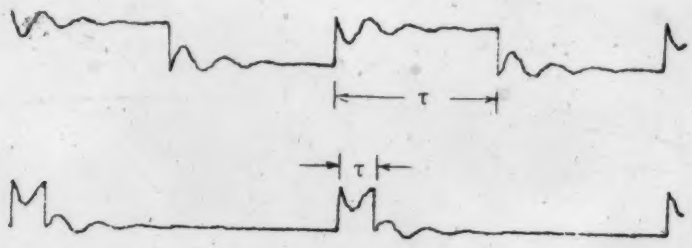

τ = 50 msec

τ = 10 msec

Figure A.8 The Pulse Response of a High-Q Twin-T Filter

A.3 THE 60-HZ PEAKED AMPLIFIER

As noted in Sections A.1 and A.2, both the low-Q and the high-Q versions of the twin-T notch filter display poor transient responses, although the steady-state frequency response can be shaped as required. One approach to an improvement of the pulse response is to use the high-Q twin-T network to form a 60-Hz peaked amplifier, and use its steady-state output to "buck out" the interfering 60 Hz in an auxiliary amplifier.

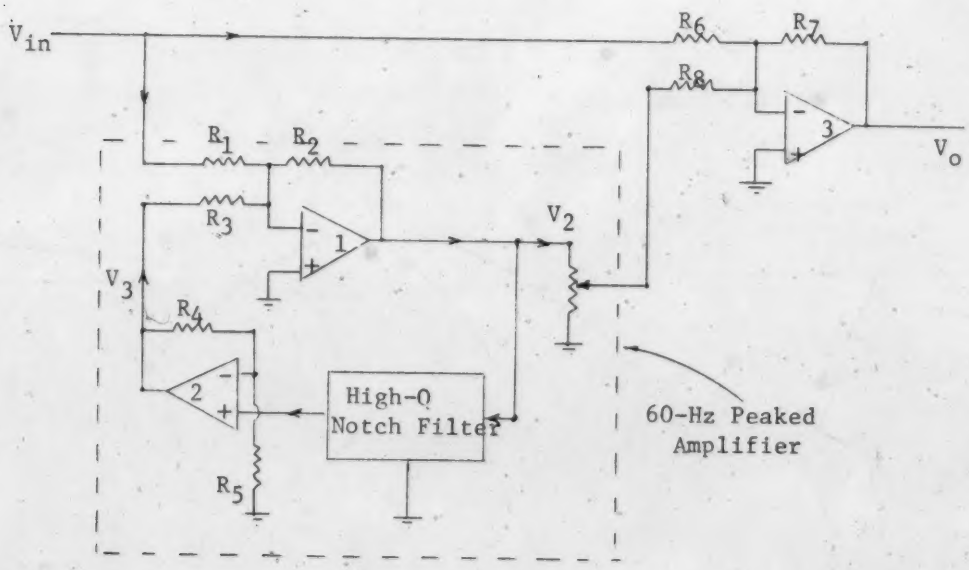

Figure A.9 The 60-Hz Peaked Amplifier

For the peaked-amplifier section of Figure A.9, using the high-Q transfer function $H_1(s)$ of Eqn. (A-3),

$$\frac{V_2(s)}{V_{in}(s)} = -\frac{R_2}{R_1}\left[\frac{1}{1 + H_1(s)R_2(R_4 + R_5)/(R_3R_5)}\right]$$

Using typical resistance values (as noted in Fig. 3.21), R_1 = 47Kohms, R_2 = 47Kohms, R_3 = 10Kohms, R_4 = 33Kohms, and R_5 = 2.2Kohms,

$$\frac{V_2(s)}{V_{in}(s)} = H_2(s) = -\left[\frac{1}{1 + 75\left[\frac{s^2 + \omega_o^2}{s^2 + .34\omega_o s + 1.34\omega_o^2}\right]}\right]$$

$$H_2(s) = -.013\left[\frac{s^2 + .34\omega_o s + 1.34\omega_o^2}{s^2 + .0045\omega_o s + 1.01\omega_o^2}\right] \qquad \text{(A-6)}$$

Evaluating $|H_2(j\omega)|$ gives the frequency response:

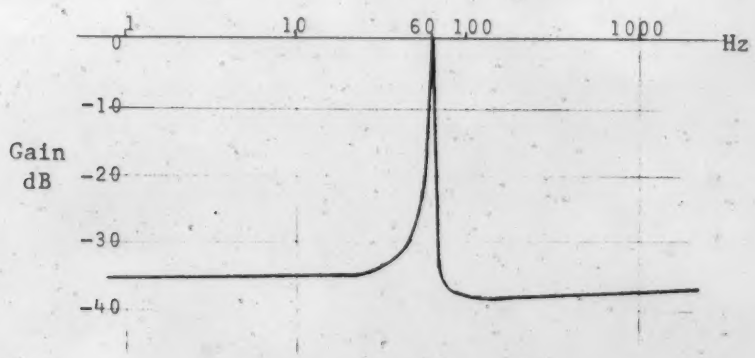

Figure A.10 The Frequency Response of the 60-Hz Amplifier

The pole-zero locations for this peaked amplifier are of interest. From the transfer function $H_2(s)$, (Eqn. A-6), it can be shown that:

The zeros are at: $s = (-0.18 \pm j1.15)\omega_o$

The poles are at: $s = (-.002 \pm j1.005)\omega_o$

The complex pole and zero in the upper-half S plane, with an expanded scale, are shown in Figure A.11.

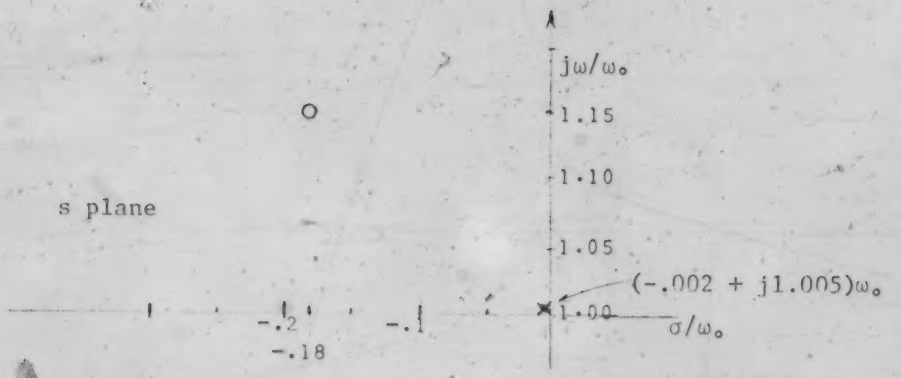

Figure A.11 Pole-Zero Locations for the 60-Hz Peaked Amplifier

Note that the pole is safely in the left-half plane for stability, but its nearness to $j = \omega_o$ indicates the very high effective Q ($\simeq$ 220). The zero location gives a slightly higher attenuation on the high-frequency side of ω_o, as is evident in the frequency-response curve of Figure A.10.

A.4 THE MODIFIED 60-HZ NOTCH FILTER

As is well known, if H(s) is a band-pass function, then [1 - H(s)] is the equivalent band rejection. This is the effective response of Figure A.12 if certain precautions are taken:

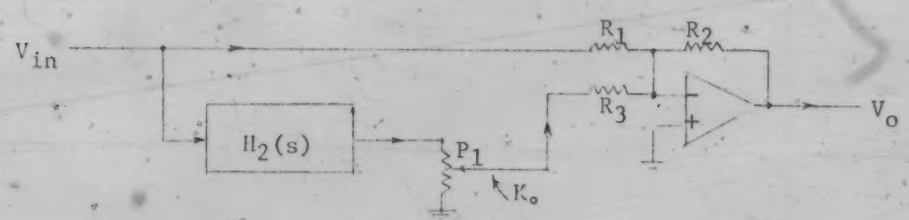

Figure A.12 Block Diagram of the Modified Notch Filter

The voltage transfer function of Figure A.12 is:

$$\frac{V_o(s)}{V_{in}(s)} = H_3(s) = -R_2\left[\frac{1}{R_1} + \frac{K_o H_2(s)}{R_3}\right]$$

Substituting for $H_2(s)$ from Eqn. A-6, and letting resistor $R_1 = R_2$, gives:

$$H_3(s) = -\left[1 - .043\frac{R_2}{R_3}K_o\left(\frac{s^2 + .34\omega_o s + 1.34\omega_o^2}{s^2 + .0045\omega_o s + 1.01\omega_o^2}\right)\right]$$

Letting $K_1 = K_o\frac{R_2}{R_3}(.013)$, rearranging, and ignoring the sign inversion of the summing amplifier, the transfer function can be rewritten as:

$$H_4(s) = |H_3(s)| = (1-K_1)\left[\frac{s^2 + \left(\frac{.0045-.34K_1}{1-K_1}\right)\omega_o s + \left(\frac{1.01-1.34K_1}{1-K_1}\right)\omega_o^2}{s^2 + .0045\omega_o s + 1.01\omega_o^2}\right]$$

By taking the precaution that resistor $R_3 < R_2$, (and that the nominal gain of $H_2(s)$ was unity at f_o), a point can be found on potentiometer P_1 such that its fractional setting $= K_o \approx \frac{R_3}{R_2}$. For this setting, the 2nd term in the bracketed numerator can be made equal to zero, leaving:

$$H_4(s) \approx .99\left[\frac{s^2 + 1.005\omega_o^2}{s^2 + .0045\omega_o + 1.01\omega_o^2}\right] \qquad (A\text{-}7)$$

In terms of the pole-zero locations:

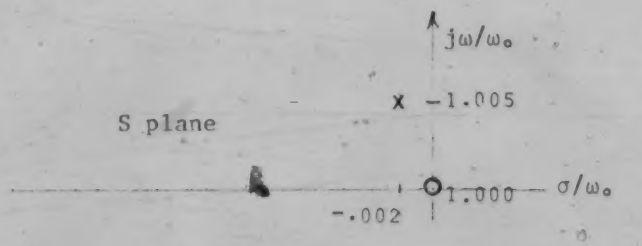

Figure A.13 Pole-Zero Locations of the Modified Notch Filter

Note in Figure A.13 that the complex pole location remains the same as in Figure A.11 but the zero has been restored to the jω axis, very close to the desired j = ω_o. In practice of course, the frequency-trim adjustment in the twin-T notch permits a precise location of the frequency null.

Figure A.14 shows the character of the high-Q notch, and since the Q is now over 200, the bandwidth has been reduced to about 60/200 = 0.3 Hz. (If such a notch width is considered too narrow, the Q can be reduced as required by reducing the resistance value of R_L in Fig. A.5(a) which manipulates the pole location as in Figure A.6.)

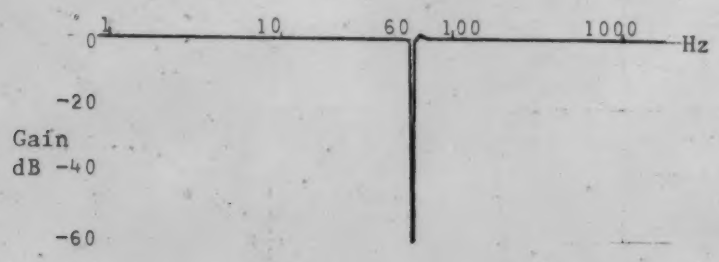

Figure A.14 Frequency Response of the Modified Notch Filter

While the frequency response of the modified notch filter is simply that of a high-Q filter, the impulse and transient responses are much different. The impulse response can be derived from Eqn. A-7 as follows:

$$H_4(s) = .99\left[\frac{s^2 + 1.005\omega_o^2}{s^2 + .0045\omega_o s + 1.01\omega_o^2}\right]$$

$$H_4(s) = .99\left(1 - \frac{.0045\omega_o s + .01\omega_o^2}{s^2 + .0045\omega_o s + 1.01\omega_o^2}\right)$$

$$= .99\left[1 - 1.7\left(\frac{s + .002\omega_o}{(s + .002\omega_o)^2 + (1.005\omega_o)^2} + \frac{2.2(1.005\omega_o)}{(s + .002\omega_o)^2 + (1.005\omega_o)^2}\right)\right]$$

which gives a time domain response, with f_o = 60 Hz, t = msec, and $t > 0_+$

$$h_4(t) = -1.67\, e^{-.0007t}\,(\cos.38t + 2.2\sin.38t) \qquad \text{(A-8)}$$

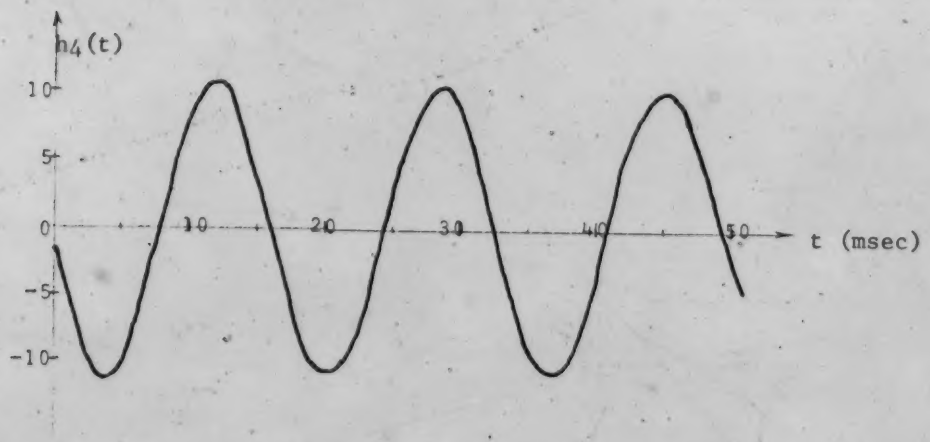

Figure A.15 The Impulse Response of the Modified Notch Filter

The impulse response now reflects the changed pole location; its proximity to the jω axis produces very little damping of the sinusoid, but since the pole is very close to the zero the amplitude of the sinusoid is only about one tenth that of the straight high-Q twin-T filter (as shown in Fig. A.7).

The pulse response of the modified notch filter, with a unit-amplitude input pulse of duration τ, can now be derived from the transfer

function of Eqn. A-7, giving:

$$Y_4(s) = X(s)H_4(s)$$

$$= \left(\frac{1-e^{-\tau s}}{s}\right)(.99)\left(\frac{s^2 + 1.005\omega_o^2}{s^2 + .0045\omega_o s + 1.01\omega_o^2}\right)$$

$$= (1-e^{-\tau s})\left(\frac{.99}{s} + \frac{.01s - .0045\omega_o}{s^2 + .0045\omega_o s + 1.01\omega_o^2}\right)$$

$$= (1-e^{-\tau s})\left[\frac{.99}{s} + \frac{.01(s + .0022\omega_o)}{(s + .0022\omega_o)^2 + (1.005\omega_o)^2} - \frac{.0044(1.005\omega_o)}{(s + .0022\omega_o)^2 + (1.005\omega_o)^2}\right]$$

Returning again to the time domain with f_o = 60 Hz and t = msec, the pulse response becomes:

$$y_4(t) = \left[.99 + e^{-.0008t}\ (.01\cos.38t - .004\sin.38t)\right] u(t)$$
$$- \left[.99 + e^{-.0008(t-\tau)}\ (.01\cos.38(t-\tau) - .004\sin.38(t-\tau)\right] u(t-\tau)$$

.....(A-9)

which is illustrated by the following test results, for several input-pulse widths:

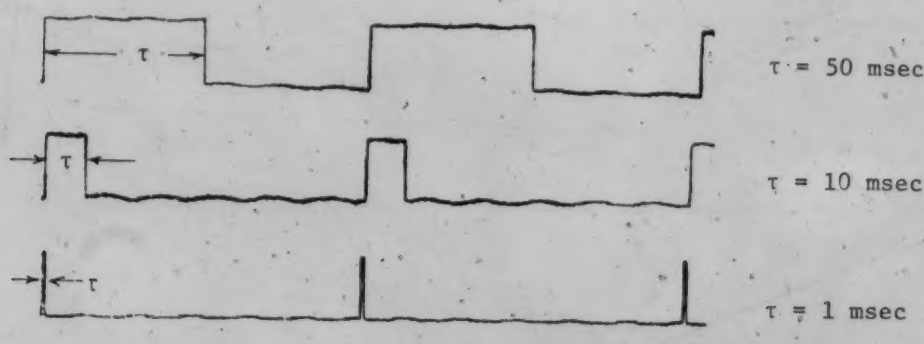

Figure A.16 The Pulse Response of the Modified Notch Filter

It is apparent from Figure A.16 that the pulse response of the modified notch filter is a considerable improvement over that of the standard high-Q twin-T filter (as shown in Fig. A.8).

From Eqn. A-9 for the time-domain response $y_4(t)$, it can be seen that the (.02) cosine coefficient represents a nominal 2% 60-Hz ripple on the pulse response, and its exponential damping is negligible. This ripple originates as the "error" signal at the output of the 60-Hz peaked amplifier after each excitation by a pulse edge: it is not related to the 60-Hz content of the incoming signal. (If desired, the level of this ripple could be reduced by a higher loop gain and further optimization of the 60-Hz peaked amplifier.)

A.5 PHASE RESPONSES

It is of some interest to compare the phase responses of the various versions of the notch filter. From Eqn. A-1 for the transfer function of the passive twin-T network:

$$H_o(s) = \frac{s^2 + \omega_o^2}{s^2 + 4\omega_o s + \omega_o^2}$$

$$H_o(j\omega) = \frac{1 - (\omega/\omega_o)^2}{1 - (\omega/\omega_o)^2 + j(4\omega/\omega_o)}$$

The phase angle is therefore:

$$\theta_o(\omega) = - \tan^{-1}\left[\frac{4\omega/\omega_o}{1 - (\omega/\omega_o)^2}\right] \qquad \text{(A-10)}$$

In a similar manner, from the transfer function Eqn. A-3 for the high-Q twin-T notch filter, the phase response can be expressed as:

$$\theta_1(\omega) = - \tan^{-1}\left[\frac{.35\omega/\omega_o}{1.35 - (\omega/\omega_o)^2}\right] \qquad \text{(A-11)}$$

and from Eqn. A-7 for the modified notch filter transfer function,

$$\theta_4(\omega) = - \tan^{-1}\left[\frac{.0045\omega/\omega_o}{1.01 - (\omega/\omega_o)^2}\right] \qquad \text{(A-12)}$$

The phase responses given by equations A-10, A-11 and A-12 are plotted below:

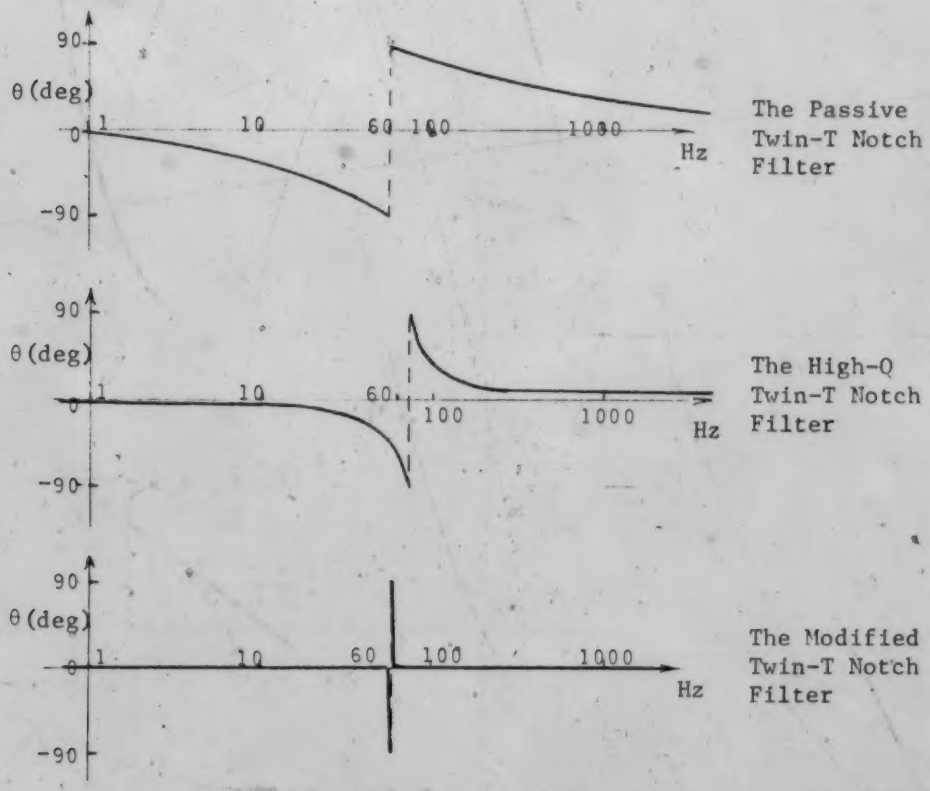

Figure A.17 The Phase Responses of the Various Notch Filters

A.6 EFFECTIVENESS AND LIMITATIONS

The effectiveness of the modified notch filter is shown in Figure A.18. The input signal consisted of a 13-Hz square wave plus a superimposed 60-Hz sine wave, of equal peak-to-peak amplitudes. The recorded output is shown (a) with the notch filter switched OUT, and (b) with the notch filter switched IN. (The square-wave droop is due to the capacitive coupling into the amplifier section which precedes the notch filter.)

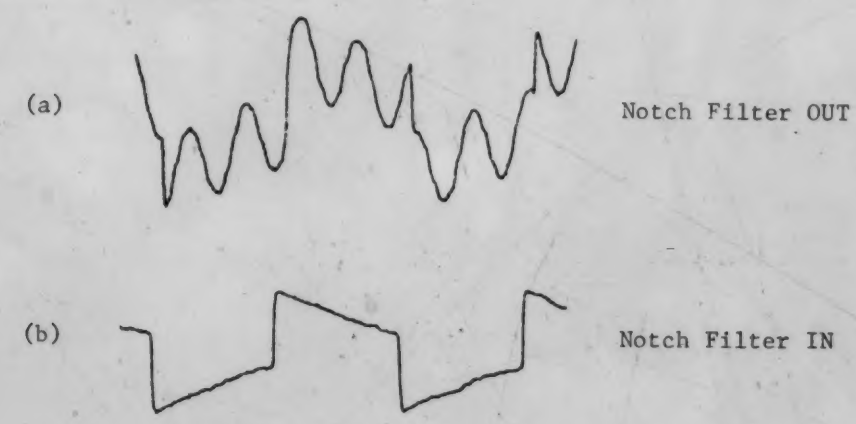

Figure A.18 The Effectiveness of the Modified Notch Filter

The limitations of this modified notch filter are related to the very high "internal Q" of the 60-Hz peaked amplifier. The approach to steady-state operation of the system is determined by the exponential term of Eqn. A-9, which in units of seconds is $\exp(-0.8t)$. The time constant is therefore 1.25 seconds, and to settle to within 1% of the steady-state value will require about 5.8 seconds. This is illustrated

in Figure A.19, which was generated by abruptly gating a constant-amplitude 60-Hz signal into the notch-filter system.

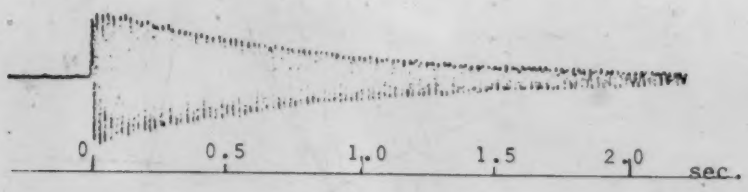

Figure A.19 Settling Time of the Modified Notch Filter

Under the usual field conditions, the 60-Hz interference is essentially constant, so that after the initial turn-on settling time of 6 or 7 seconds, this long time constant is of little concern. However, an occasional field record has shown a short damped train of 60-Hz oscillations, presumably due to power-demand switching in the relatively distant power-line distribution systems, with a resultant step change in the amplitude of the local 60-Hz interference field.

A second limitation of the modified notch filter is that the nominal 2% ripple due to pulse excitation can be driven to 5% - 10% if the pulse repetition rate is a precise sub-multiple of 60-Hz. To date, this has not been observed in field recordings, perhaps due to the random time distribution of the natural ELF transients and the short coherence times of the low-frequency components.

APPENDIX B

THE "GYRATOR" NOTCH FILTER

B.1 SCHEMATIC AND TRANSFER FUNCTION

The basic circuit of the so-called "gyrator" notch filter, using integrated-circuit operational amplifiers such as the common type "741", is shown in Figure B.1.

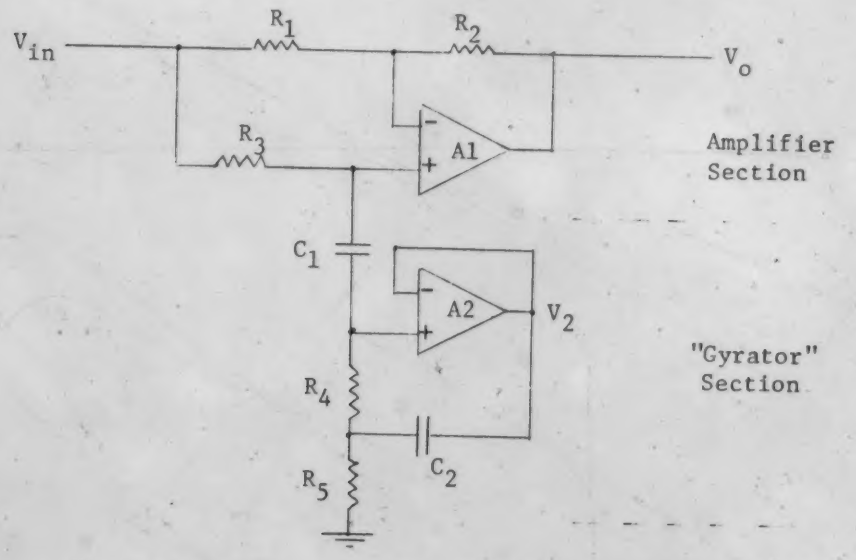

Figure B.1 The Gyrator Notch Filter

The voltage transfer function for this notch filter can be shown to be:

$$H(s) = \left[\frac{s^2 + \frac{(R_4 + R_5 - R_2R_3/R_1)}{\sqrt{C_1C_2R_4R_5}} C_1\omega_o s + \omega_o^2}{s^2 + \frac{(R_3 + R_4 + R_5)}{\sqrt{C_1C_2R_4R_5}} C_1\omega_o s + \omega_o^2} \right] \qquad \text{(B-1)}$$

where $\omega_o = \sqrt{C_1C_2R_4R_5}$.

B.2 POLE-ZERO LOCATIONS

From the transfer function for H(s), it is evident that a zero will occur (the desired frequency notch) if the centre term of the numerator is made equal to zero. This will occur if:

$$R_4 + R_5 - R_2R_3/R_1 = 0$$

i.e., if

$$R_4 + R_5 = R_2R_3/R_1$$

For convenience, make resistors $R_1 = R_2$, so that the requirement for a frequency notch becomes simply that:

$$R_4 + R_5 = R_3$$

From Eqn. B-1 the filter Q can be written as:

$$Q = \frac{\sqrt{C_1C_2R_4R_5}}{C_1(R_3 + R_4 + R_5)}$$

A further simplification results if resistance values are chosen so that:

$$R_4 = R_5 = R_3/2$$

The transfer function then reduces to:

$$H(s) = \frac{s^2 + \omega_o^2}{s^2 + 4\sqrt{C_1/C_2}\,\omega_o s + \omega_o^2} \qquad \text{(B-2)}$$

where now $\omega_o = 1/(R_4\sqrt{C_1C_2})$, and the expression for Q becomes:

$$Q = \frac{1}{4}\sqrt{\frac{C_2}{C_1}} \qquad \text{(B-3)}$$

This leaves the Q defined by the ratio of capacitances C_1 and C_2, while the notch frequency is related to their product via $\omega_o = 1/(R_4\sqrt{C_1C_2})$.

Since the gyrator-section gain is manipulated by the capacitance ratio C_2/C_1, the complex-pole location relative to the zero can be readily defined in terms of C_2/C_1.

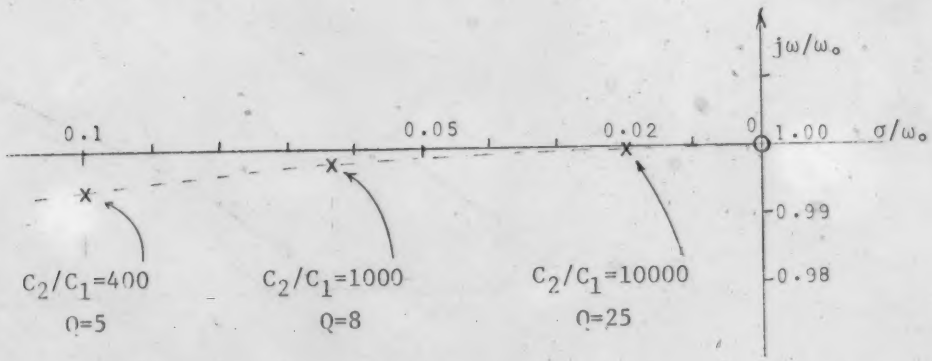

Figure B.2 Pole-Zero Locations for the Gyrator Notch Filter

B.3 PRACTICAL LIMITATIONS

There are two practical considerations which limit the application of the gyrator notch filter:

(a) The maximum useful Q is about 20. From the expression for Q in terms of the capacitance ratio (Eqn. B-3) it can be seen that for Q = 20 the capacitance ratio C_2/C_1 = 6,400. With resistor R_4 = 100Kohms (about the highest practical value in view of the operational amplifier input resistance) and f_o = 60 Hz, the required capacitance values become:

$$C_1 = 330 \text{ pF}$$
$$C_2 = 2.1 \mu\text{F}$$

Such a value of C_2 can be secured in a metallized-foil capacitor, but it

is close to the practical limit of cost and size.(Electrolytic capacitors are not acceptable because of the A.C. non-polarized operation, and because of their capacitance instability.) Even with a capacitance ratio of 6400/1 it is difficult to secure the two units with similar temperature coefficients of capacitance. As a result, the notch-frequency drift with temperature may be a problem.

(b) The maximum permitted level of the interference component of V_{in} is a function of Q. This is related to the large capacitance ratio C_2/C_1 which implies that the amplitude of the 60-Hz oscillation (in this case) at the output of amplifier A2 (the voltage V_2 in Fig. B.1) must be very much greater than its amplitude at the (+) input of amplifier A1. For a maximum signal amplitude of perhaps 10 V (peak) at V_2, the maximum amplitude of the 60-Hz component of V_{in} will be:

$$V_{in(60\ Hz)} \approx \frac{V_2}{Q} = \frac{10}{20} = 0.5\ V\ (peak)$$

It is necessary that this interference-level restriction be observed in any application of this type of notch filter, since peak clipping of V_2 can introduce transient distortions into the output signal V_o.

B.4 ADVANTAGES

For applications where a Q of less than 20 is adequate, the gyrator notch filter is a simple, stable approach, with relatively few components. Minor frequency adjustments can be easily made if resistor R_4 is variable; alternatively, if the required capacitance is sufficiently low, capacitor C_1 can be chosen as a trimmer capacitor. It should be noted

that to secure a valid null at the notch frequency, resistor R_1 may have to be somewhat reduced from its theoretical value, to allow for the finite input resistances of the operational amplifiers.

Figure B.3 shows that the pulse response is free of leading and trailing-edge differentiation, and the "shock-excited" 60-Hz ripple is sufficiently low for most applications. Note that this 60-Hz ripple is a constant percentage of the pulse amplitude, and is not a feed through of 60-Hz interference from the input signal; in the illustration of Fig. B.3(a) no 60-Hz interference was present on the input pulse.

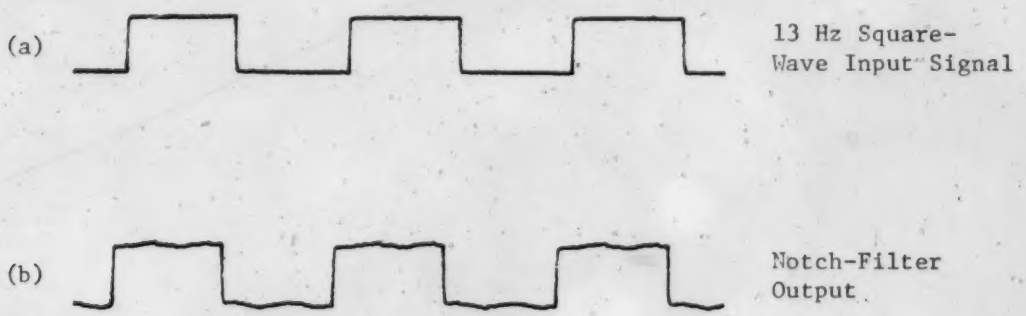

Figure B.3 Pulse Response of the Gyrator Notch Filter